ER-7798-F

0292

480

NONDESTRUCTIVE EVALUATION OF CERAMICS

T. Derkacs
I. M. Matay
W. D. Brentnall

TRW, Inc.
Cleveland, OH. 44117

July 1976

Final Technical Report
Contract No. N00019-75-C-0238

Approved for public release; distribution unlimited

Prepared for
NAVAL AIR SYSTEMS COMMAND
Department of the Navy
Washington, D. C. 20361

SECURITY CLASSIFICATION OF THIS PAGE (When Data Entered)

REPORT DOCUMENTATION PAGE

READ INSTRUCTIONS BEFORE COMPLETING FORM

1. REPORT NUMBER
2. GOVT ACCESSION NO.
3. RECIPIENT'S CATALOG NUMBER

4. TITLE (and Subtitle)

NONDESTRUCTIVE EVALUATION OF CERAMICS

5. TYPE OF REPORT & PERIOD COVERED

Final Technical Report

6. PERFORMING ORG. REPORT NUMBER

TRW - ER-7798-F

7. AUTHOR(s)

TRW Inc.
23555 Euclid Avenue
Cleveland, Ohio 44117

8. CONTRACT OR GRANT NUMBER(s)

N00019-75-C-0238

9. PERFORMING ORGANIZATION NAME AND ADDRESS

Naval Air Systems Command
Department of the Navy
Washington, D.C. 20361

10. PROGRAM ELEMENT, PROJECT, TASK AREA & WORK UNIT NUMBERS

11. CONTROLLING OFFICE NAME AND ADDRESS

12. REPORT DATE

19 May 1976

13. NUMBER OF PAGES

14. MONITORING AGENCY NAME & ADDRESS (if different from Controlling Office)

T. /Derkacs, I. M. /Matay
W. D. /Brentnall

15. SECURITY CLASS. (of this report)

Unclassified

15a. DECLASSIFICATION/DOWNGRADING SCHEDULE

16. DISTRIBUTION STATEMENT (of this Report)

Approved for public release; distribution unlimited.

Final technical rept.
20 Jan 75 - 19 Apr 76

17. DISTRIBUTION STATEMENT (of the abstract entered in Block 20, if different from Report)

18. SUPPLEMENTARY NOTES

19. KEY WORDS (Continue on reverse side if necessary and identify by block number)

Nondestructive evaluation (NDE); ceramics; high frequency ultrasonics; flexural strength; hot pressed silicon carbide; hot pressed silicon nitride; sintered silicon carbide; reaction bonded silicon carbide; flaws; fracture origins.

20. ABSTRACT (Continue on reverse side if necessary and identify by block number)

An ultrasonic nondestructive evaluation (UNE) method was developed to successfully detect small defects in gas turbine quality ceramic materials. A high frequency (25-45 MHz), longitudinal wave mode, pulse-reflection UNDE method was developed to evaluate a range of densities (2.2 to 3.2 g/cm^3) of ceramics (reaction bonded Si_3N_4, sintered SiC, hot pressed Si_3N_4 and hot pressed SiC) for various types of defects (open pores and seeded inclusions of low (Al_2O_3) and high (WC) densities) of various small sizes (10 to 130μm).

DD FORM 1 JAN 73 1473 EDITION OF 1 NOV 65 IS OBSOLETE
S/N 0102-014-6601

SECURITY CLASSIFICATION OF THIS PAGE (When Data Entered)

PRICES SUBJECT TO CHANGE

20. Conventional mechanical tests were also performed to verify defect sizes and to correlate material strength with UNDE results.

FOREWORD

This Final Technical Report describes the work performed for the Naval Air Systems Command, Department of the Navy, under NASC Contract N00019-75-C-0238, during the calendar period of 1975 January 20 through 1976 April 19. The work involved the nondestructive evaluation (NDE) of ceramic materials, under the technical direction of Mr. Irving Machlin, AIR-52031B, Naval Air Systems Command, Washington, DC 20361.

This contract with TRW Inc. was carried out in the Materials Development Department - Dr. I. J. Toth, Manager - of TRW Materials Technology. TRW personnel contributing to this program, and their areas of involvement, were: Mr. T. Derkacs, Principal Investigator; Mr. I. M. Matay, Program Manager and instrumentation optimization; and Mr. W. D. Brentnall, mechanical testing and metallurgical evaluations. Technical support to this program was provided by Messrs. J. Touhalisky and J. O. Rowe, ultrasonic inspections; Mr. A. V. Stan, instrumentation modifications; Mr. C. A. Tyndall, mechanical testing; Mr. W. G. Curtis, scanning electron microscope fractography; and Mr. C. E. Harris, electron beam microprobe analysis.

This Final Technical Report has been given an internal TRW report number of ER-7798-F.

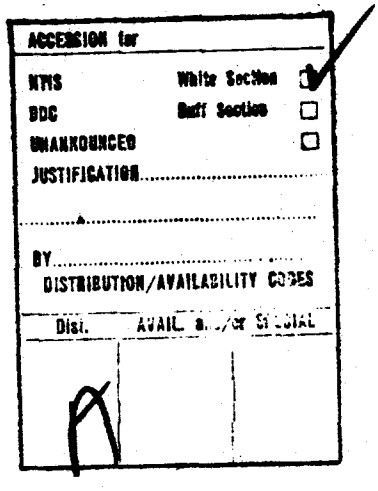

ABSTRACT

An ultrasonic nondestructive evaluation (UNDE) technique was developed to successfully detect small defects in gas turbine quality ceramic materials. A high frequency (25-45 MHz), longitudinal wave mode, pulse-reflection UNDE method was developed to evaluate a range of densities (2.2 to 3.2 g/cm^3) of ceramics (reaction bonded Si_3N_4, sintered SiC, hot pressed Si_3N_4 and hot pressed SiC) for various types of defects (open pores and seeded inclusions of low (Al_2O_3) and high (WC) densities) of various small sizes (10 to 130 μm). Conventional mechanical tests were also performed to verify defect sizes and to correlate material strength with UNDE results.

TABLE OF CONTENTS

TABLE OF CONTENTS (Cont'd)

LIST OF ILLUSTRATIONS

LIST OF ILLUSTRATIONS (Cont'd)

LIST OF ILLUSTRATIONS (Cont'd)

LIST OF ILLUSTRATIONS (Cont'd)

LIST OF TABLES

LIST OF ABBREVIATIONS AND SYMBOLS

Symbol	Quantity	Unit
A	geometric constant	———
A	electrical current	ampere
$\mathring{A}$	length	Angstrom
Al_2O_3	aluminum oxide	———
B	constant	second-square root of cubic meter per kilogram
B	boron	———
b	specimen width	meter
C	carbon	———
C	temperature	Celsius
c	crack size	meter
Ca	calcium	———
°	temperature or angle	degree
E	elastic modulus	newton per square meter
EMP	electron beam microprobe	———
F	temperature	Fahrenheit
Fe	iron	———
f	fundamental frequency of ultrasonic wave	hertz
g	mass	gram
γ	fracture energy	joule per square meter
h	specimen height	meter

LIST OF ABBREVIATIONS AND SYMBOLS (CONT.)

Symbol	Quantity	Unit
H.P.	hot pressed	———
Hz	frequency	hertz
I	moment of inertia	quadric meter
IEEE	Institute of Electrical and Electronics Engineers, Inc.	———
K	stress intensity factor	newton per square root of cubic meter
Kc	critical stress intensity factor	newton per square root of cubic meter
Ksi	stress	thousand pound per square inch
L_c	material grain size	meter
L_d	defect size	meter
l	specimen length	meter
λ	ultrasonic wavelength	meter
M	moment	newton-meter
m	length	meter
MgO	magnesium oxide	———
min.	time	minute
N	nitrogen	———
N	force	newton
n	constant	———
O_2	oxygen	———
P	force	newton
psi	stress	pound per square inch

LIST OF ABBREVIATIONS AND SYMBOLS (CONT.)

Symbol	Quantity	Unit
R.B.	reaction bonded	
ρ	density	gram per cubic centimeter
S	sulfur	——
S	strength	meganewton per square meter
s	time	second
SEM	scanning electron microscope	——
Si	silicon	——
SiC	silicon carbide	——
Si_3N_4	silicon nitride	——
σ_b	stress on specimen tensile surface	meganewton per square meter
σ_y	stress at defect location	meganewton per square meter
t	billet thickness	meter
UNDE	ultrasonic nondestructive evaluation	——
V	crack velocity	meter per second
V	electrical potential	volt
V_0	potential on transmitter	volt
V_1	potential at receiver with no specimen	volt
V_2	potential at receiver with specimen inserted	volt

LIST OF ABBREVIATIONS AND SYMBOLS (CONT.)

Symbol	Quantity	Unit
v	velocity of sound	meter per second
W	tungsten	—
WC	tungsten carbide	—
x	distance from end of specimen	—
y	depth of defect below specimen tensile surface	meter
Z	acoustic impedance	kilogram per square meter-second

PREFIXES

Decimal multiples and submultiples of the engineering units listed above are formed by means of the following prefixes:

Symbol	Prefix	Multiplication Factor
M	mega	10^{6}
K	kilo	10^{3}
c	centi	10^{-2}
m	milli	10^{-3}
μ	micro	10^{-6}
n	nano	10^{-9}

1.0 INTRODUCTION

The trend in both military and commercial aircraft is toward turbofan engines having a compact, high-temperature gas generator. Although directionally solidified superalloy and composite materials may solve the short-term requirements for high-temperature, high strength materials, the long-term requirements for temperatures approaching 2500°F (1370°C) can only be satisifed by ceramic materials.

Silicon nitride and silicon carbide are the two ceramics commonly being considered for gas turbine and other high temperature engineering applications because of their high strength combined with good oxidation and thermal shock resistance. Both ceramics can be fabricated either as a fully-dense, hot-pressed material with high strength but limited shape capability, or as a more porous reaction sintered material, weaker but with quite extensive shape capability. Because of trade-offs between cost, fabricability and strength requirements, both forms warrant consideration for gas turbine applications. In addition, recent efforts have been directed towards development of sintered materials with properties approaching those of hot pressed material (Ref. 1).

In order to make the use of ceramic materials practical for gas turbines not only must suitable materials be developed, but nondestructive techniques must be found to inspect these materials. The brittle failure tendencies of ceramic materials, with catastrophic failure propagating under stress from small defects, make flaw detection highly important. However, in many cases, failure of these materials is controlled by internal voids, inclusions and microcracks that are beyond the detection limits of existing inspection techniques.

The object of this program is to develop a nondestructive evaluation technique capable of detecting defects in the 10 to 100 μm range in silicon nitride and silicon carbide. The approach that has been selected is high frequency ultrasonic evaluation.

2.0 SUMMARY

In order to cover in this program the range of materials and material densities considered candidates for use in gas turbine engines, specimens were obtained of hot pressed and sintered silicon carbide and hot pressed and reaction bonded silicon nitride. These materials were procured seeded with 125 μm low and high density particles in specified locations for use as defect reference standards. The material thicknesses were selected to be typical for turbine airfoils.

Initially, investigation was concentrated on determining the physical and acoustic properties of these materials. Of particular interest were the density of the material, the velocity of sound in the material, and the acoustic insertion loss as a function of ultrasonic frequency. In addition to these investigations, the materials were inspected by X-radiography and conventional ultrasonics in order to provide baseline data. This initial work showed that the hot pressed materials were of higher quality and were more suitable for detection of smaller size defects using higher frequency ultrasound. It also allowed specification of high frequency ultrasonic transducers.

Preliminary high frequency inspections were performed using various combinations of parameters in order to establish the best technique (combination of available equipment and method) to use for each material. Final inspections were then performed using the best available technique with particular emphasis on achieving thorough inspection of the material. Four point-bend testing was used to expose the ultrasonically detected defects so that they could be examined by scanning electron microscope fractography and electron beam microprobe analysis. Flexural strength data was also recorded and analyzed for a possible correlation with ultrasonic inspection results.

The results of the ultrasonic inspections verified that increasing the inspection frequency from 15 to 25 and then to 45 MHz allowed ever smaller defects to be detected, as expected from theoretical considerations. The hot pressed silicon carbide billet showed so few defects that no mechanical testing was performed. The sintered silicon carbide billet showed some particular patterns of ultrasonic indications that were found to correlate with areas of secondary fragmentation on the fracture surfaces. However, since fracture did not initiate from these defects, no correlation was found with flexural strength. The 45 MHz inspection of the sintered silicon carbide billet showed a general pattern of indications which seemed to correlate with the pores in the material which are not larger than about 20 μm. The reaction bonded silicon nitride billet showed a general background of indications which was almost continuous at 25 MHz. These indications were identified as originating from pores in the material on the order of about 20 μm in diameter. The frequency of these indications was found to correlate with flexural strength. However, it was also found that the indications from the pores masked indications from larger inclusions which were strength limiting. It is therefore recommended that further

investigation of reaction bonded silicon nitride be directed toward using a lower frequency inspection to detect large, strength limiting defects, while avoiding indications from the general porosity.

The billet of hot pressed silicon nitride was the only one in which a large number of individual defects were detected, including the seeded defects. This billet was machined into four point-bend specimens in which individual ultrasonically detected defects were located near the center of the tensile surface during testing. Specimens from defect free areas were also tested to provide baseline material strength data. No correlation was established between ultrasonic inspection results and the flexural strength of the hot pressed silicon nitride, because only four of the sixteen specimens could definitely be said to have failed through the ultrasonically detected defects. Three conclusions were drawn from the test results:

1. The smallest defect that could be definitely correlated with an ultrasonic signal was a 25 μm void (detected using an inspection frequency of 25 MHz).

2. Due to the difference in acoustic impedance mismatch, there is about a factor of ten difference between the signal level reflected from a low density (Al_2O_3) and high density (WC) inclusion of about the same size, shape and depth in the material.

3. The defects were deformed by the hot pressing, making them favorably oriented for ultrasonic detection but not for affecting material strength. For this type of specimen/defect geometry, ultrasonic shear wave inspection should give a much better correlation with flexural strength than the longitudinal wave inspection used in this program.

In conclusion, the results of this program show that the basic goal of detecting defects in the 10 to 100 μm size range was accomplished by high frequency ultrasonics. They also show that the primary effort of future work should be an attempt to correlate flexural strength with the results of ultrasonic shear wave inspection. Development of somewhat higher frequency inspection is also warranted, particularly for hot pressed silicon carbide.

3.0 CERAMIC MATERIALS

3.1 General

A variety of ceramic materials have been considered for use in gas turbine engines and other engineering applications where high temperature, oxidizing environments are encountered. Because of an outstanding combination of oxidation resistance, high-temperature strength and resistance to thermal shock, Si_3N_4 and SiC have emerged as the most promising materials for use as gas turbine engine components. Figure 1 shows temperature capabilities for turbine blades fabricated from various materials. For 1000-hour rupture life under typical operating stresses, of the systems currently being investigated only Si_3N_4 and SiC have potential for the 2300°F (1260°C) to 2500°F (1370°C) temperature range.

Both Si_3N_4 and SiC can be fabricated by one of several methods, so that there exists a series of materials with different sets of properties represented by each chemical formula (Ref. 2). Si_3N_4, for example, can be formed by reaction sintering (Refs. 3-6), hot pressing (Ref. 7), conventional sintering (Ref. 8), and chemical vapor deposition (Ref. 9). Each of these methods produces different amounts of porosity, different microstructure, and therefore different properties. In addition, for hot pressing and conventional sintering, where additives are used to aid sintering, the properties of the material depend on the additives used (Ref. 10). Finally, the properties of the final materials depend on the processing parameters used and the purity, grain size and phase type of the ceramic powders (Ref. 11). With the wide variety of materials available and with the rapid changes that are occurring as a result of the continuing effort to improve these materials, a program designed to develop an inspection method for whatever form is finally used, cannot investigate all of the materials available nor can it be limited to only one. Rather, it must investigate enough representative samples to cover the range of parameters that are likely to be encountered in the general population of gas turbine quality ceramics.

It is well established that the strength of ceramic materials is controlled by the size of cracks or crack precursors (inclusions) in the materials. In other words, a ceramic material will fail at a stress lower than the theoretical strength of a perfect specimen because of the defects present in it. Fracture mechanics attempts to relate the size of the defect present to the strength of the material. The Griffith-Irwin thermodynamic approach relates the material strength (S) to the crack size (c), the elastic modulus (E) and the fracture energy (γ) through a dimensionless geometric factor (A):

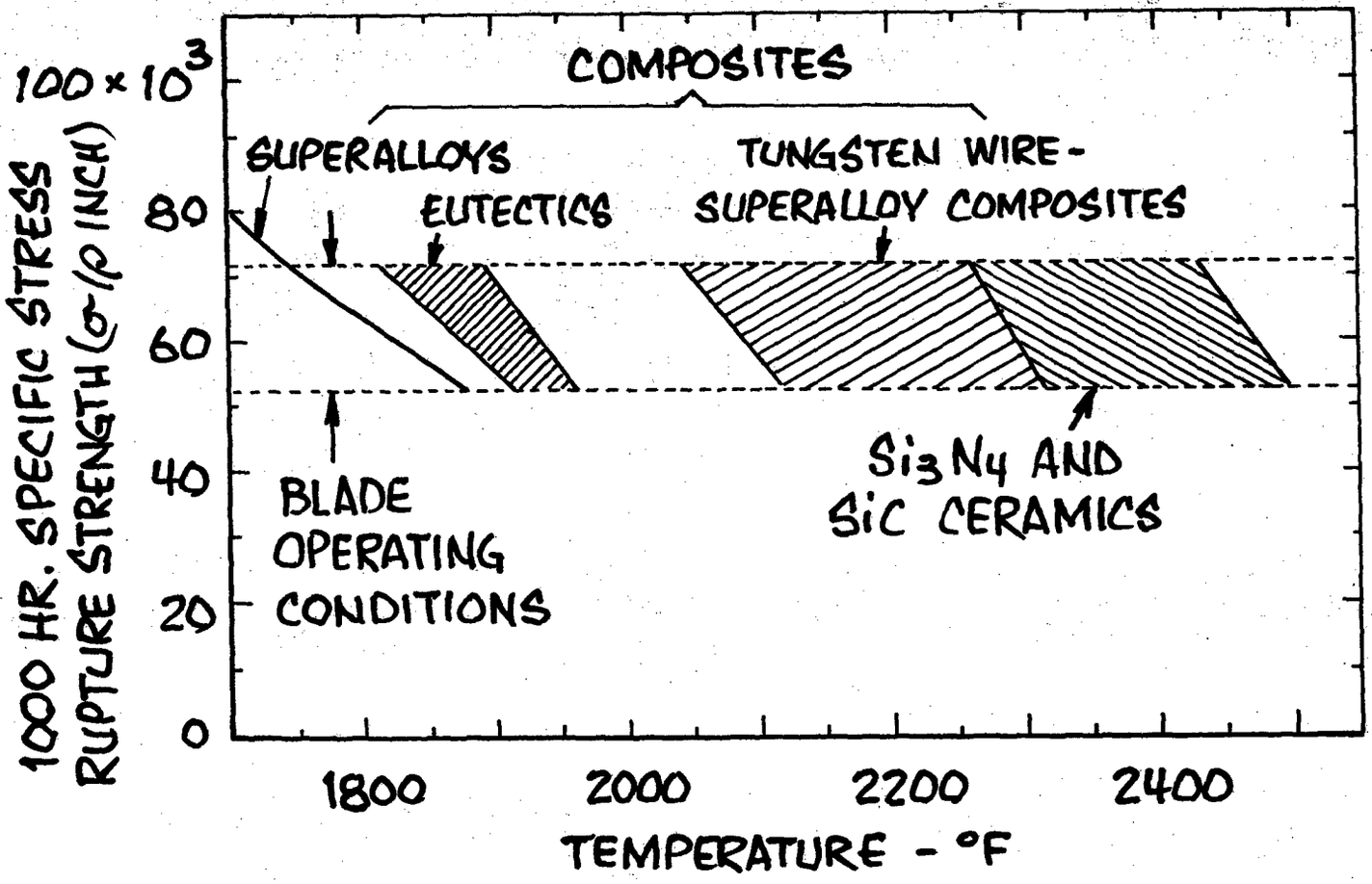

Figure 1. Potential Turbine Blade Use Temperatures for 1000 Hour Life with Various Material Systems.

$$S = \frac{AK_c}{\sqrt{c}} \qquad (1)$$

where $K_c = \sqrt{2\gamma E}$ is called the critical stress intensity factor and is directly related to the magnitude of the stresses in the immediate vicinity of the crack front. It can be seen from this equation that material strength is increased by increasing γ and E, which are material properties related to microstructure, and by reducing crack length, c. Since porosity tends to decrease E, it must be considered a defect along with cracks and their precursors, inclusions (Refs. 12 and 13).

In some materials cracks remain at their initial length until fracture stress is reached; then propagate catastrophically to failure (Ref. 14). In such a case, knowledge of the material properties and the stress field to which the part is to be subjected enables equation (1) to be used to calculate the maximum allowable initial crack size. A nondestructive inspection method is then needed to ensure with a specified reliability at a specified confidence level that no crack exists equal to or greater than this specified maximum crack length.

In other materials, stress levels lower than the fracture stress cause the initial cracks to slowly extend until the critical crack size to satisfy equation (1) is reached for the applied stress; then the crack propagates catastrophically to failure. This phenomena, known as subcritical crack growth (Refs. 15 and 16), causes material strength to be dependent on the time spent under stress. Many materials have been found to follow the relation:

$$V = BK^n \qquad (2)$$

where V is the crack velocity, K is the stress intensity factor and B and n are constants that can be determined for a particular material experimentally (Refs. 17 and 18). For transient conditions, such as thermal stress, experiments must be run to determine strength as a function of stressing rate (Ref. 19). For these materials it is not enough to calculate the maximum allowable initial crack size based on fracture stress. Rather, it is necessary to assume a lifetime for a part and to calculate the maximum initial crack size that would not propagate to critical size in this lifetime, assuming a certain pattern of stresses and stress rates. Since the maximum allowable crack in this case is much smaller than for materials that do not experience subcritical crack growth, a much more sensitive nondestructive evaluation method is required to ensure that a part meets the criteria used in making fracture mechanics calculations. Furthermore, the more sensitive the inspection technique, the longer the lifetime that can be assumed for the part.

The mode of failure for Si_3N_4 and SiC depends on the fabrication method and the operating temperature. Lange (Ref. 20) has shown that, for hot pressed Si_3N_4, fracture at low temperature results from critical stress, with fracture propagating from cracks or inclusions in the 80 to 150 μm range. For the high temperatures of interest for gas turbine applications, however, subcritical crack growth occurs resulting in lower fracture strength than at low temperatures. Terwilliger (Ref. 21) has shown that the same pattern occurs with reaction sintered material when an impurity (5% MgO) is added as an aid to densification. As can be seen from Figure 2, reaction sintered material made without such additives, while lower in strength at low temperatures, maintains its strength at high temperatures. It is concluded from these observations that the impurities added to aid densification lower the viscosity of the glassy phase at the grain boundaries resulting in subcritical crack growth at high temperatures.

In conclusion, it can be seen from the above discussion that the ceramic materials that are eventually used in gas turbine applications may fail either due to application of critical fracture stress or due to subcritical crack growth. In the former case defects on the order of 100 μm must be detected, although detection of smaller defects would certainly be of economic benefit. In the latter case, much smaller defects must be detected, possibly as small as 10 to 25 μm (Ref. 22), in order to ensure that the criteria assumed in fracture mechanics calculations are met. It is therefore necessary to develop a nondestructive evaluation technique capable of detecting defects in the 10 to 100 μm range with a high degree of reliability.

3.2 Material Selection and Procurement

The specimens were selected for this program to cover the range of material types that seem promising for gas turbine applications. The specimens were selected to be a convenient size for C-scan inspection as well as for manufacture and to be a thickness typical of turbine blades. Finally, it was decided that the specimens should be seeded with known defects in order to provide a calibration point for determining the size of other defects detected ultrasonically.

The specimens purchased for this program were 6 x 6-inch (15 x 15 cm) billets, seeded as shown in Figure 3, of the following types:

1. Cerralloy* 146A, hot pressed silicon carbide 0.25 inches (0.064 cm) thick, densified using boron nitride with 1/2 to 1 percent impurities such as calcium, aluminum and iron.

*Ceradyne, Inc., Chatsworth, CA.

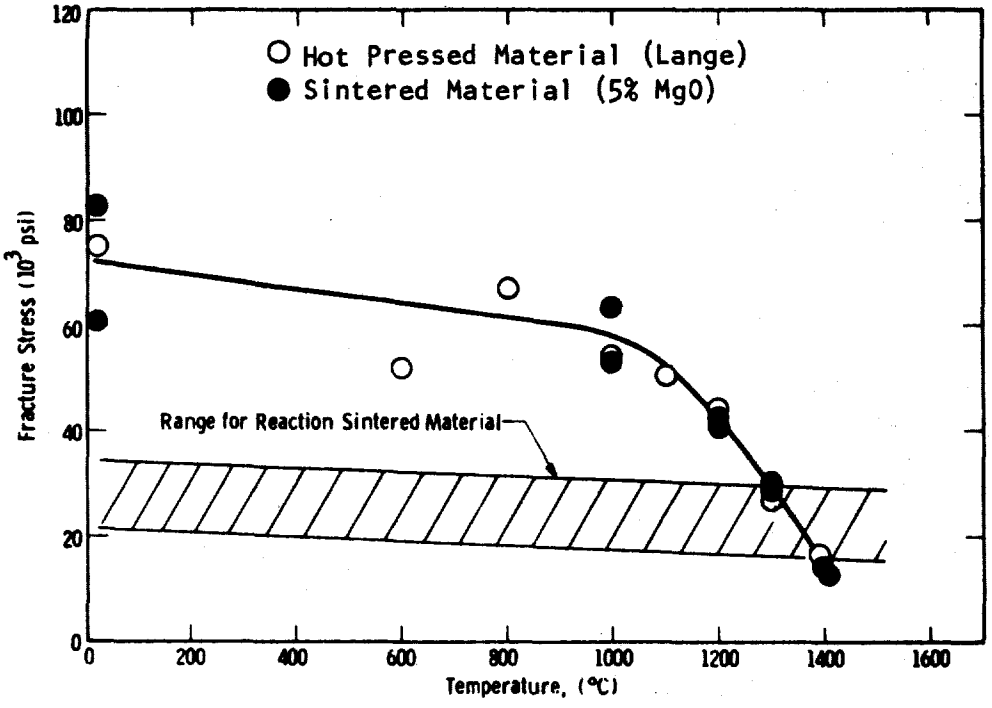

Figure 2. Strengths of Silicon Nitrides (Reference 21).

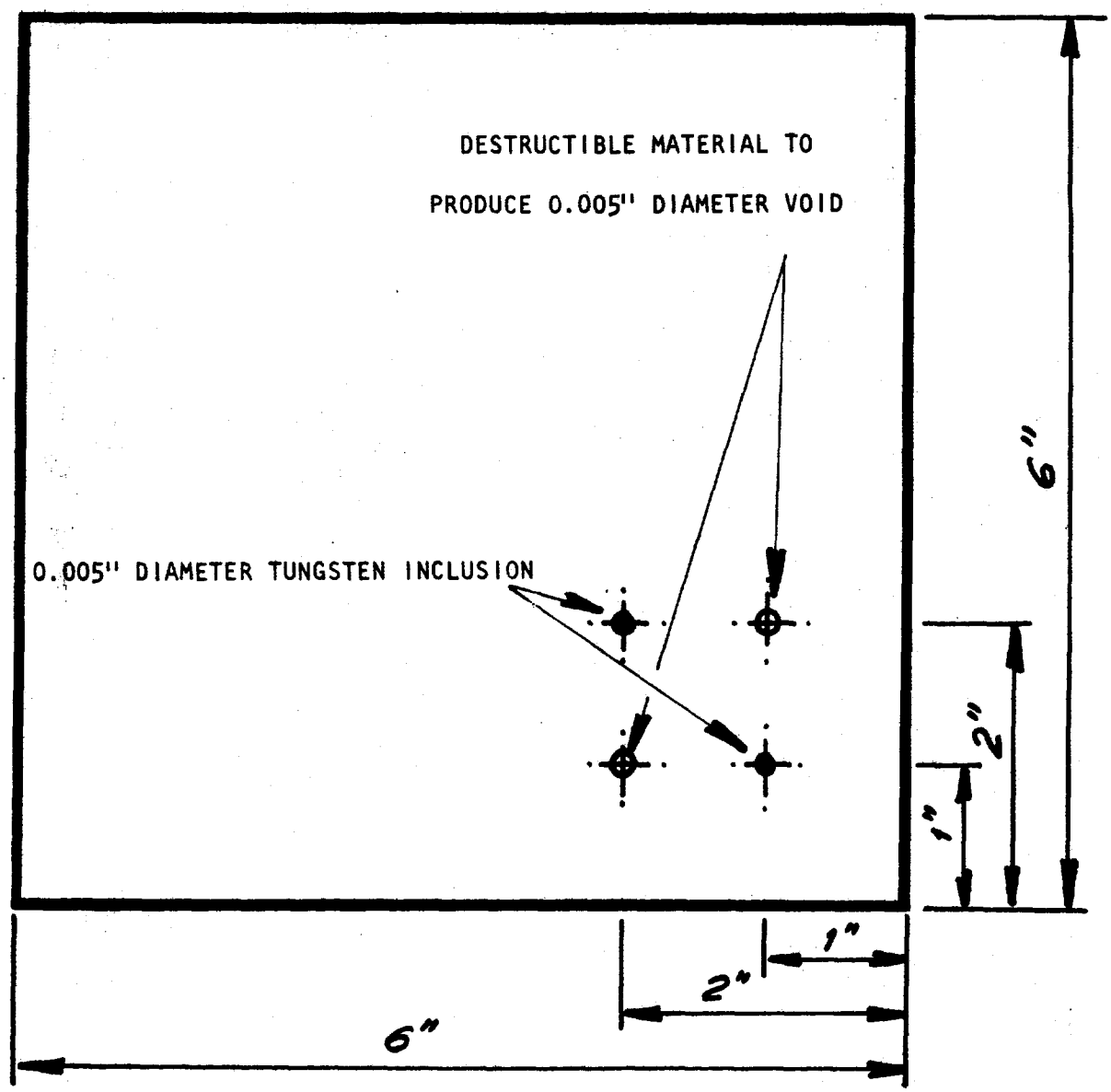

Figure 3. Seeding Scheme for Ceramic Specimens.

2. Cerralloy* 147, hot pressed silicon nitride 0.25 inches (0.64 cm) thick, densified using one percent magnesium oxide with 1/2 to 1 percent impurities such as calcium, aluminum and iron.

3. NC+435, silicon carbide 0.17 inches (0.43 cm) thick, sintered using an additive to achieve 100 percent of theoretical density with fine grain structure (3 μm).

4. NC+350, reaction bonded silicon nitride 0.25 inches (0.64 cm) thick, expected to contain small (<50 μm) well distributed pores.

Each specimen was ground to a 15 to 20 microinch surface finish on the large surfaces. The seeded defects were selected to simulate typical ceramic defects. Voids were used to simulate low density defects such as pores, unreacted silicon and boron nitride. Tungsten carbide particles were used for high density defects because this material may be found in ceramic powders. The 0.005-inch (125 μm) size was chosen because it is the smallest size that could be conveniently handled by the manufacturer. The selection of a source for the hot pressed materials was based primarily on the excellent delivery time offered by Ceradyne.

3.3 Specimen Properties Determination

Before equipment and parameters could be selected for ultrasonic inspection of these specimens, it was necessary to measure some of the material properties. Of particular interest was the density of each material. Since the billets were of a regular rectangular shape, their densities were determined by measuring their dimensions accurately and by weighing them. The results are listed in Table 1.

The densities of the hot pressed materials are comparable to the 3.2 g/cm^3 reported in other studies (Ref. 23). The density of the sintered silicon carbide, assuming 12% unreacted silicon, represents about 2.5% void volume. The density of the reaction bonded silicon nitride is about 69% of theoretical density.

In addition to density measurements, the billet specimens were also evaluated for gross defects by X-radiography. Figures 4, 5, 6 and 7 are X-radiographs of the four billets. Figures 4 and 5 are 2 percent X-radiographs of the sintered silicon carbide and reaction bonded silicon nitride taken by the manufacturer prior to final machining. The mottled appearance of the sintered silicon nitride is due in part to unreacted silicon which was removed from the surface during final machining. Figures 6 and 7 are X-radiographs of the hot pressed silicon nitride taken with a Picker Minishot II on Kodak Type M film at 40 KV and 3mA for 2 minutes at a focal distance of 24 inches. X-radiography was not able to detect the seeded defects in any of these specimens.

+Norton Co., Worcester, MA.

TABLE I

CERAMIC SPECIMEN DENSITIES

Material Type	Bulk Density (g/cm^3)
Sintered Silicon Carbide	2.95
Hot-pressed Silicon Carbide	3.24
Hot-pressed Silicon Nitride	3.17
Reaction Bonded Silicon Nitride	2.20

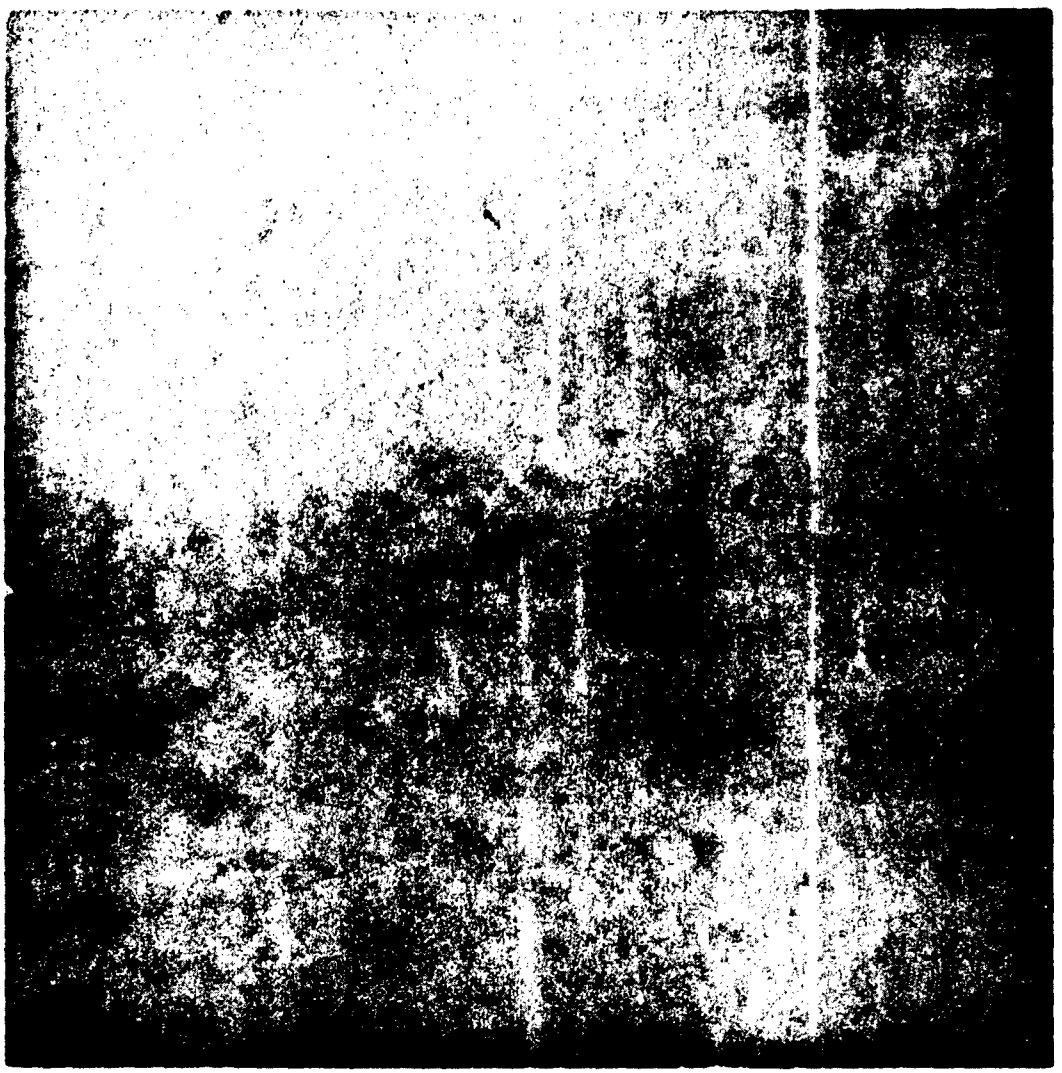

Figure 4. X-Radiograph of NC-435 Sintered Silicon Carbide Billet Before Final Machining.

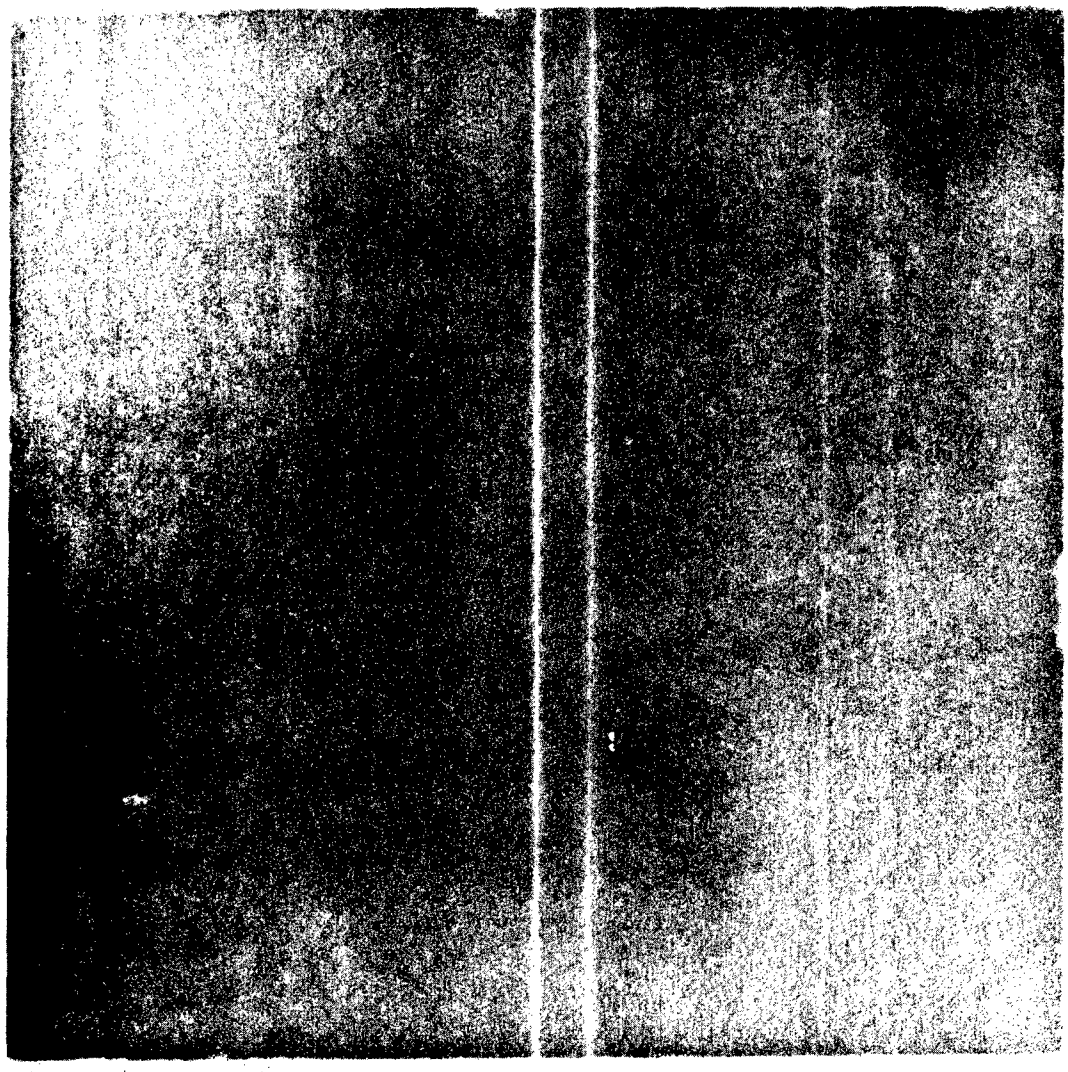

Figure 5. X-Radiograph of NC-350 Reaction Bonded Silicon Nitride Billet Before Final Machining.

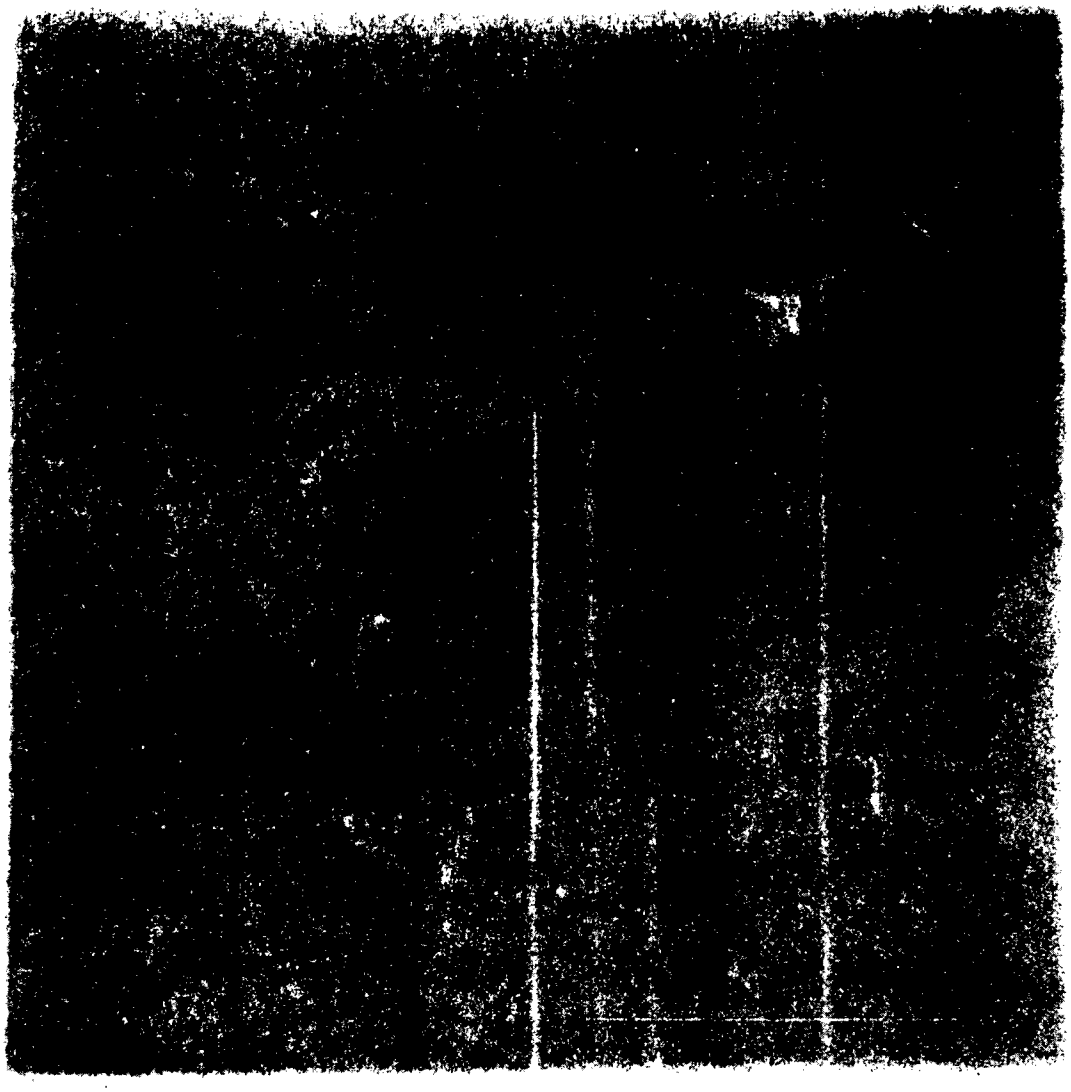

Figure 6. X-Radiograph of Cerralloy 146A Hot Pressed Silicon Carbide Billet.

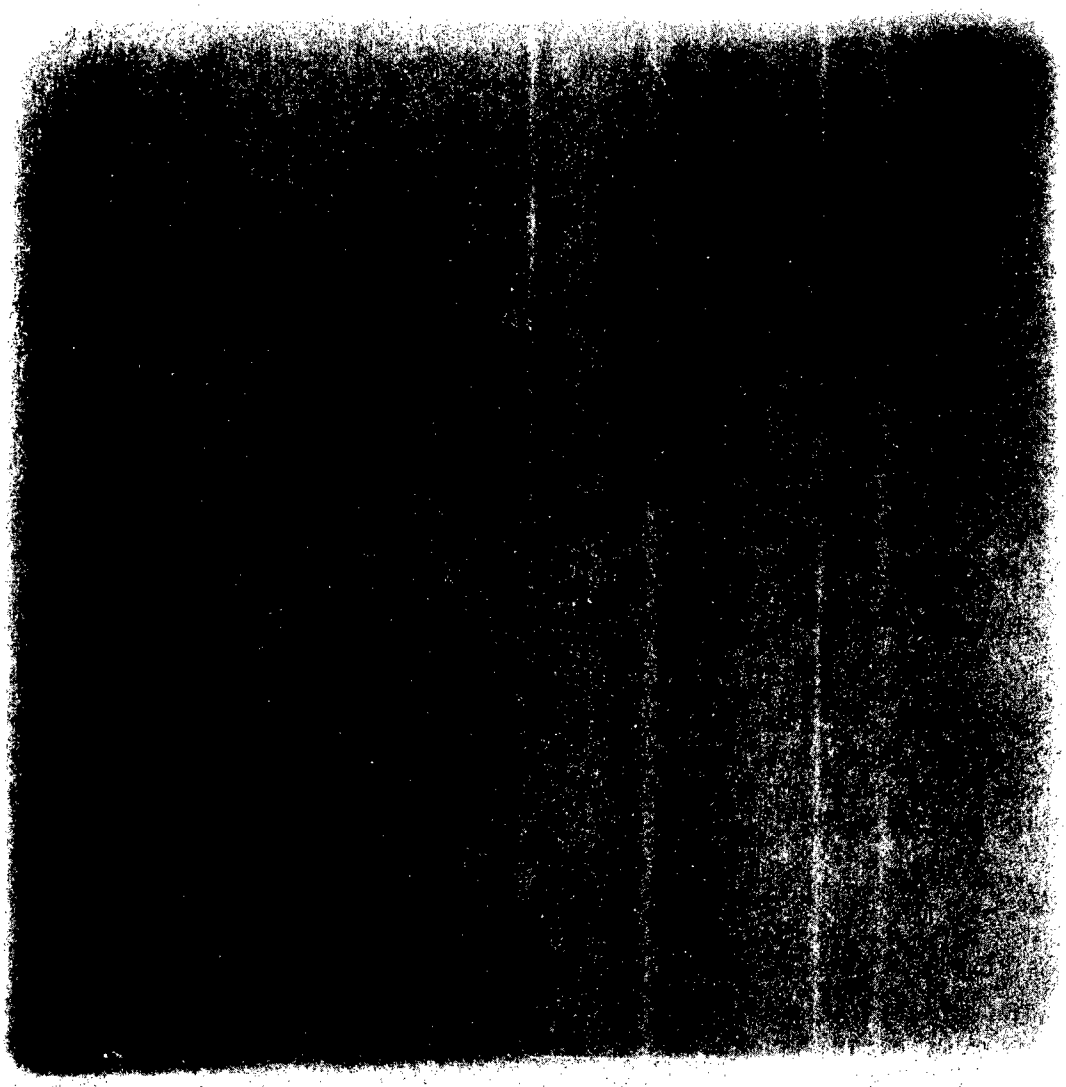

Figure 7. X-Radiograph of Cerralloy 147 Hot Pressed Silicon Nitride Billet.

4.0 NONDESTRUCTIVE EVALUATIONS

4.1 General

A number of nondestructive evaluation methods are available for detection of internal flaws in ceramics. Among these are established techniques, such as ultrasonics, X-radiography, and, to a lesser extent, neutron radiography and those still in developmental stages, such as microwave, infrared and acoustical holography. Evaluation of these techniques for gas turbine ceramics (Ref. 24), however, has shown that the present detection sensitivity of the established techniques is not within the 10 to 100 μm range of interest in this program. Efforts to improve ultrasonic sensitivity by computer enhancement (Ref. 25) have shown the potential for detecting defects down to 60 μm. However, the poor surface resolution of this technique (5 mm) makes it unsuitable for thin sections such as airfoils. In evaluating the potential for further development of the available techniques, it was concluded that high frequency ultrasonics is the most promising technique with the theoretic capability to detect defects in the size range of interest.

The ability of ultrasonic waves to detect a defect depends on several factors. The wavelength, λ, of the ultrasound must be equal or smaller than the flaw dimension, L_d, so that the waves will interact with the flaw. The neighboring particle size (grain structure), L_c, of the media under test must be smaller by a factor of three, or more, than the wavelength in order to avoid undesired acoustic scattering. These two requirements are expressed by the following formula:

$$L_d > \lambda > 3L_c \qquad (3)$$

The acoustic impedance mismatch between the flaw and the material being inspected must be large enough to cause a significant reflection or scattering of energy. For pulse-echo testing the flaw must be oriented so that the signal returns to the transducer. Finally, the attenuation of the material must not be too great, so that sufficient energy reaches the receiving transducer to allow amplification of the defect signal above the level of electronic noise.

In view of formula (3), the probing acoustic wave must be designed for the particular material/defect application in mind. Conventional ultrasonic equipment is primarily designed for inspection of metals, where the relatively coarse grain structure limits the ultrasonic frequency that can be used. The fine grain size in Si_3N_4 and SiC, however, makes it possible to use frequencies higher than those offered by commercial ultrasonic instrumentation, thus making it possible to detect smaller flaws than has generally been the case in metals.

The frequency, f, of a sound wave in a material with acoustic velocity, v, is given by

$$f = \frac{v}{\lambda} \tag{4}$$

where λ is the acoustic wavelength. The ultrasonic frequency, therefore, must be selected based on the acoustic velocity of the particular material under test to give a wavelength at least as small as the defect to be detected, but large enough to avoid interference from grain structure.

4.2 Acoustic Properties Determination

In order to tailor the interrogating ultrasonic energy to be the most suitable to the material/defect relationship described in Section 4.1, it was necessary to determine certain acoustic properties of the ceramic materials. Accordingly, acoustic velocity impedance and insertion loss measurements were carried out on the billet specimens.

Figure 8 is the diagram of a typical A-scan display used to measure the acoustic velocity. A large reflection is received from the front surface of the material followed by a diminishing series of reverberation reflections from the surfaces. The time between any two successive echoes is the time required for the waves to travel through the material and back. Therefore, the velocity is equal to twice the material thickness divided by the elapsed time between successive pulses. Since the acoustic velocity is independent of frequency for a given material, the velocity was measured only at 10 megahertz (MHz). This frequency was selected because it is high enough to allow resolution of the pulses from the front and back surfaces of these relatively thin materials and yet low enough so that numerous multiple reflections of the back surface can be seen, thereby increasing the accuracy of the measurement.

The acoustic impedance, Z, of a material is given by

$$Z = \rho v \tag{5}$$

where ρ is the material density and v is the acoustic velocity. The density of each specimen was determined by direct measurement of the specimen dimensions and weight. This along with the acoustic velocity was used to calculate the acoustic impedance.

The attenuation of the acoustic beam during immersion inspection of a material is the result of reflections at the material to couplant (usually water) interfaces, attenuation in the material and divergence of the acoustic beam to a diameter larger than the receiving transducer. The latter depends on the divergence (or convergence) of the beam from the transucer, the geometry of the part being inspected and the acoustic impedance mismatch between the material and the couplant. While it is difficult to separate

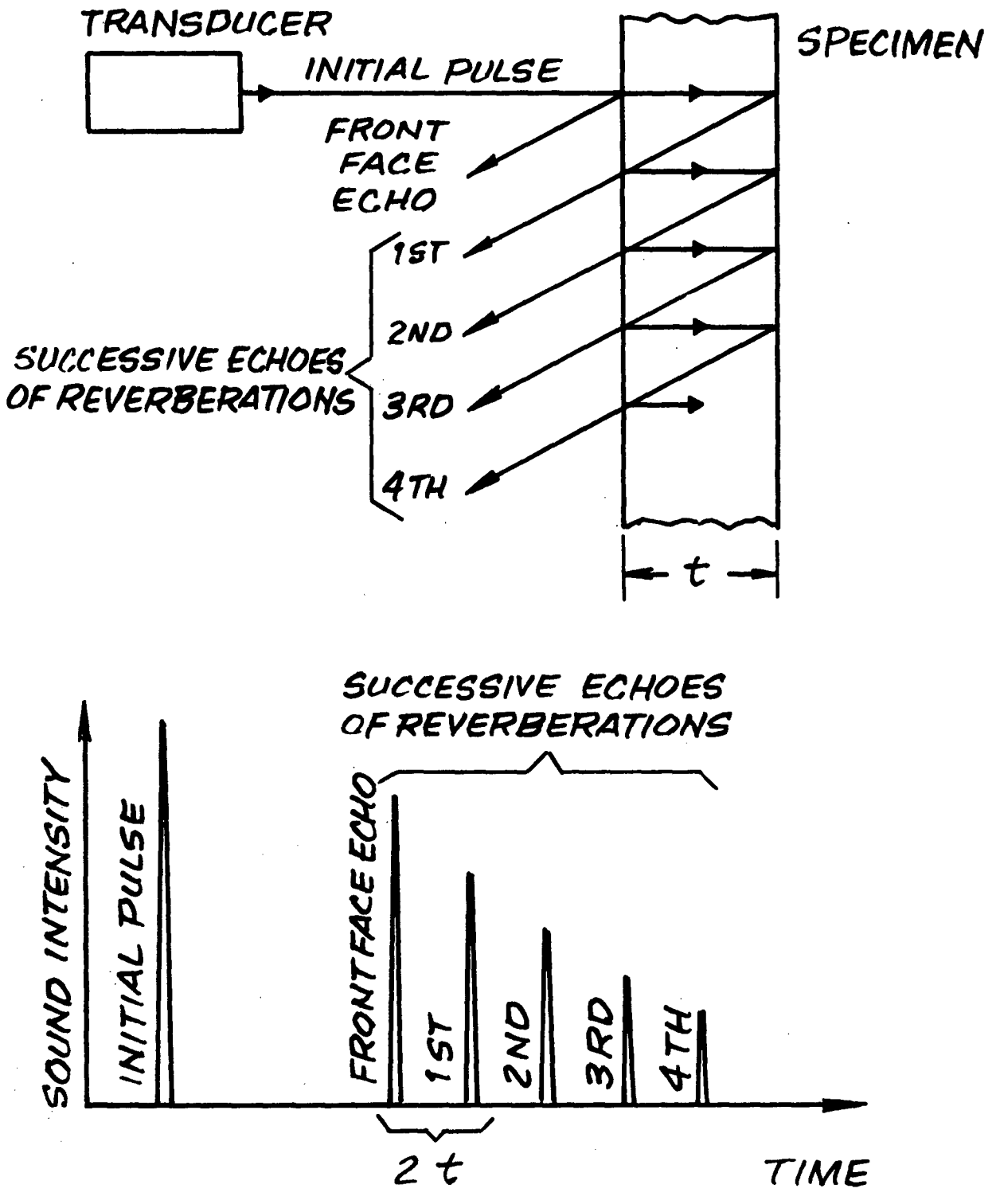

Figure 8. Symbolic Representation of Sound Propagation in Specimen and Time Domain (A-Scan) Presentation of Sonic Reverberations.

the effects of these factors, for the purposes of this program it is not necessary to do so. The total signal loss caused by the material as a function of frequency is the primary factor of interest. This was measured by the arrangement shown in Figure 9. Two transducers were placed a fixed distance apart and the voltage, V_1, at the receiver was measured. The specimen was then placed between the transucers and the voltage, V_2, at the receiver was again measured. One minus the ratio of these two voltages is the insertion loss caused by the material.

In order to evaluate the uniformity of the acoustic properties, each of the specimens was divided up into twenty-five one-inch square cells. The thickness, acoustic transit time and acoustic insertion loss were measured at the center of each cell. The insertion loss was measured at 1, 5, 10, 15, 25 and 45 MHz. All acoustic properties data are shown in Table II.

The acoustic velocities measured were quite high, about a factor of two higher than for common metals in all but one ceramic material. The density measured for the reaction bonded silicon nitride indicates a 31 percent void volume. This, it is believed, in turn caused an acoustic velocity that is much lower, about equivalent to metals. The density and velocity values for the silicon nitride are in excellent agreement with the work of McLean, et al (Ref. 26), who showed that the sonic velocity is directly proportional to the density of silicon nitride over the density range 2.2 to 3.2 g/cm^3.

The acoustic velocity was not found to vary significantly in any of the materials except the reaction bonded silicon nitride. In this material the velocity varied from 5910 to 6545 m/s. Based on the velocity to density relationship mentioned above, this is a density variation from 2.14 to 2.30 g/cm^3. The acoustic impedances fall within the range of values found for metals. The value for reaction bonded silicon nitride is similar to that for titanium or aluminum, while the values for the other materials are higher, but below those of steels or nickel base alloys. The insertion loss did not vary appreciably from one point to another on any of the specimens, except the reaction bonded silicon nitride. Figure 10 is a plot of the average insertion loss versus transducer resonant frequency for all four specimens. This data has been normalized for specimen thickness. It should be emphasized that the insertion loss depends on many factors other than frequency. Also, as will be discussed in more detail in Appendix 8.1, the 25 and 45 MHz transducers put out a broad range of frequencies the most predominant of which is not necessarily the resonant frequency. This data was obtained to determine a first estimate of the difficulty of passing sound through the material. The lower insertion loss for the reaction bonded silicon nitride is due to less reflection at the water/ceramic interface due to the lower acoustic impedance of this material.

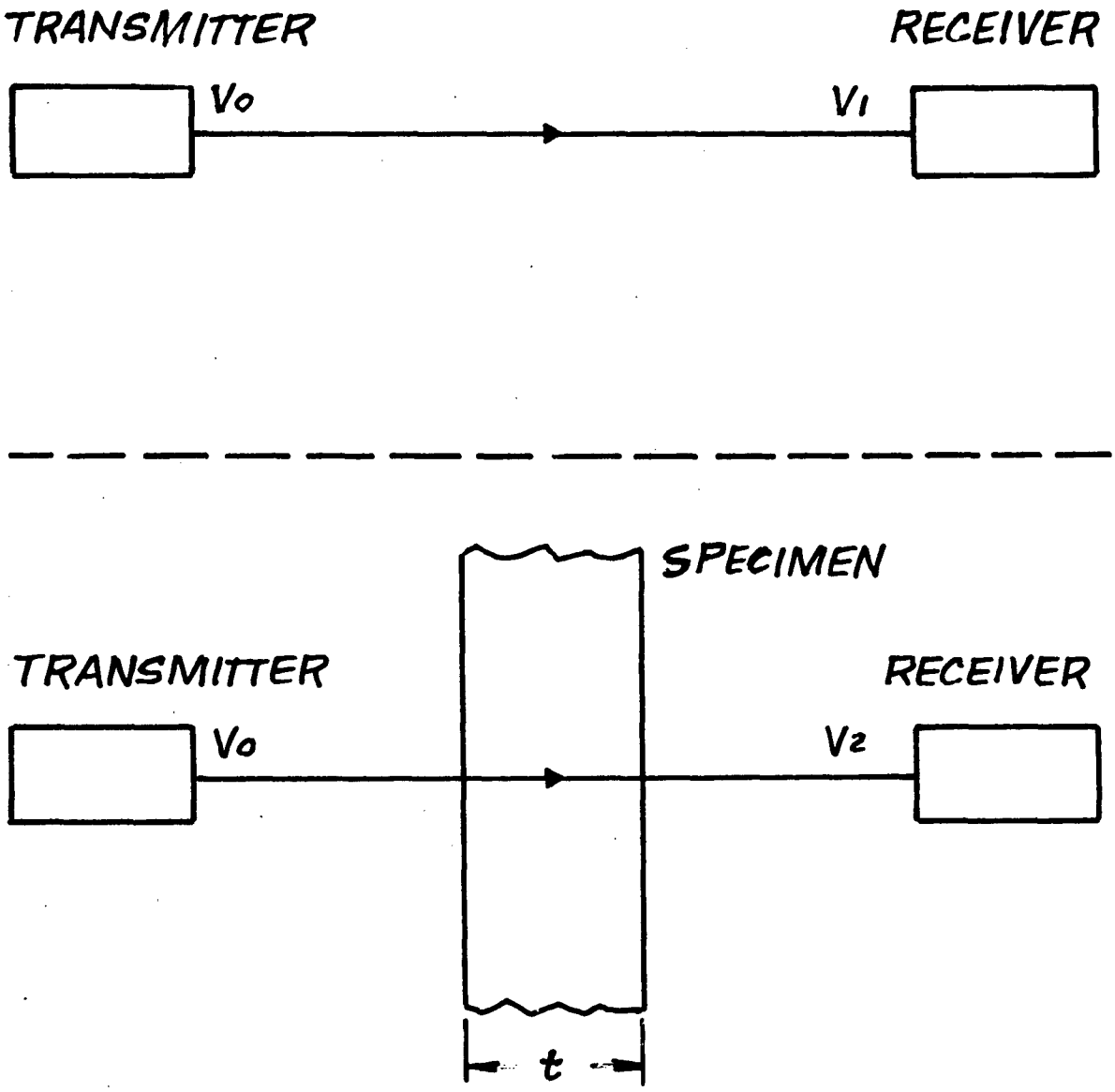

Figure 9. Block Diagram of Through-Transmission Technique to Measure Insertion Loss.

TABLE II

ACOUSTIC PROPERTIES OF CERAMIC SPECIMENS

Material Type	Velocity (m/s)	Impedance ($\times 10^6$ g/cm^{2}s)	Insertion Loss at Frequency in MHz					
			1	5	10	15	25	45
Sintered Silicon Carbide	10,670	3.15	0.817	0.887	0.883	0.892	0.922	0.903
Hot-pressed Silicon Carbide	12,250	3.40	0.841	0.863	0.859	0.881	0.952	0.939
Hot-pressed Silicon Nitride	10,500	3.88	0.856	0.846	0.840	0.875	0.938	0.932
Reaction Bonded Silicon Nitride	6,142	1.35	0.698	0.855	0.803	0.781	0.841	0.840

NOTES: 1. All data tabulated are average values of 25 discrete measurements.

2. Acoustic insertion loss data are dimensionless, and are related to corresponding material thickness of 0.427, 0.643, 0.640 and 0.6216 cm, respecitvely.

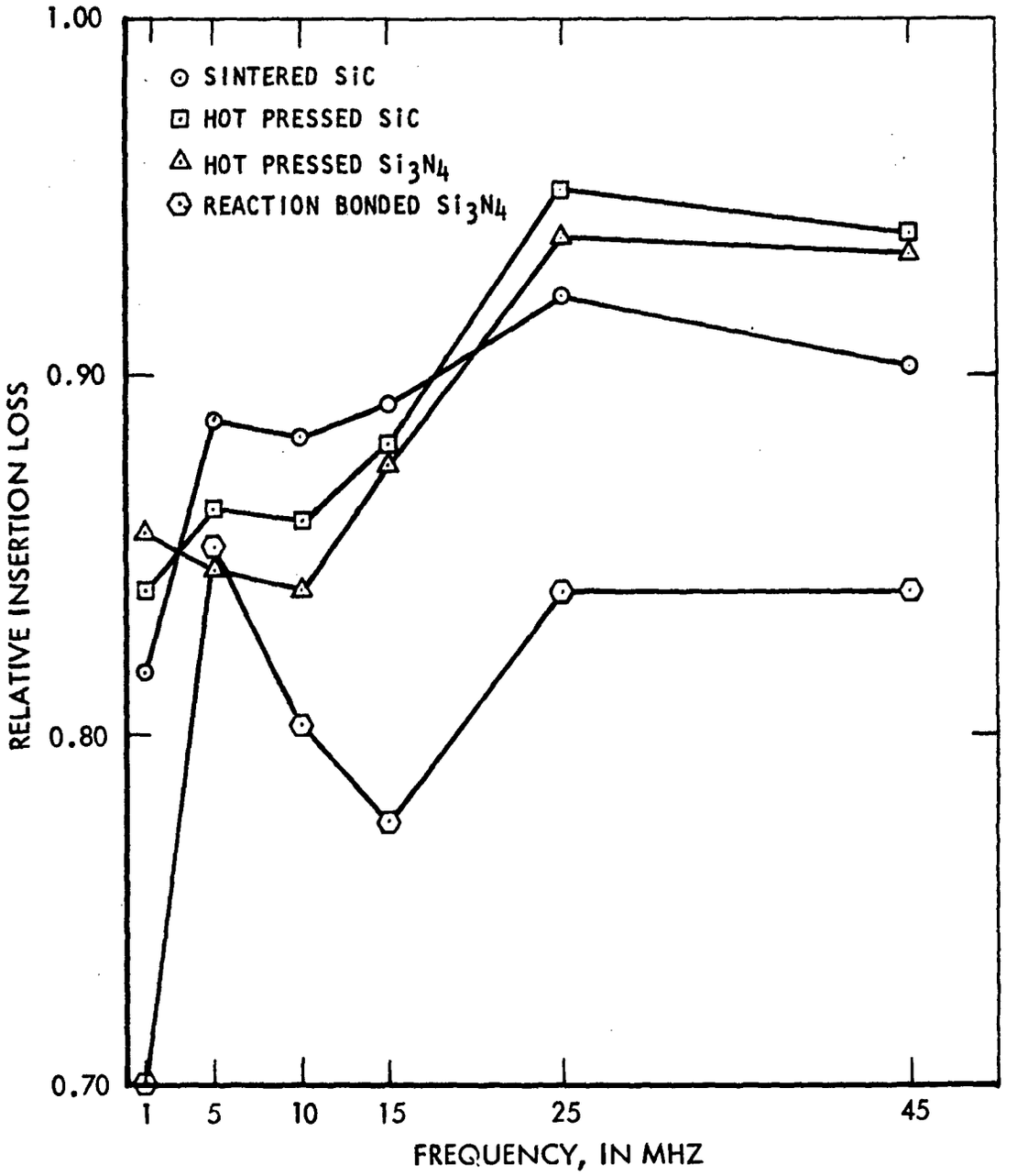

Figure 10. Graph of Relative Insertion Loss Versus Transducer Resonant Frequency for Four Ceramic Materials.

4.3 Conventional Ultrasonic Inspection

The initial inspections of the ceramic materials were conducted using conventional techniques to establish baseline data and to assist in establishment of the final inspection procedure. These inspections were performed at a frequency of 15 MHz, using a Sperry UM 700 ultrasonic instrument with a UFN pulser/receiver unit and a 1/4 inch diameter focused transducer. When no defects were found on either part using the conventional pulse-echo technique, a loss of back-surface-reflection technique was used. This latter technique is similar in concept to through-transmission inspection, but uses only one transducer. The defect gate was set to detect a drop in the reflection from the back surface of the part due to scattering of the beam at a defect. Figures 11, 12 and 13 show C-scan recordings made using this technique on the hot pressed silicon carbide, hot pressed silicon nitride and on the sintered silicon carbide materials, respectively. The reaction bonded silicon nitride specimen was received too late in the program to be inspected by this technique. This conventional ultrasonic technique did not show a defect in the hot pressed silicon carbide (Figure 11) even when the sensitivity was adjusted to gate on the surface texture of the part. Figure 12, however, shows several of the larger defects in the hot pressed silicon nitride that were detected by the pulse-echo technique at higher frequencies. In this case a defect indication is a light spot outlined by dark indications caused by scattering at the defect edges. Figure 13 shows a considerable number of indications scattered throughout the sintered silicon carbide. It should be noted that the darkening at the corners of the specimens is a result of a slight taper at the corners. The dark indentations on the sides are the grips used to hold the specimens during C-scan.

As a result of these conventional ultrasonic inspections, as well as the material properties determinations, the need was identified to reinspect the materials using both instrumentation and transducers of higher frequencies. It was also determined that longer focal length transducers were needed to compensate for the high acoustic velocities of these materials.

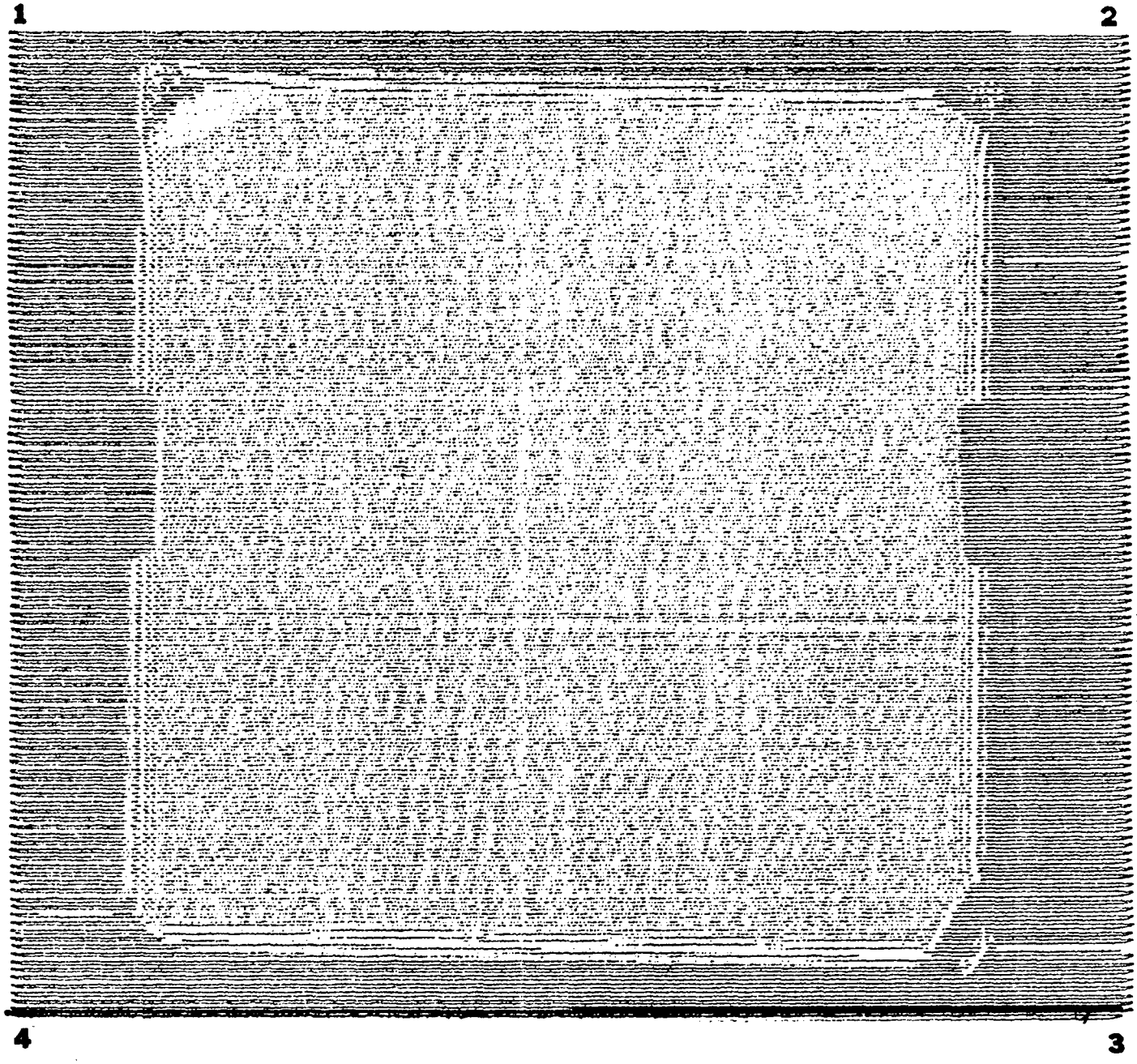

Figure 11. C-Scan Recording of Hot-Pressed Silicon Carbide Specimen Using Loss-of-Back-Reflection Method at a Frequency of 15 MHz.

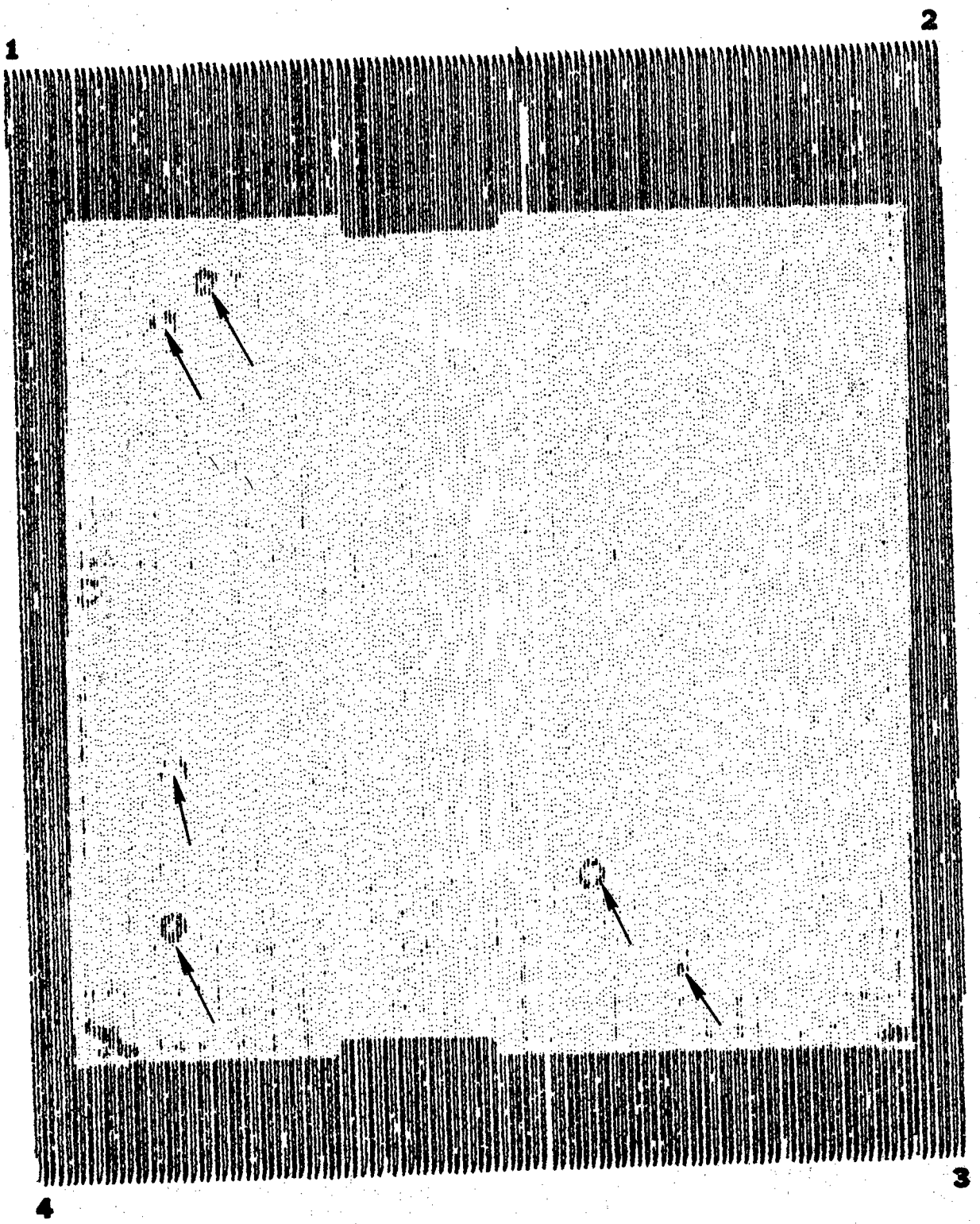

Figure 12. C-Scan Recording of Hot-Pressed Silicon Nitride Specimen Using Loss-of-Back-Reflection Method at a Frequency of 15 MHz.

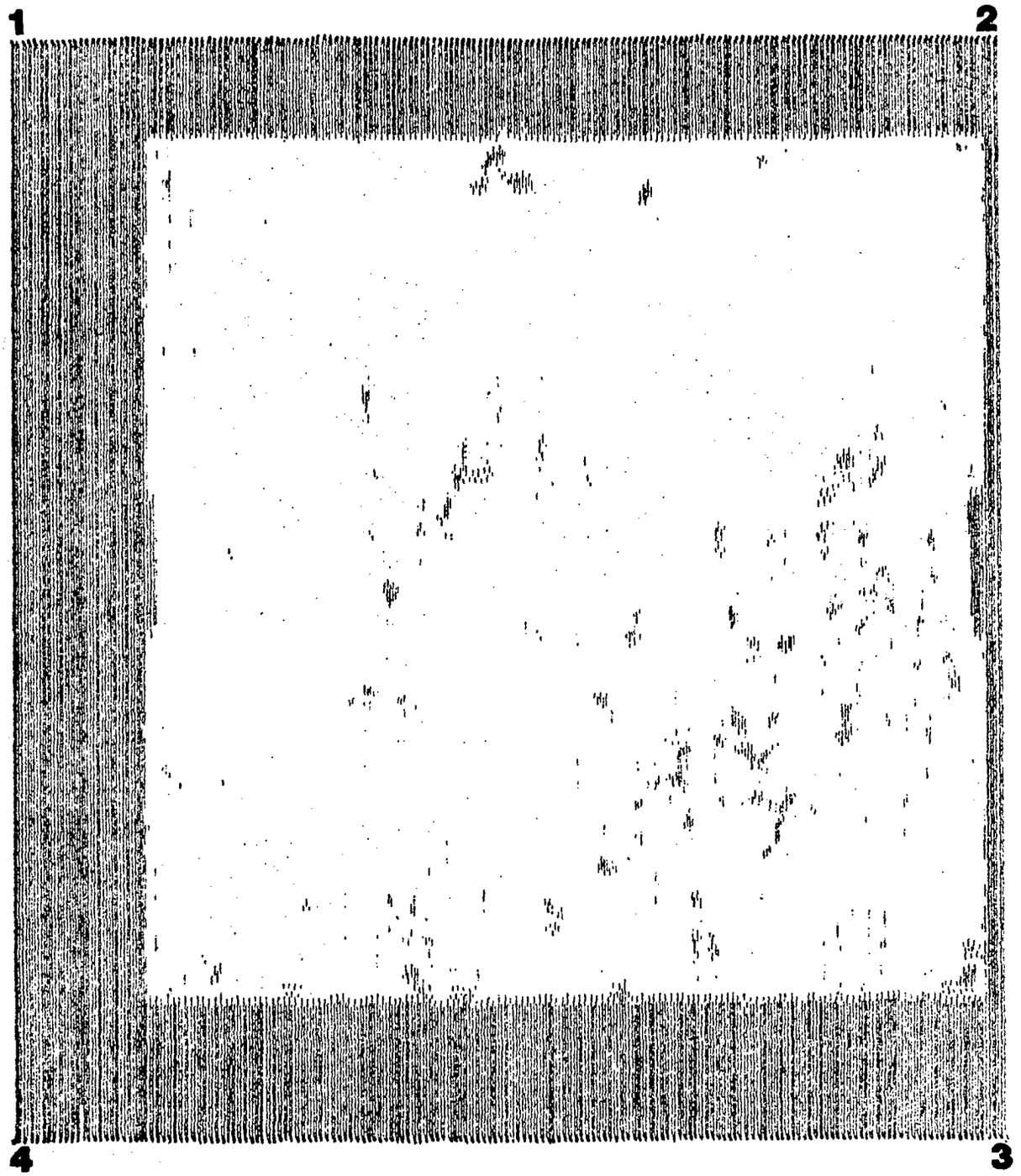

Figure 13. C-Scan Recording of Sintered Silicon Carbide Specimen Using Loss-of-Back-Reflection Method at a Frequency of 15 MHz.

5.0 HIGH-FREQUENCY ULTRASONIC EVALUATIONS

Using high frequencies to inspect the ceramic materials required some developmental efforts in both instrumentation modifications and new transducer procurements. These efforts are discussed in Section 8.0, Appendices.

5.1 Initial Inspection

Initial high frequency inspections were made of all four ceramic specimens using the pulse-echo technique with two newly acquired 25 and 45 MHz transducers and employing an Erdman Model 1177B pulser/receiver. C-scan recordings of these inspections are shown in Figures 14 through 17, at 25 MHz, and Figures 18 through 23 at 45 MHz. No C-scan recording is included of the hot pressed silicon carbide at 25 MHz because the result was the same as at 45 MHz (Figure 21). No defects were detected.

The C-scan recording of sintered silicon carbide shows extensive areas of indications at 25 MHz (Figure 14) and even more at 45 MHz (Figure 18). However, Figure 19 made at a different focal plane, shows only a few scattered indications. This result indicates that the indications result from clusters of small defects isolated in one plane in the material so that they only are detected when the transducer is focused close to this plane.

The C-scan recordings of reaction bonded silicon nitride show extensive indications throughout the part at 25 MHz (Figure 15) and even more indications at 45 MHz (Figure 20). Figure 16 was made at 25 MHz at reduced sensitivity in order to identify any particularly bad areas. The fact that the side of the specimen that shows fewer indications (side 1, 2) also shows higher acoustic velocity and, therefore, higher density, tends to substantiate the theory that these indications are caused by the porosity in this material.

Figure 17, a C-scan recording of the hot pressed silicon nitride at 25 MHz, shows several of the same large defects that were detected at 15 MHz by the loss-of-back-reflection method. Figures 22 and 23 are of the same part at 45 MHz at two different focal planes, one-third and two-thirds of the specimen thickness below the top surface of the specimen, respectively. The defects labeled A are those previously detected. Those labeled D are defects first detected in Figure 22. The indication labeled C is caused by a chip in the top surface of the part. The indications labeled E in Figure 23 are defects that did not appear in the previous recordings.

A number of conclusions were drawn from these initial high frequency inspections:

1. It was confirmed that increasing the inspection frequency improves defect detectability,

2. The need was identified to inspect at several different focal planes in order to obtain complete coverage of the part.

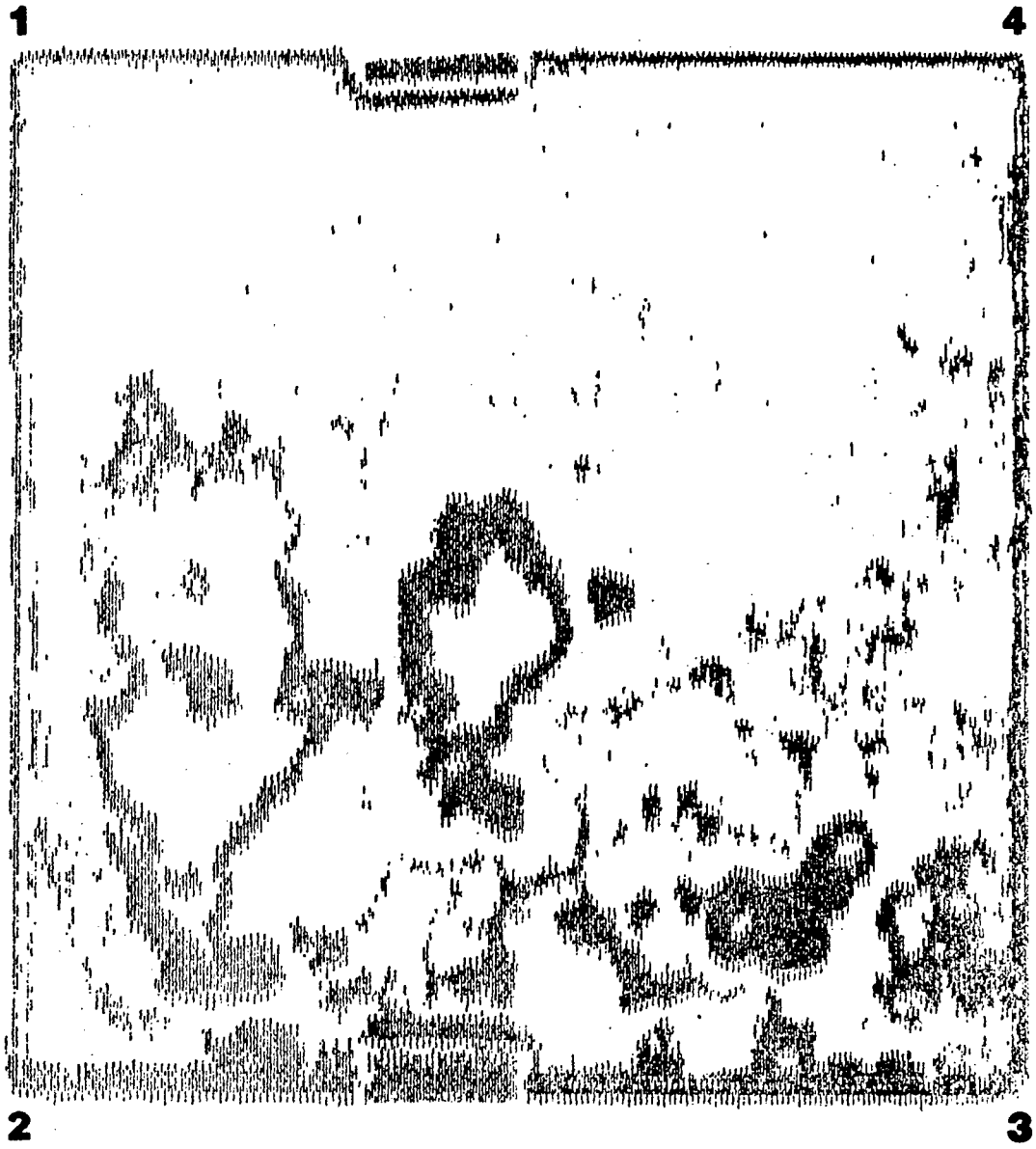

Figure 14. C-Scan Recording of Sintered Silicon Carbide Specimen Using Pulse-Echo Method at a Frequency of 25 MHz.

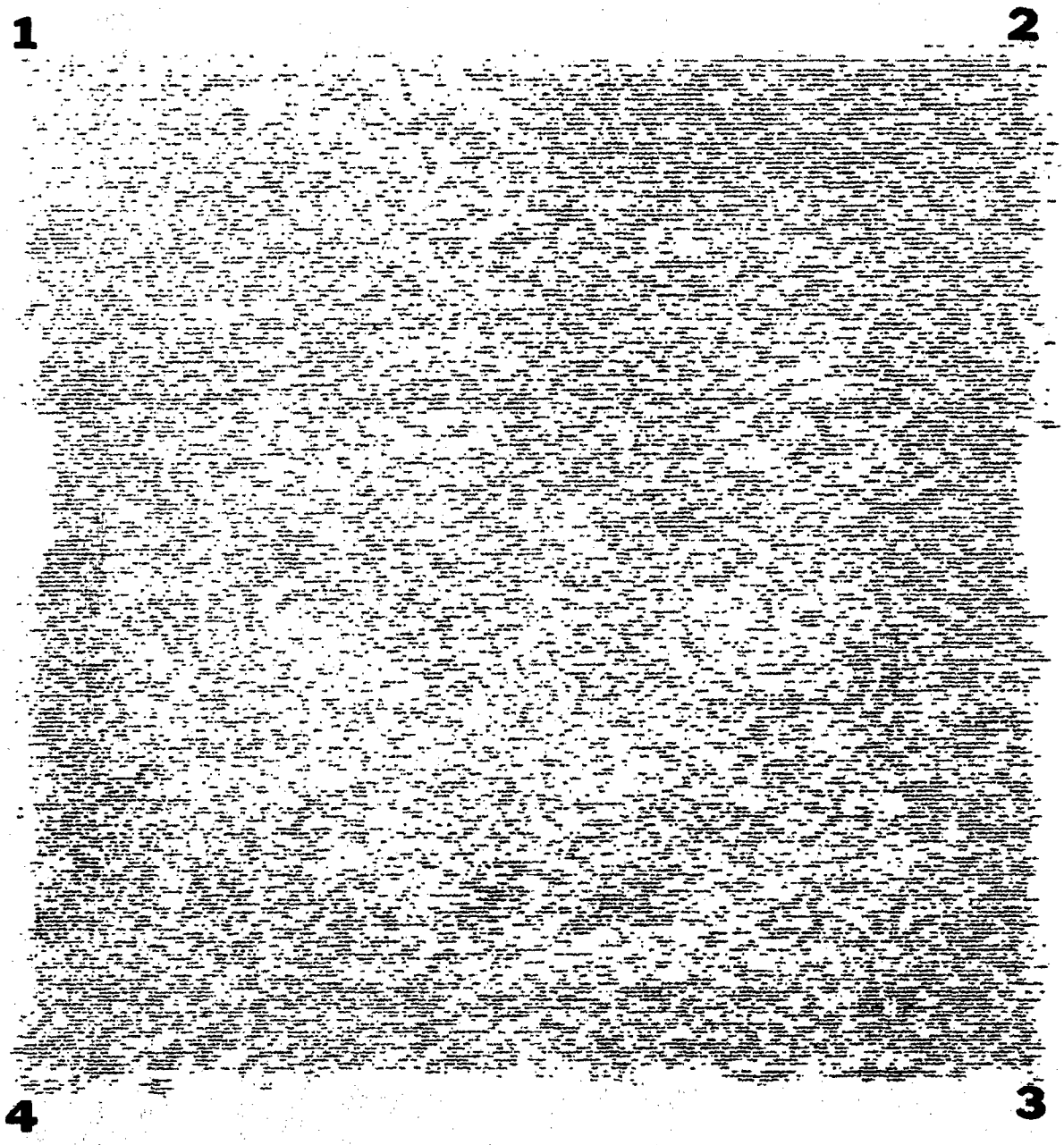

Figure 15. C-Scan Recording of Reaction Bonded Silicon Nitride Specimen Using High Sensitivity Pulse-Echo Method at a Frequency of 25 MHz.

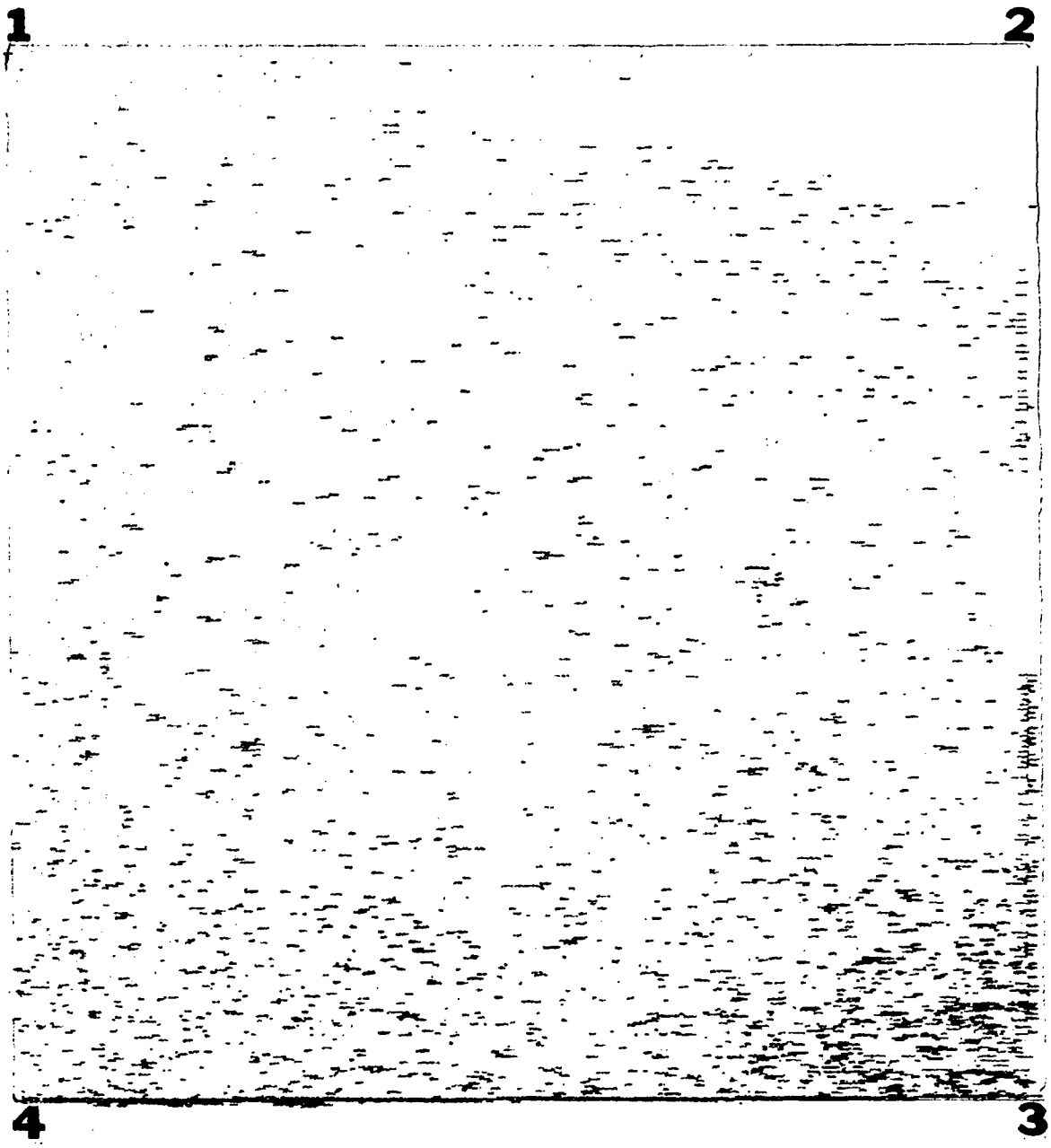

Figure 16. C-Scan Recording of Reaction Bonded Silicon Nitride Specimen Using Low Sensitivity Pulse-Echo Method at a Frequency of 25 MHz.

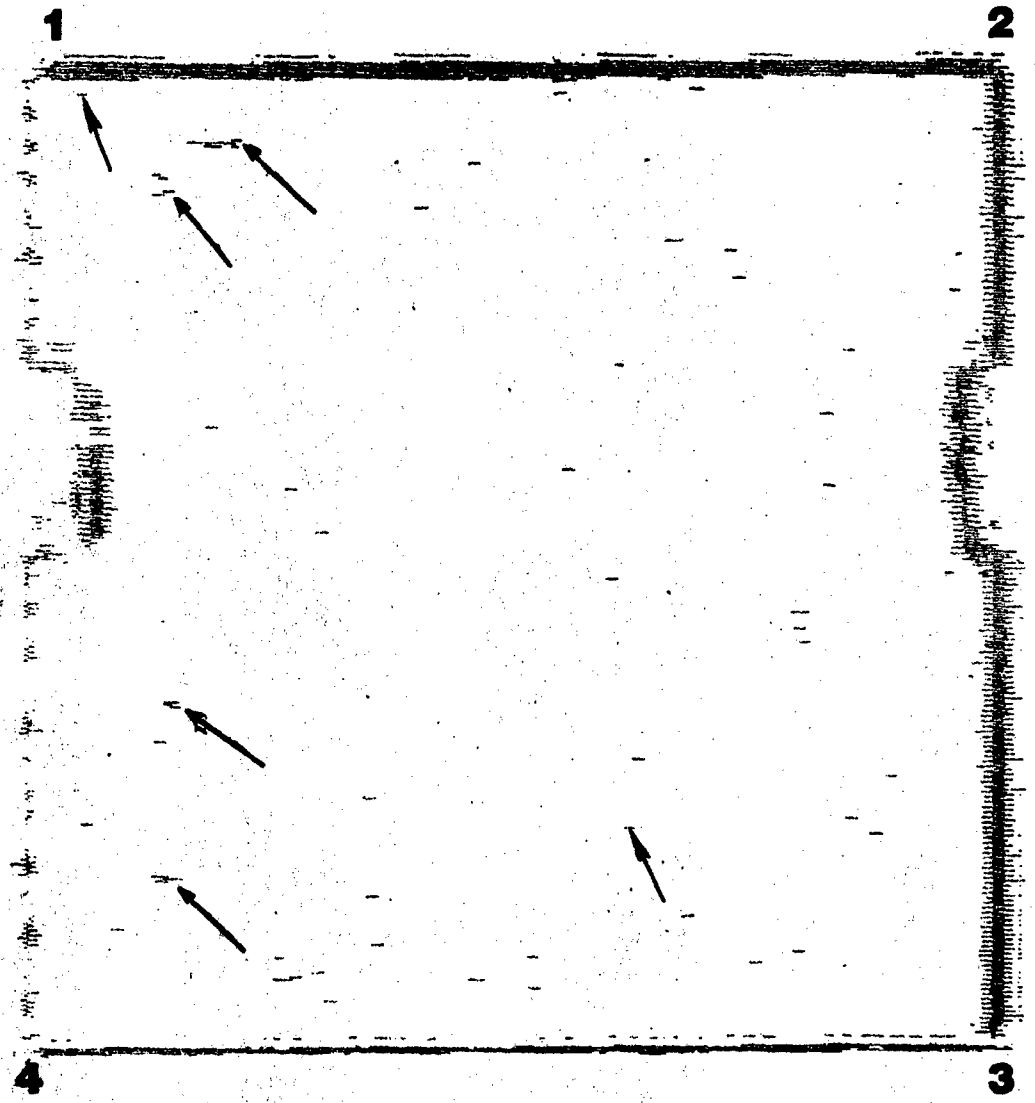

Figure 17. C-Scan Recording of Hot Pressed Silicon Nitride Specimen Using Pulse-Echo Method at a Frequency of 25 MHz.

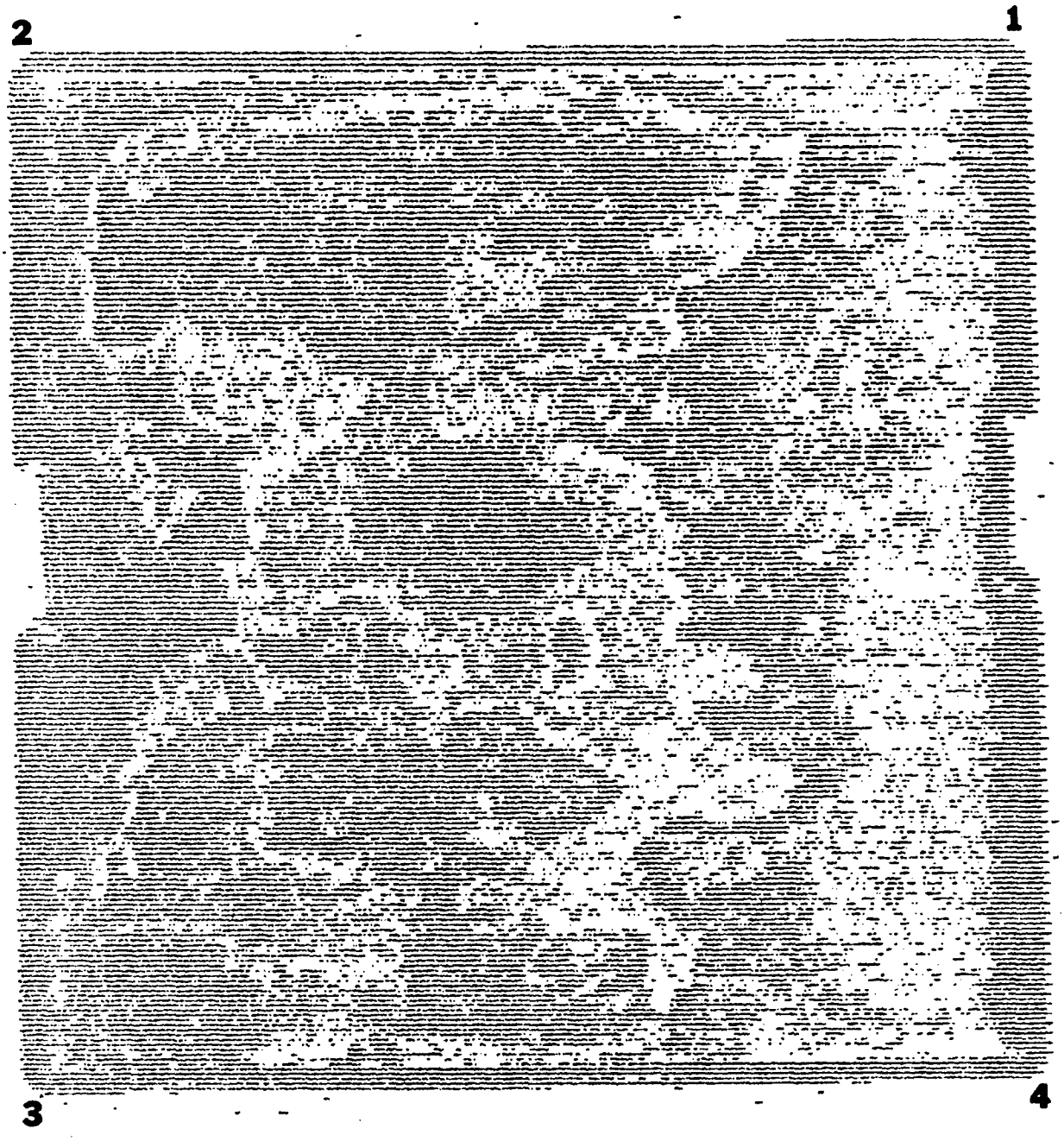

Figure 18. C-Scan Recording of Sintered Silicon Carbide Specimen Using High Sensitivity Pulse-Echo Method at a Frequency of 45 MHz with the Transducer Focal Point Two-Thirds of the Specimen Thickness Below the Top Surface.

Figure 19. C-Scan Recording of Sintered Silicon Carbide Specimen Using High Sensitivity Pulse-Echo Method at a Frequency of 45 MHz with the Transducer Focal Point One-Third of the Specimen Thickness Below the Top Surface.

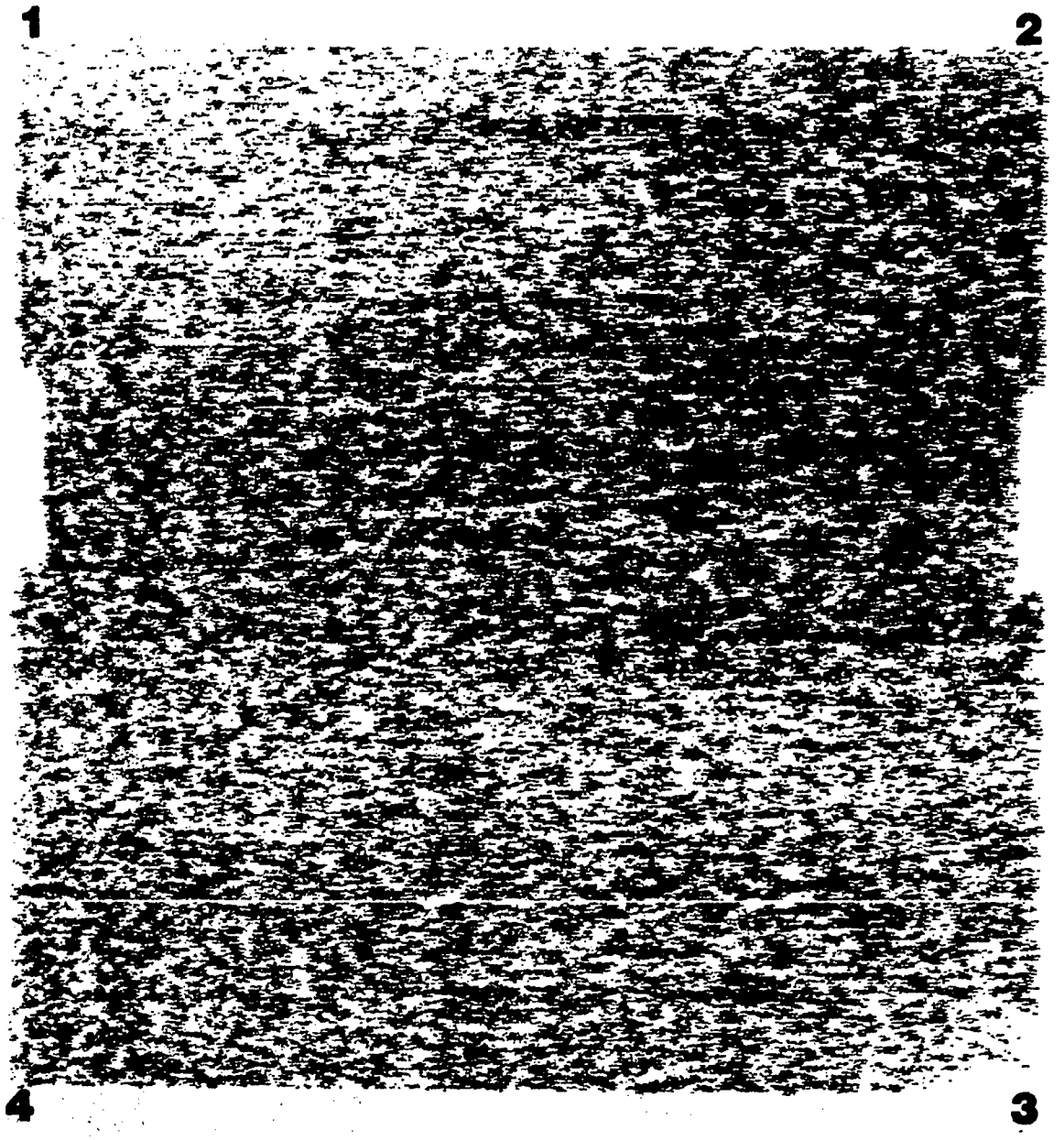

Figure 20. C-Scan Recording of Reaction Bonded Silicon Nitride Specimen Using High Sensitivity Pulse-Echo Method at a Frequency of 45 MHz.

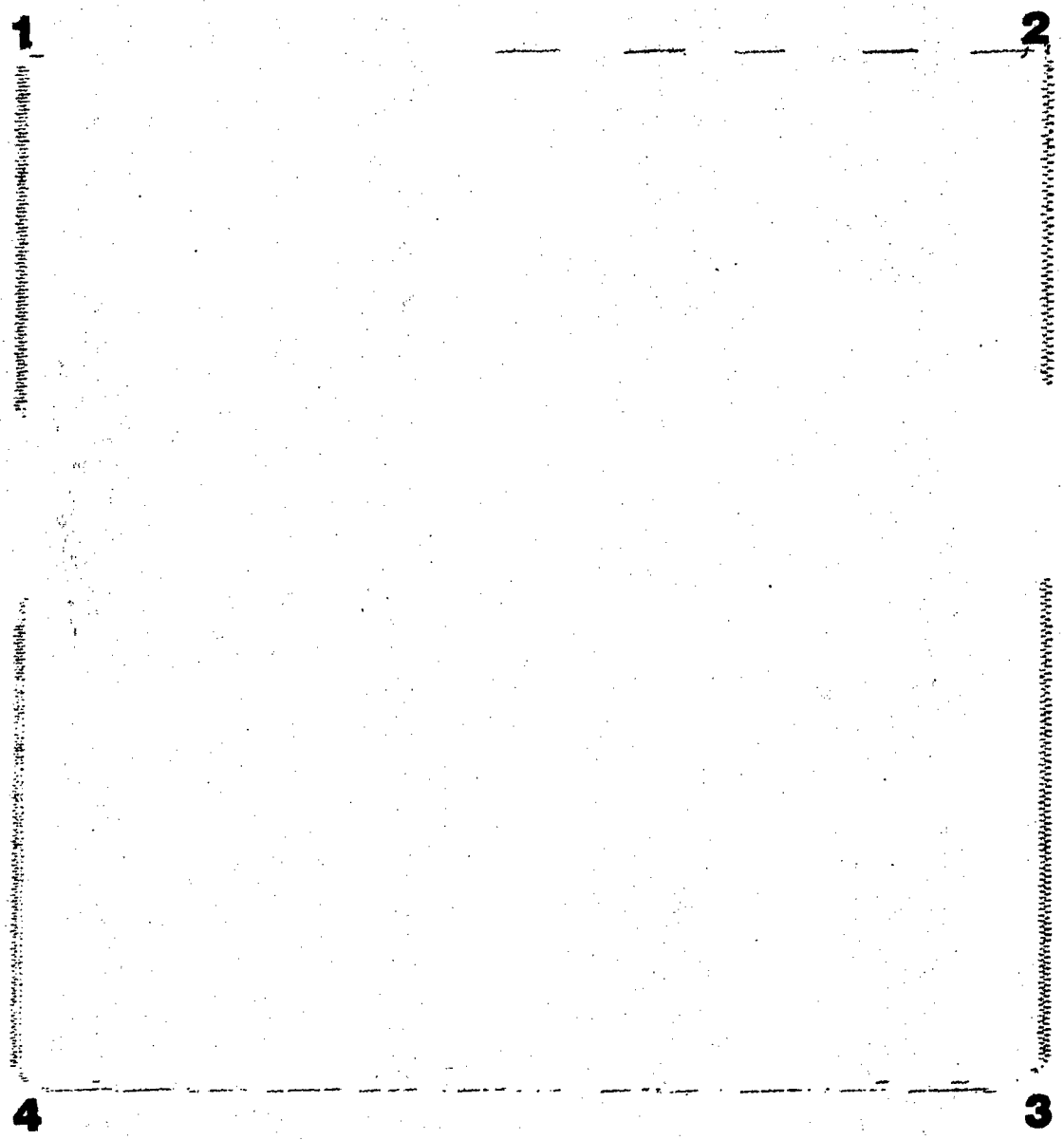

Figure 21. C-Scan Recording of Hot Pressed Silicon Carbide Specimen Using High Sensitivity Pulse-Echo Method at a Frequency of 45 MHz.

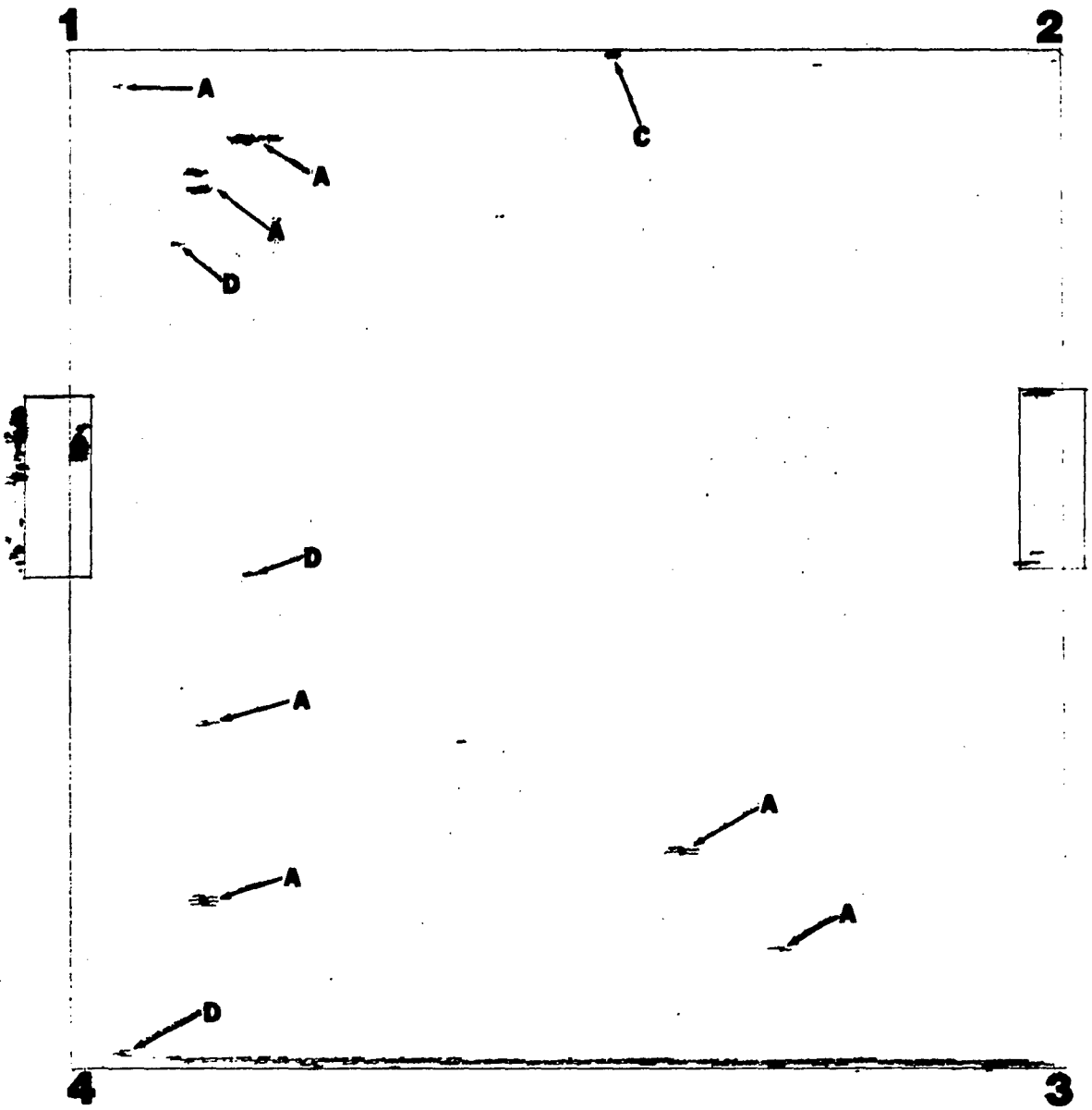

Figure 22. C-Scan Recording of Hot Pressed Silicon Nitride Specimen Using High Sensitivity Pulse-Echo Method at a Frequency of 45 MHz with the Transducer Focal Point One-Third of the Specimen Thickness Below the Top Surface.

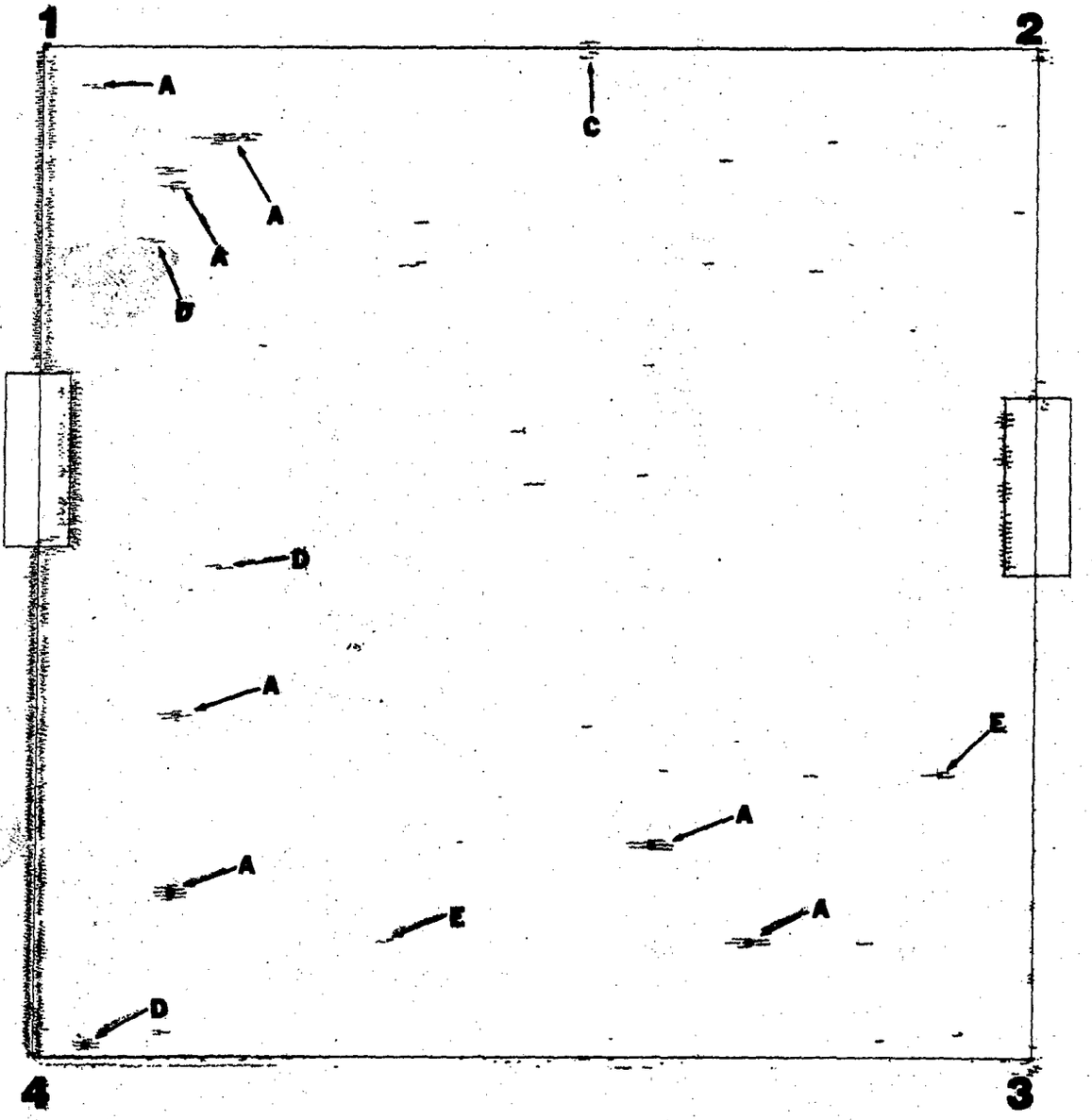

Figure 23. C-Scan Recording of Hot Pressed Silicon Nitride Specimen Using High Sensitivity Pulse-Echo Method at a Frequency of 45 MHz with the Transducer Focal Point Two-Thirds of the Specimen Thickness Below the Top Surface.

7788-c

3. It was shown that specimens of reaction bonded silicon nitride and sintered silicon carbide are not suitable for higher sensitivity inspections because they already give practically continous indications.

5.2 High-Frequency Inspections

As a result of the initial inspections and the studies of transducer response as a function of the driving pulse characteristics (refer to Appendix 8.1, Transducer Characterization), it became evident that an improved pulser would provide a much enhanced defect detectability. Accordingly, instrumentation modifications were carried out which are discussed in Appendix 8.2, Instrumentation Considerations.

5.2.1 Inspection of Hot Pressed Silicon Nitride

In order to investigate the effect of the focal depth of the ultrasonic transducers, the billet of hot pressed silicon nitride was inspected at seven focal planes at a frequency of 25 MHz. It was found that when the water path was long enough to focus on the top half of the specimen, the sensitivity fell off. Therefore, scans were made at focal planes from the middle down to the back surface from each side. This procedure was then used to scan the same billet at seven focal planes at 45 MHz. The C-scan recordings of these inspections have not all been presented in this report because they would become repetitious. The following figures, however, illustrate the major conclusions drawn from these inspections.

The first conclusion drawn from these inspections is that, using the modified instrumentation (Section 8.2), the inspection is much more sensitive, even with the 25 MHz transducer than with the previously used pulser and the 45 MHz transducer. Second, all four of the seeded defects are detectable with this technique. These points are illustrated by Figure 24, a C-scan recording made using the pulse-echo method with the 25 MHz transducer focused near the center of the part. The defects previously detected (see Figure 17 at 25 MHz and Figures 22 and 23 at 45 MHz) are labeled D. Two of these are the seeded 0.005 inch (125 μm) voids also labeled SV. The new defects are labeled N. Two of these are the 0.005 inch (125 μm) tungsten carbide particles also labeled SWC. These four seeded defects form a one-inch square near corner #3 of the billet just as indicated by the manufacturer. (It should be noted in comparing Figure 24 to the seeding diagram, Figure 3, that the original six-inch square billet was chipped on the edges and was machined down to five and one-half inches. thereby moving the seeded defects closer to the edge).

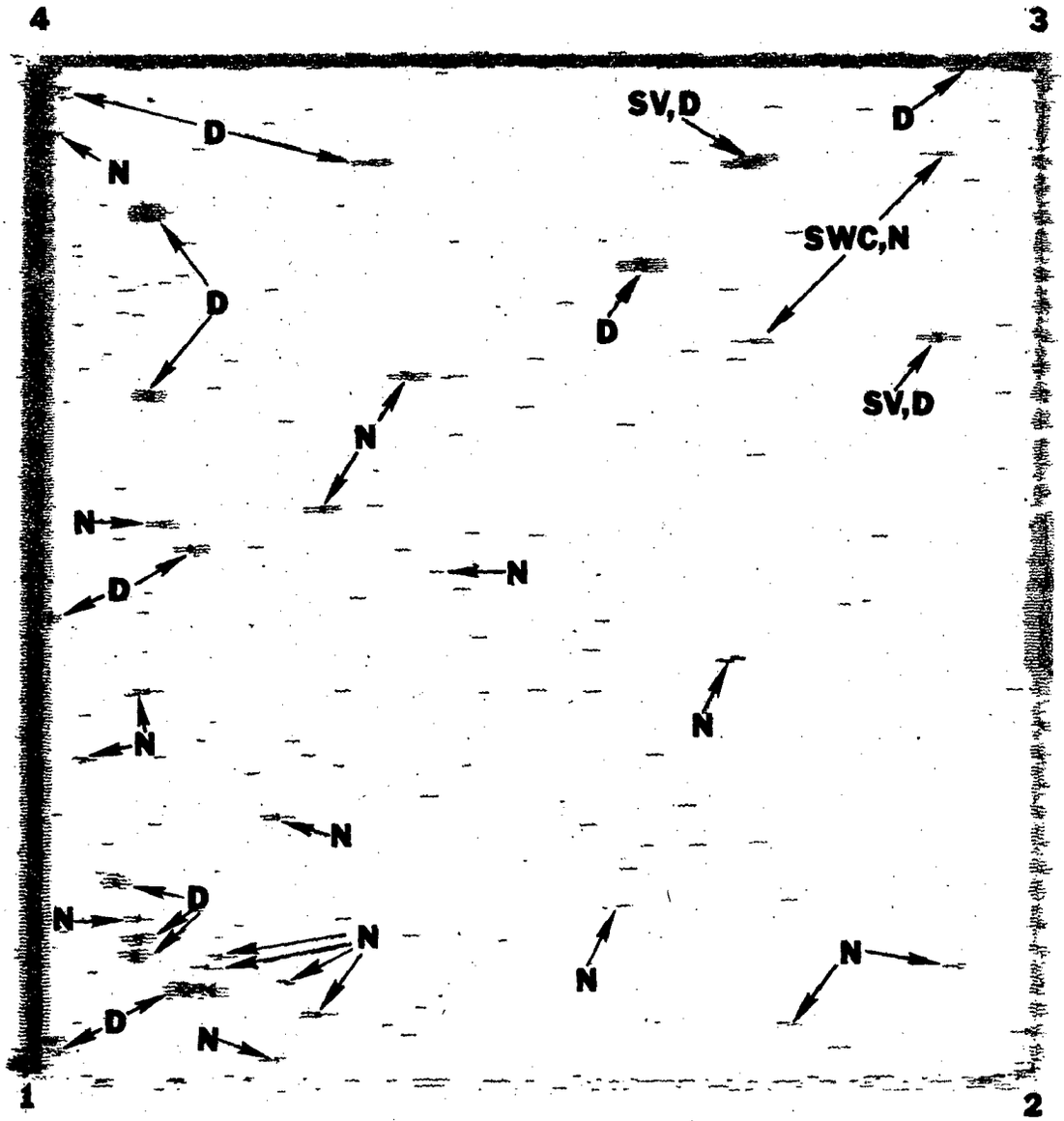

Figure 24. C-Scan Recording of Hot Pressed Silicon Nitride Specimen Using the Pulse-Echo Ultrasonic Inspection Method at a Frequency of 25 MHz with the Transducer Focused Near the Center of the Part.

The third conclusion is that inspection at 45 MHz is not dramatically better than inspection at 25 MHz. This is illustrated by Figure 25, a C-scan recording equivalent to Figure 24, but using the 45 MHz transducer. In Figure 25, defects labeled N are new ones that do not appear in Figure 24. Letter O's mark locations where defects appearing in Figure 24 do not appear in Figure 25. A more detailed examination of all the scans reveals that most of the defects appear on scans at both frequencies. A few very small defects do appear only at 45 MHz, indicating improved resolution with frequency. Finally, by comparing the scans at different focal planes it is concluded that most of the defects appear either on those made with the transducer focused near the center of the part or on those made with the transducer focused near one surface. Figures 26 and 27 are C-scans made with the 25 and 45 MHz transducers, respectively, focused near the surface of the part. The defects labeled N in these figures are ones that did not appear in the C-scan with the transducer focused at the center of the part at the same frequency. Another factor that varied between focal planes was background noise. Three sources of spurious indications were identified: reflections from turbulence in the water, which can be controlled by scan speed and water depth; electronic noise from the receiver caused by the necessity for using a very high gain setting; and false gating caused by problems in synchronizing the pulser to the receiver and by fluctuations in the front interface pulse. This latter condition is caused either by surface texture or by surface defects. Since the defect gate is synchronized to the front interface pulse, these fluctuations can cause the defect gate to shift momentarily to include the rear interface pulse, thus causing a false defect signal. This effect was observed to vary considerably from one focal plane to another apparently depending on how the ultrasonic beam interacts with the surface. Further investigation is needed to obtain a better understanding of this phenomenon.

The seeded defects were included in the part to use in setting the instrument gain in order to obtain an estimate of the size of the other defects observed. It turned out, however, that the signal from a seeded void saturated the receiver with the gain at the minimum setting. Therefore, an attenuator had to be installed at the output of the pulser to reduce the signal strength to bring it into the range of the receiver. With this arrangement, the gain was set to give a signal just below saturation for the seeded void. The pulser height from the other defects was then measured, in each case with the transducer height adjusted to focus on the defect in order to peak the signal. The depth of the defect in the part was also measured. Based on these results a map of the part was made showing relative defect size and defect depth (Figure 28). The depth is designated as bottom, middle or top third of the part. The figure also shows those defects that are detected only at 45 MHz. These defects were either very small (0.10 or less) or were very close to the top or bottom surface (i.e., 2.2 BF and 0.70 TF). This map was used to select defects for destructive examination.

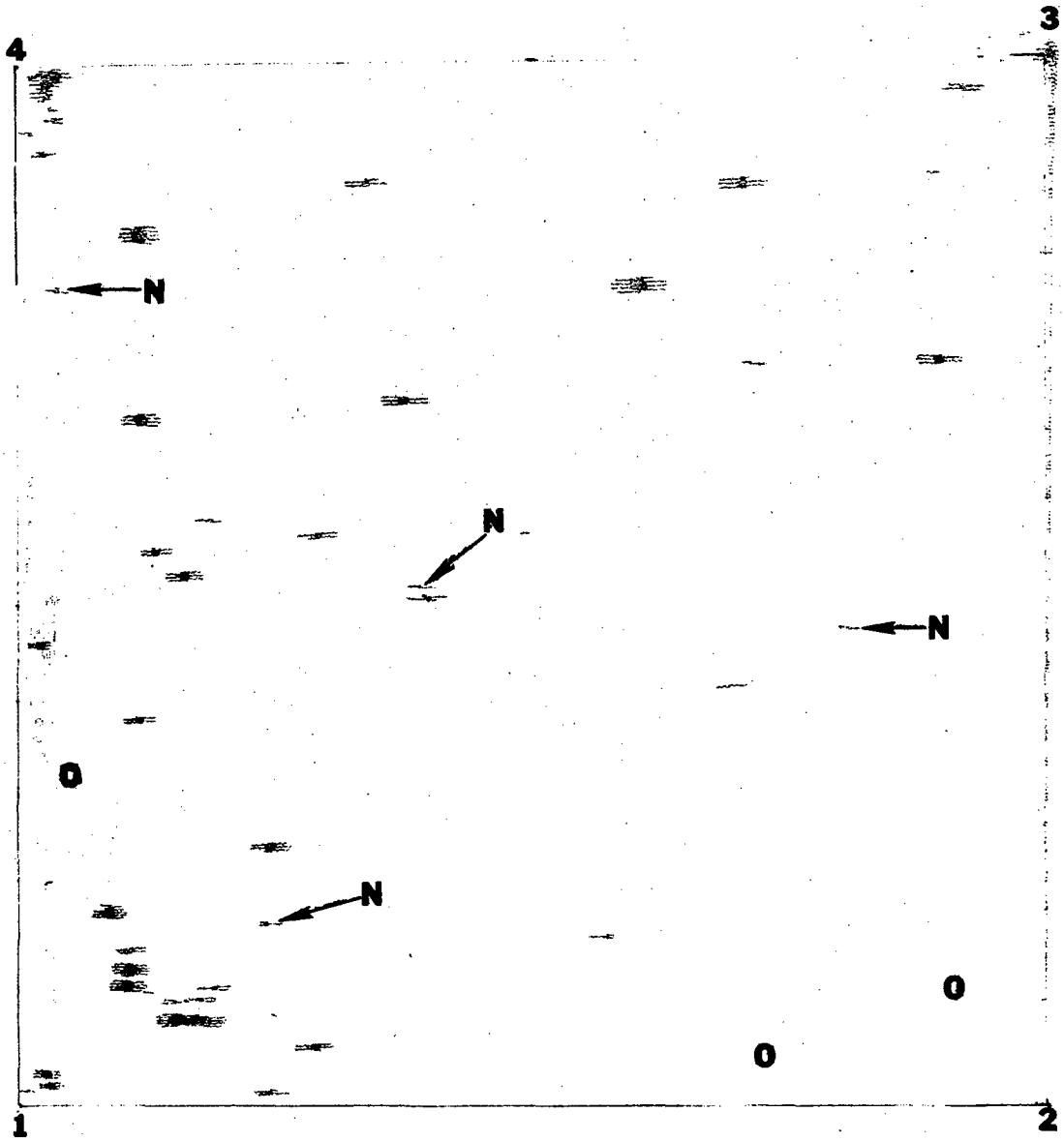

Figure 25. C-Scan Recording of Hot Pressed Silicon Nitride Specimen Using the Pulse-Echo Ultrasonic Inspection Method at a Frequency of 45 MHz with the Transducer Focused Near the Center of the Part.

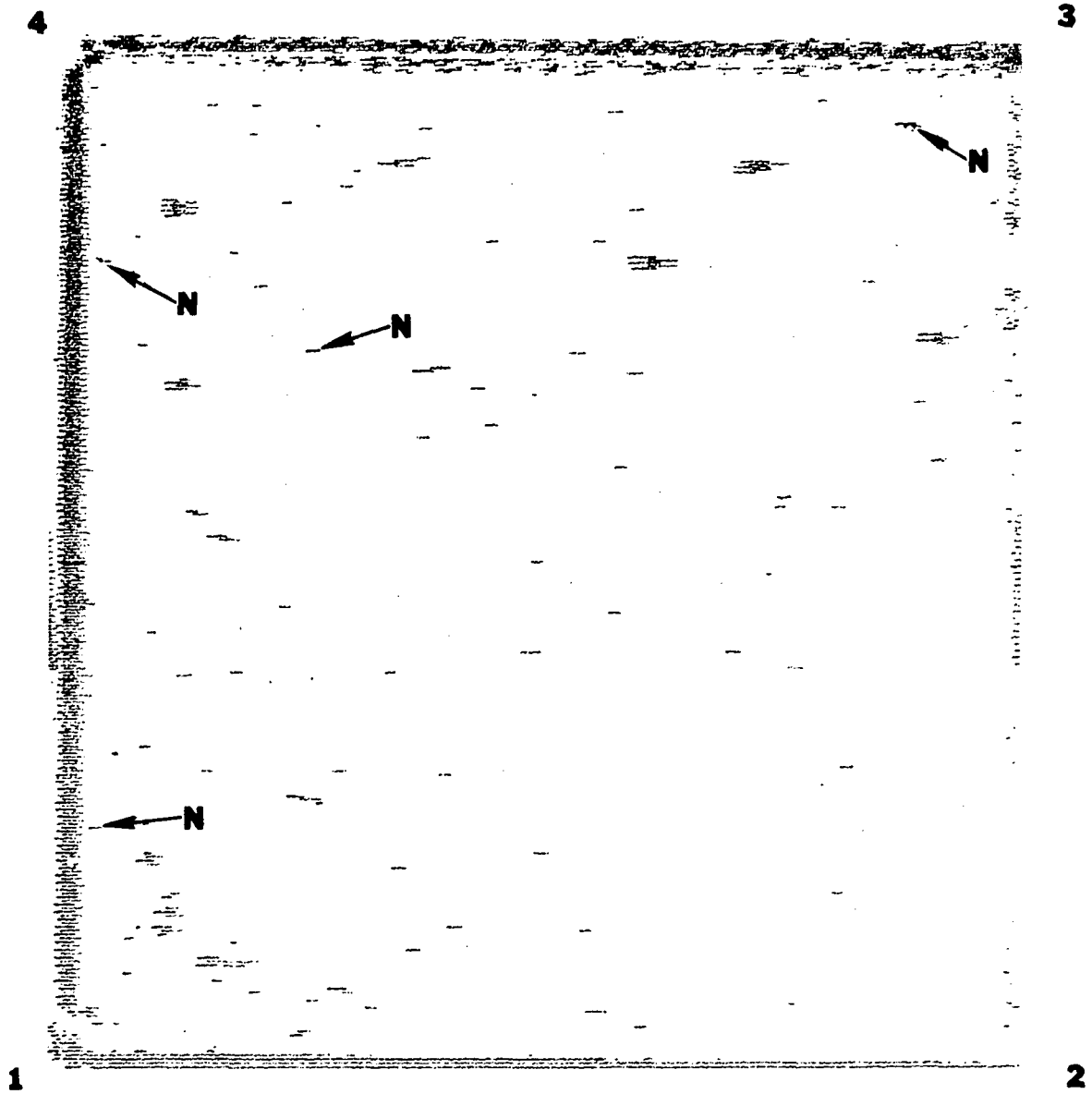

Figure 26. C-Scan Recording of Hot Pressed Silicon Nitride Specimen Using the Pulse-Echo Ultrasonic Inspection Method at a Frequency of 25 MHz with the Transducer Focused Near the Back Surface of the Part.

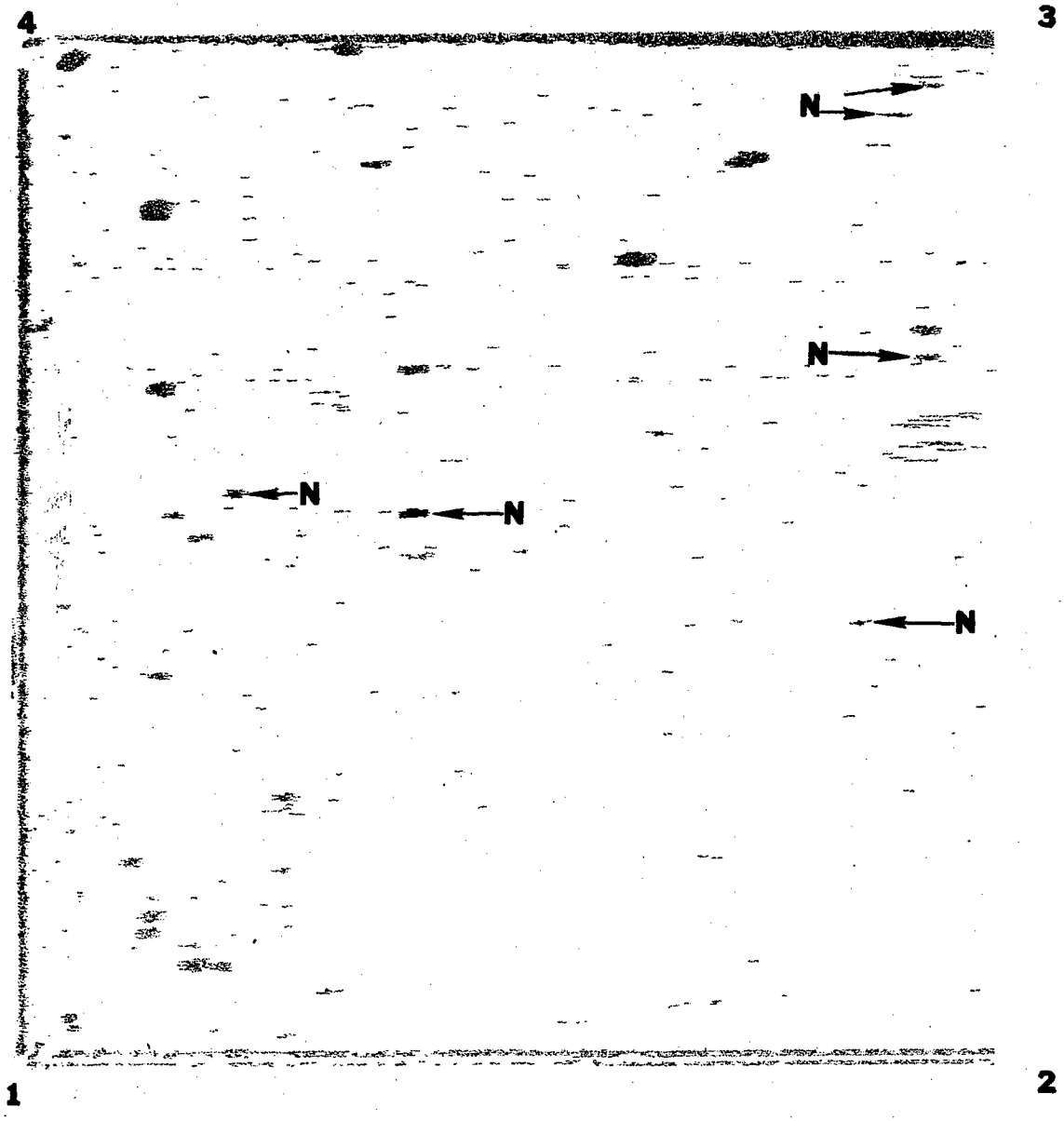

Figure 27. C-Scan Recording of Hot Pressed Silicon Nitride Specimen Using the Pulse-Echo Ultrasonic Inspection Method at a Frequency of 45 MHz with the Transducer Focused Near the Back Surface of the Part.

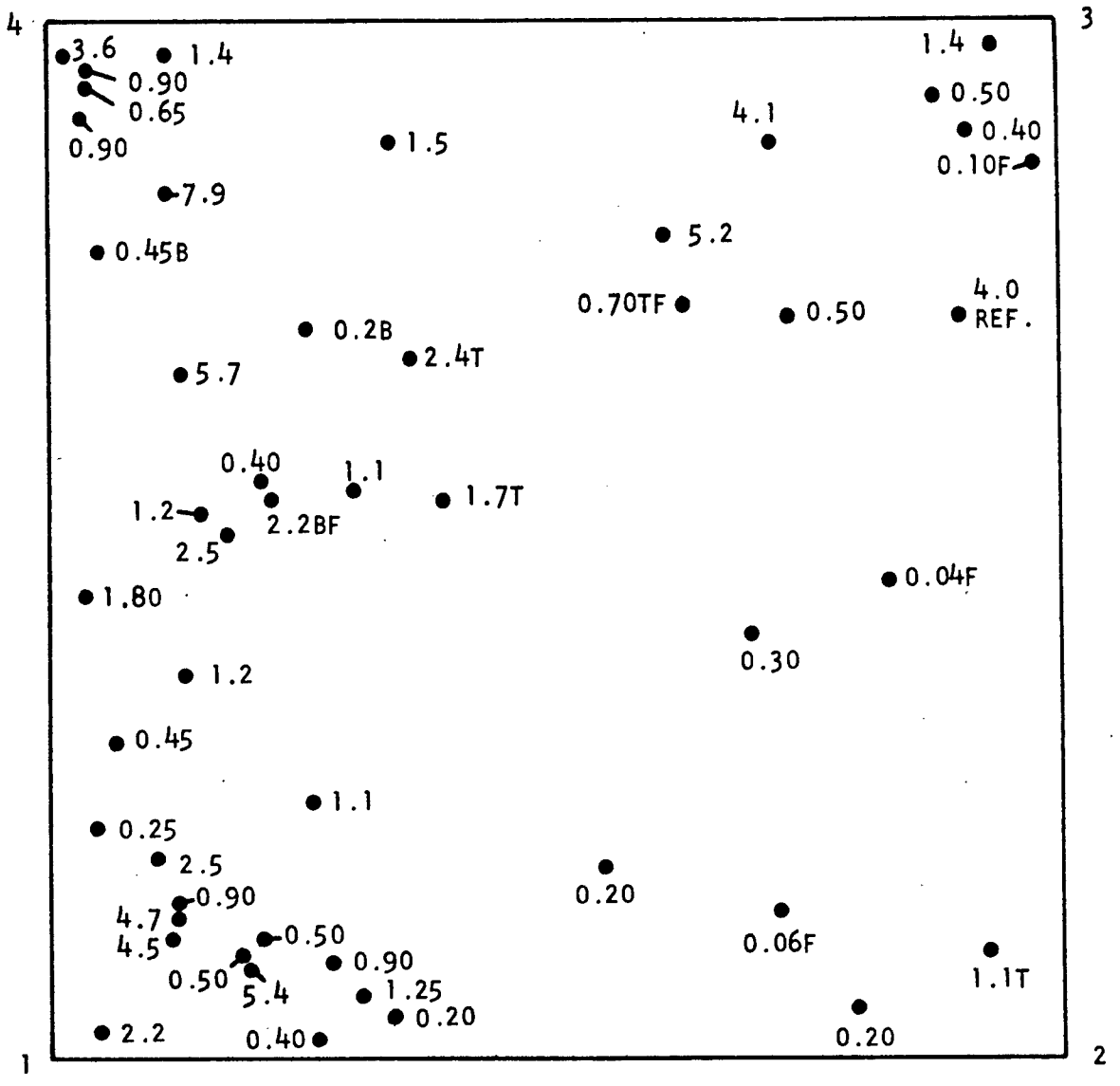

DEFECT SIGNAL AMPLITUDE IN cm CRT SCREEN HEIGHT REFERENCED TO 4.0 cm FOR SEEDED VOID.

T - IN TOP THIRD OF PART

B - IN BOTTOM THIRD OF PART

F - SEEN ONLY AT 45 MHz

Figure 28. Defect Size and Location Distribution in Billet of Hot Pressed Silicon Nitride.

The seeded tungsten carbide particle gave pulse heights about 10% of those from the seeded voids. The smallest defect observed gave a signal 1% of that from a seeded void and 10% of that from a seeded tungsten carbide particle. Assuming that the pulse height is proportional to the defect area, the ratio of defect sizes is proportional to the square root of the ratio of pulse heights. Therefore, these results indicate that the smallest defect detected is no greater than one-third of the size of the seeded tungsten carbide particles and could be much smaller.

5.2.2 Inspection of Hot Pressed Silicon Carbide

Based on the results of the inspection of the hot pressed silicon nitride, it was decided to inspect the hot pressed silicon carbide at three focal planes, at the center and near each surface from the back side, at both 25 MHz and 45 MHz. During inspection this material exhibited a severe noise response. Nevertheless, in order to maintain the desired high degree of defect detection, the inspection was carried out with high instrument sensitivity. In order to overcome the billet's poor signal-to-noise ratio, the following signal enhancing technique was used.

Two inspections were carried out yielding C-scan recordings. Comparing the two recordings (by overlaying one on another with the aid of transparencies) similar indications were identified. These were then re-inspected and diagnosed for their response with the aid of the instrument's A-scan display.

The procedure described helped to identify three small defects in the billet. Figures 29 and 30 show the C-scan recordings for 25 and 45 MHz frequencies, respectively, both revealing these defects. The noise problem was less severe at 45 MHz.

Since the seeded defects were not found in this billet there is no direct way to estimate the defect sizes. An indirect method was therefore used. The instrument was set up using a seeded void in the billet of hot pressed silicon nitride. The billet of silicon carbide was then examined using these same instrument settings. The three defects were found to have signal amplitudes on the CRT display of 2.1, 1.5 and 0.7 cm compared to a pulse height of 4.0 cm for the seeded void. However, the material difference makes these values only rough estimates.

Based on the results of both the frequency response tests described in Appendix 8.1 and the ultrasonic inspections, the following appraisal may be made. The ultrasonic transducers are operating at a broad spectrum of frequencies. The combination of the transducer and instrumentation characteristics and the preferential attenuation of higher frequencies by the acoustic media causes the amplitude response to be a maximum at a

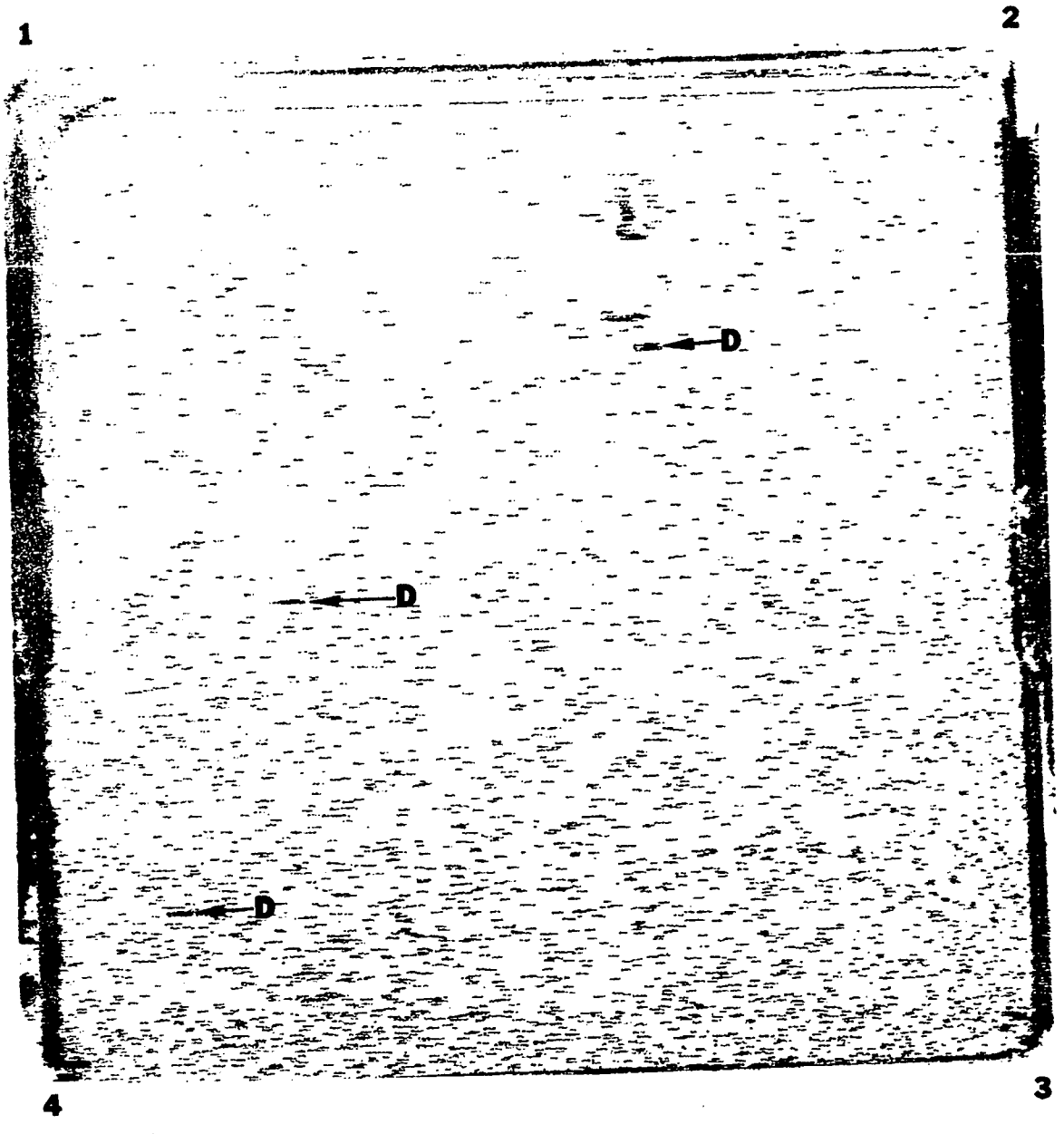

Figure 29. C-Scan Recording of Hot Pressed Silicon Carbide Specimen Using the Pulse-Echo Ultrasonic Inspection Method at a Frequency of 25 MHz with the Transducer Focused Near the Center of the Part.

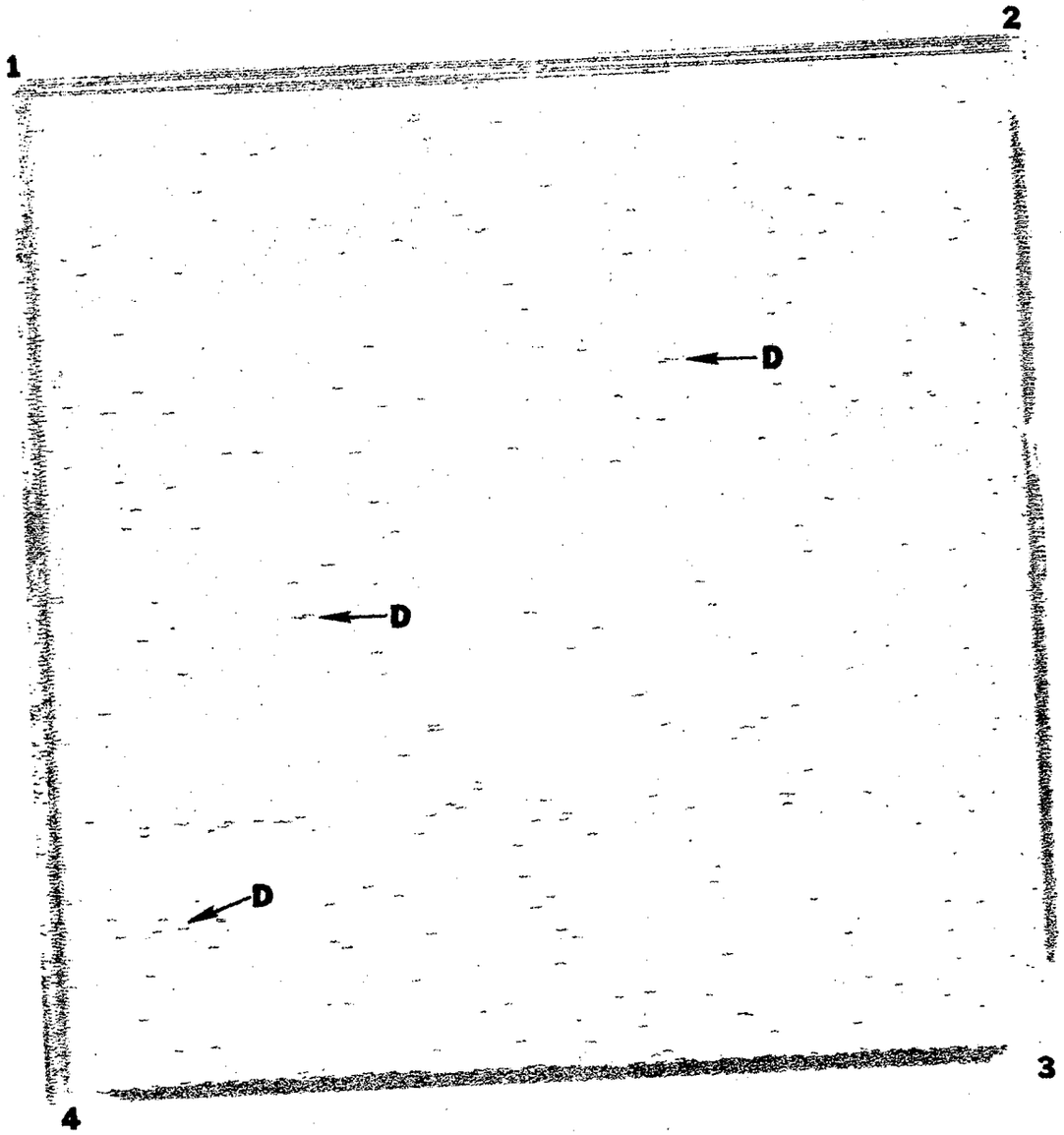

Figure 30. C-Scan Recording of Hot Pressed Silicon Carbide Specimen Using the Pulse-Echo Ultrasonic Inspection Method at a Frequency of 45 MHz with the Transducer Focused Near the Center of the Part.

frequency lower than the transducer resonant frequency. The favorable defect detection experienced at 25 MHz is a result of the fact that the receiver has its maximum sensitivity at this frequency. The lack of significant improvement in going to 45 MHz is due to a sharp drop-off in receiver sensitivity with increasing frequency. It seems likely that further receiver instrumentation modifications for improved high frequency response to be used for ceramic inspection would result in significantly improved detection capability.

6.0 VERIFICATION OF ULTRASONIC EVALUATIONS BY MECHANICAL TESTING

6.1 General

Since the primary objective of this program was to demonstrate that high frequency ultrasonics is capable of detecting defects in the 10 to 100 μm size range in gas turbine quality ceramics, the primary purpose of the mechanical testing was to expose the ultrasonically detected defects to the surface, in order to allow defect characterization by scanning electron microscope (SEM) fractography and electron microprobe (EMP) analysis. A secondary objective was to obtain a preliminary indication of the ultrasonically detected defect/mechanical property correlation by measuring the flexural strength of the specimens. Standard four-point bend testing procedures were used, but with specially machined specimens, to accomplish these goals. Procedures used with each of the three program materials tested, hot pressed and reaction bonded silicon nitride and sintered silicon carbide, are discussed in detail in the following sections. Mechanical testing was not performed on the hot pressed silicon carbide, because so few defects were detected, that there was little hope of obtaining any meaningful data.

6.2 Test Procedures

Standard bend tests were performed at room temperature using a tensile loading bend test jig with universal-joint coupling to ensure load alignment. Specimens with a two-to-one width-to-thickness ratio were tested at a constant crosshead speed of 0.02 inches/min. (0.51 mm/min.) with load pins having an inner span of 1/4 inch (0.64 cm) and an outer span of 3/4 inch (1.91 cm) to provide a "third point" load span. Moment and stress distributions during testing are shown schematically in Figures 31 and 32 with relevant dimensions and formulae. In Figure 32 the simple tensile stress, at some location Y above the neutral axis and between the inner loading pins, is indicated. If Y represents the location of a particular defect, and if a suitable stress concentration factor can be assigned to this defect, then a simple calculation would provide an estimate of the effective stress at this point from which it should be possible to predict the fracture strength of the specimen. Conversely, knowing the location of the defect and the fracture stress, a value for the stress intensity factor can be calculated.

6.3 Hot Pressed Silicon Nitride Evaluation

The billet of Cerralloy 147, hot pressed silicon nitride, was found ultrasonically to contain a random pattern of individual defects. Therefore, the specimen locations were selected to place one of these defects near the center of the tensile surface, in order to break the specimen through the defect. Based on the work of Gruver, et al (Ref. 27), it was assumed that some difficulty would be encountered in locating and classifying fracture origins. Therefore, the specimens were located to provide as many defect containing specimens as possible from the material available.

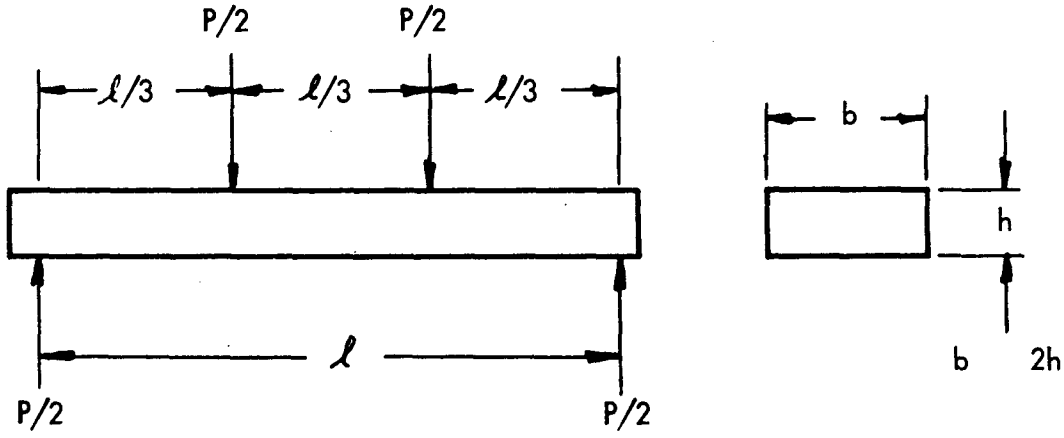

THIRD-POINT LOADING BEND TEST

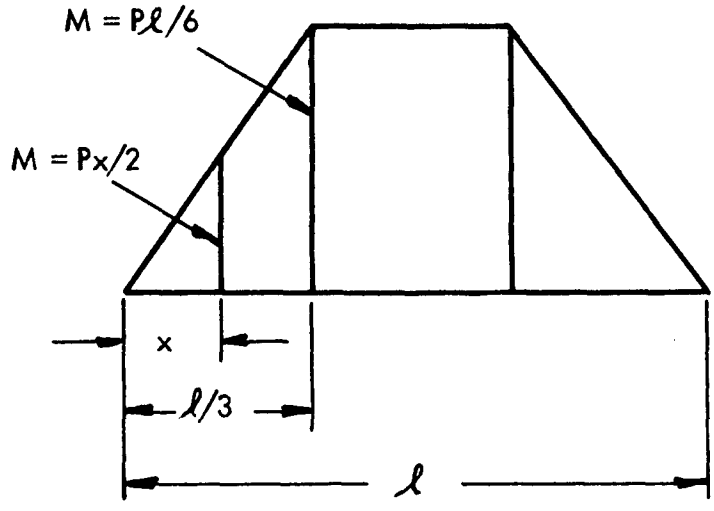

MOMENT DISTRIBUTION

Figure 31. Test Conditions for Flexural Strength Determinations.

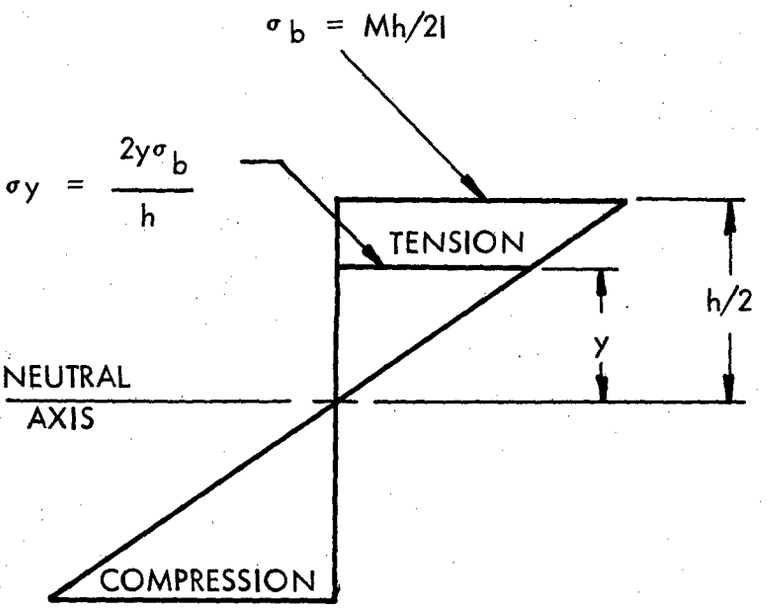

STRESS DISTRIBUTION

MOMENT OF INERTIA, I, ABOUT NEUTRAL AXIS (RECTANGULAR SECTION) = $\frac{bh^3}{12}$

$$\sigma_b \text{ (OUTER FIBER)} = \frac{Mh}{2I} = \frac{P\ell}{6}\,\frac{h}{2I} = \frac{P\ell}{bh^2}$$

$$\sigma_y \text{ (FLAW)} = K\,\frac{2y\sigma_b}{h}, \text{ WHERE } K = \text{GEOMETRIC STRESS CONCENTRATION FACTOR}$$

Figure 32. Stress Distribution and Equations for Rectangular Bar Specimens.

7811-C

6.3.1 Specimen Preparation

In order to machine specimens with defects close to the surface, it was necessary to make an accurate determination of the location of each defect. While the C-scan recordings give defect information, they are not accurate enough to use in specifying machining tolerances to achieve accurate defect location. The edges of the part are not well defined on the C-scan recording, the defects are somewhat enlarged because of the size of the ultrasonic beam, and also the system has some scanning hysteresis which obscures the defect location. In order to locate the defects more accurately, a composite transparency was made from all of the C-scan recordings so that it showed all of the defects detected. Some of the larger defects were found in the specimen ultrasonically and were used to achieve alignment between the transparency on the C-scan recorder and the part in the tank. The transparency was used to locate each defect ultrasonically and the transducer was then brought in contact with the part. The peak ultrasonic signal from the defect was obtained and then the outline of the transducer was drawn on the part. After all the defect locations had been marked, a circle template with a small hole in the center was used to locate the center of each circle. The coordinates of these points were then measured from a corner of the specimen to the nearest 0.01 inches (0.25 mm) and the value was marked on a drawing. The 1/4 x 1/8 x 1-1/4-inch (0.64 x 0.32 x 3.18 cm) four-point bend specimens were cut from the billet so that the 1/4-inch (0.64 cm) width dimension corresponded to the billet thickness (see Figure 33). This direction was chosen to facilitate machining the specimens with defects close to the surface. Since this is not one of the two directions in which testing is normally done, eight "defect free" specimens were cut parallel to each of the long sides of the billet to provide baseline data. These specimens were designated X-1 through X-4 and Y-1 through Y-4 (see Figure 34). These specimens were tested first to determine if the strength was dependent on the direction of cutting. The results. listed in Table III , showed a slight difference of questionable significance. It was determined that sufficient specimens could be cut in the Y-direction to provide the desired data. Therefore, this approach was taken to avoid any effect of anisotropy. The specimens with defects are also shown in Figure 34 and listed in Table III . Four defects in each of three size ranges were selected for specimens. The large defects gave ultrasonic signals of about the same intensity as the seeded voids. The small defects gave signals about the same as the seeded tungsten carbide particles. The medium size defects fell in between the other two groups. In addition, two specimens were made with very small defects seen only at 45 MHz and one specimen each was made with a seeded void and a seeded tungsten carbide particle. A piece of hot pressed silicon nitride approximately 7/8 x 2-7/8 inches (1.9 x 7.3 cm) with one seeded void and one seeded tungsten carbide particle was retained as a reference standard for future work.

The four-point bend specimens were machined using one of the four corners of the original billet as reference surfaces. The specimen numbers designate the corner of the billet used for reference. An attempt was made to machine each specimen so that the measured defect location

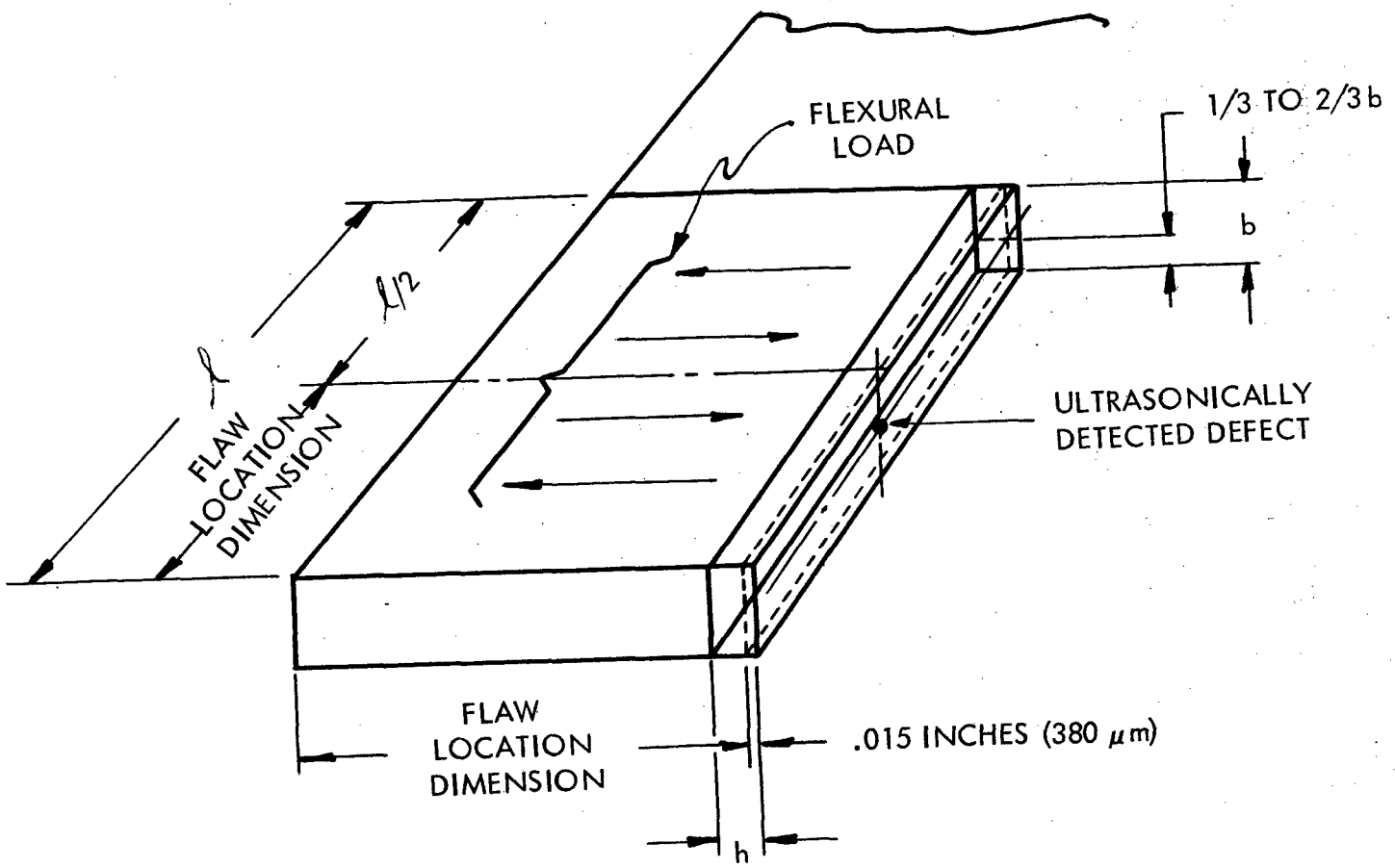

Figure 33. Planned Flaw Locations in Hot Pressed Silicon Nitride Flexural Strength Specimens.

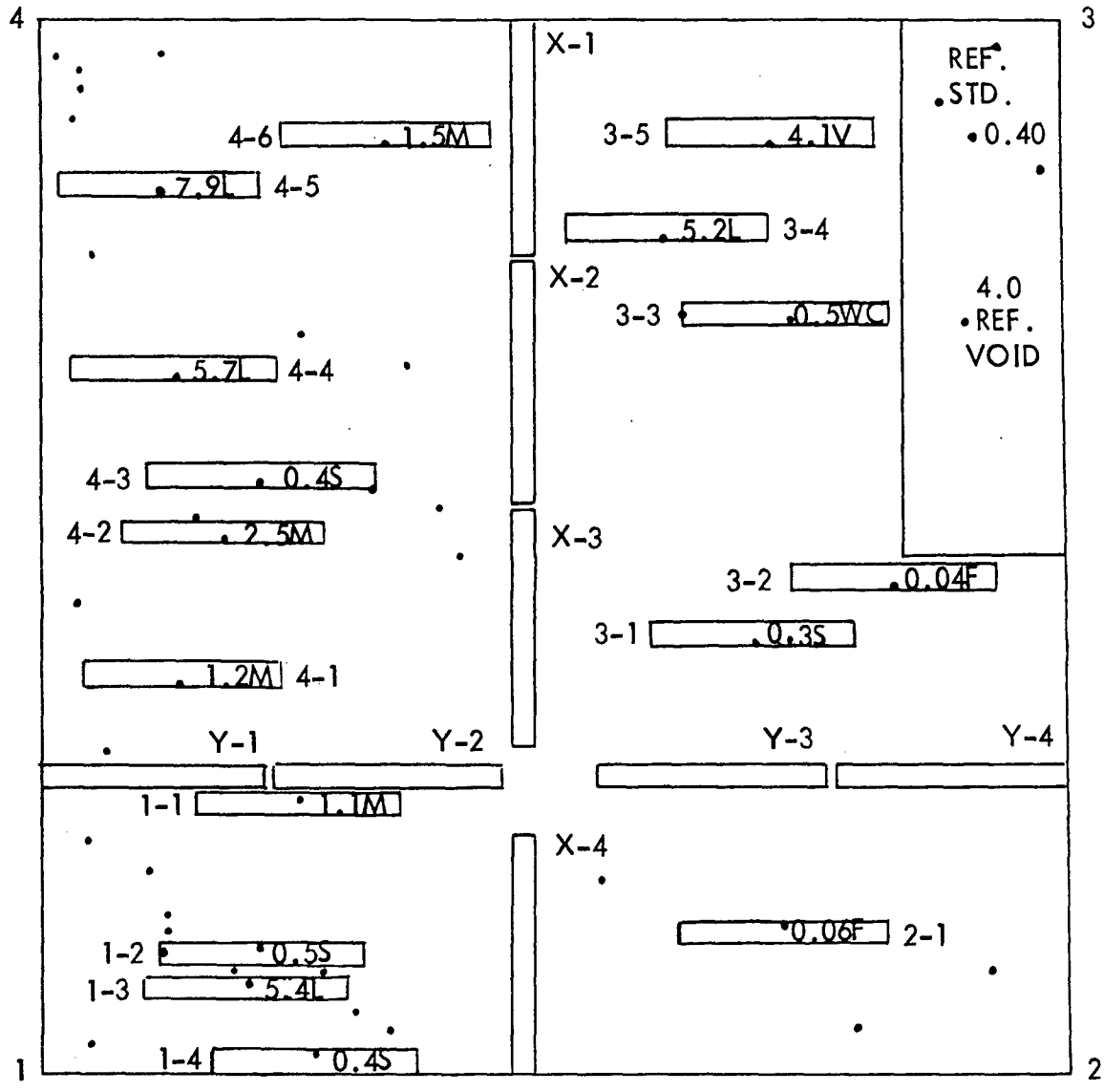

SPECIMEN NO.: X-X
ULTRASONIC SIGNAL STRENGTH: 0.0
DEFECT DESIGNATION: SMALL - S
MEDIUM - M
LARGE - L
DETECTED AT 45 MHz - F
SEEDED VOID - V
SEEDED TUNGSTEN CARBIDE - WC

Figure 34. Layout of Flexural Strength Specimens on Billet of Hot Pressed Silicon Nitride Showing Specimen Numbers and Relative Signal Amplitudes From Flaws.

TABLE III

FLEXURAL STRENGTH OF HOT PRESSED SILICON NITRIDE

Spec. No.	Indicated Defect Size	Flexural Strength MN/m^2	Flexural Strength ksi	Apparent Fracture Initiation Site/Flaw Type(2)
X-1	-	495	71.8	Failed Due to Faulty Loading Pin
X-2	-	674	97.8	NE(3)
X-3	-	645	93.5	NE
X-4	-	534	80.3	Internal Flaw/D
Y-1	-	605	87.7	NE
Y-2	-	501	72.7	"
Y-3	-	531	77.0	"
Y-4	-	558	81.0	"
1-3	Large	585	84.9	Internal Linear Defect/D
3-4	"	588	85.3	Corner/B
4-4	"	516	74.9	Internal Flaw/D
4-5	"	533	77.3	Corner/B
1-1	Medium	473	68.6	Corner/B
4-1	"	518	75.2	Corner/A
4-2	"	512	74.3	Corner/A
4-6	"	529	76.8	Adjacent to Corner/E
1-2	Small	514	74.5	Corner/B
1-4	"	612	88.8	Close to Surface/E or D
3-1	"	565	81.9	Adjacent to Corner/E
4-3	"	541	78.5	Corner/A
2-1	Very Small	583	84.6	Corner/A
3-2	"	491	71.3	Corner/B
3-3(1)	High Dens.	483	70.1	Seeded Defect/C (Tungsten Carbide)
3-5(1)	Low Dens.	293	42.5	Seeded Defect/C (Aluminum Rich Inclusion)

NOTES:

(1) Seeded inclusions

(2) Flaw Type

A	Surface Notch	D	Internal Unidentified Flaw
B	Unidentified Surface Flaw	E	Internal Void
C	Internal Inclusion	F	Surface Pore

(3) NE - Not examined by SEM

would be 0.015-inches (0.38 mm) below the surface on the tensile side of the neutral axis during testing and within 0.1-inches (0.25 cm) of the center of the specimen length. The eight "defect free" specimens were divided into two groups containing two specimens from each direction. One group had 0.002-inches (50 μm) removed from the tensile surface using a 220 grit diamond wheel to make grooves parallel to the specimen length. The second group had 0.007-inches (180 μm) removed. All the specimens were chamfered 0.005-inches (130 μm) at 45° on all four corners. After these eight specimens were tested, it was concluded that there was no significant difference either in the appearance of the fracture surfaces or in the strength data after removal of 0.002-inches (50 μm) or 0.007-inches (180 μm). Therefore, the sixteen specimens with defects were all machined to remove 0.002-inches (50 μm).

6.3.2 Flexural Strength

Results of the flexural strength determinations on hot pressed silicon nitride are listed in Table III. The first eight specimens are "defect free" control specimens. The specimens with defects are arranged in order of defect size as indicated by the ultrasonic signal strength data. The fracture initiation site and defect type are also indicated in Table III.

Based on the limited data for control samples cut in the Y direction, a mean strength level of about 517-586 MN/m^2 (75-85 ksi) might be assigned to this material. The data in Table III therefore would indicate significantly reduced strength only for specimens 1-2, 3-2, 3-3, 3-5 and 4-2. Specimens meant to contain defects which gave the highest signal strengths (1-3, 3-4, 4-4, 4-5) did not have lower than average strengths, indicating either that the defect was machined away during specimen preparation or that the identified defect did not have any influence on strength. Some of the specimens broke "off center" with apparent surface or corner fracture initiation sites, again indicating that the defect was lost during machining or did not influence fracture.

6.3.3 SEM Fractography

Fracture surfaces of selected specimens were examined by scanning electron microscopy to identify and characterize any obvious fracture initiation sites, and to obtain a size estimate of the ultrasonically detected defects. A thin coating of vapor deposited copper (<500Å) was applied to the surfaces to eliminate charging effects.

Figure 35 shows the mating fracture surfaces of one of the control specimens (X-4) with an obvious fracture initiation site just below the tensile surface and a fairly well defined "mirror" region. At higher magnifications this defect took on the appearance of a smooth amorphous looking area. A specimen tilt of about 23° was used so that there is some image foreshortening in the vertical sense. The defect shown in Figure 36 would therefore have a width dimension of about 25 μm and a length dimension somewhat greater than 60 μm. Since the hot pressing direction for the material was in the specimen width direction, it would be anticipated that the defects would be elongated in the specimen thickness direction.

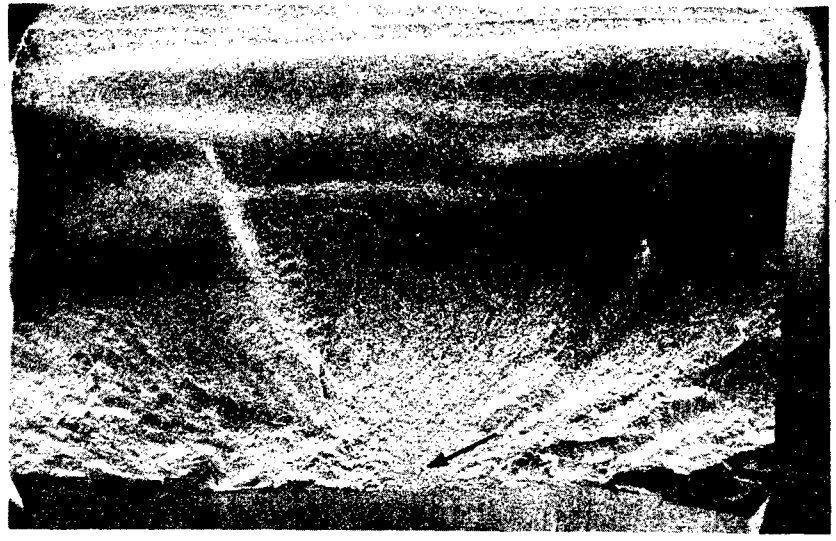

16X

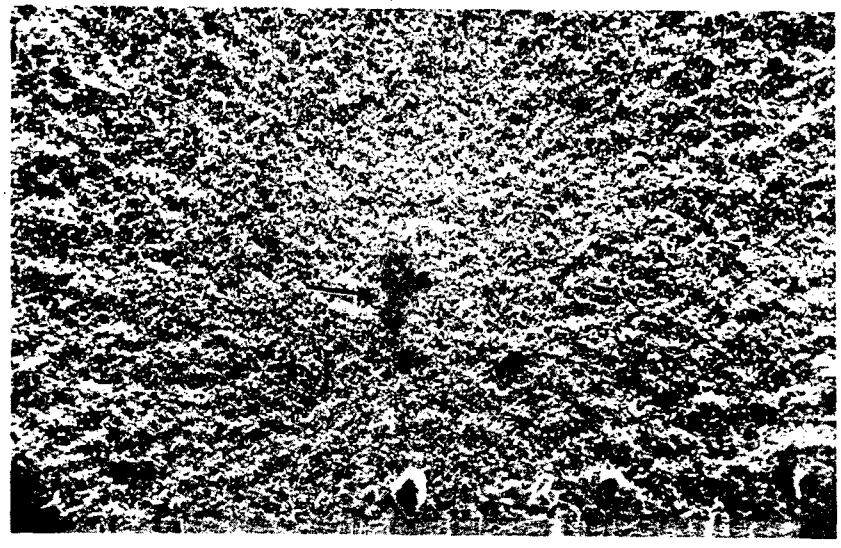

200X

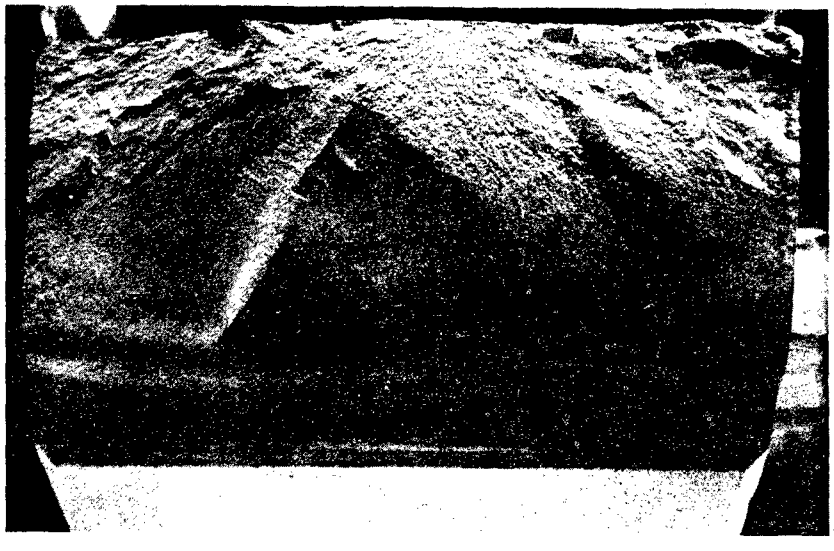

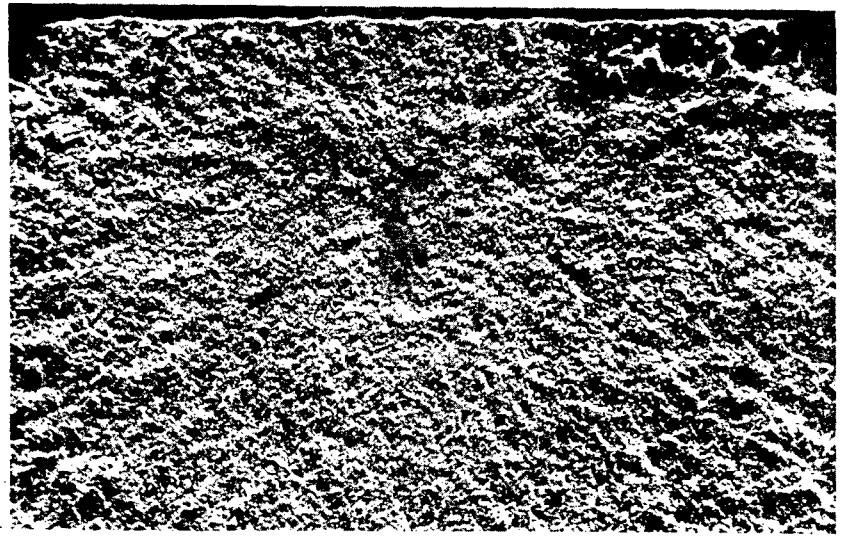

Figure 35. Fracture Surface of Hot Pressed Silicon Nitride Specimen X-4, Showing Unidentified Sub-Surface Flaw at Fracture Initiation Site.

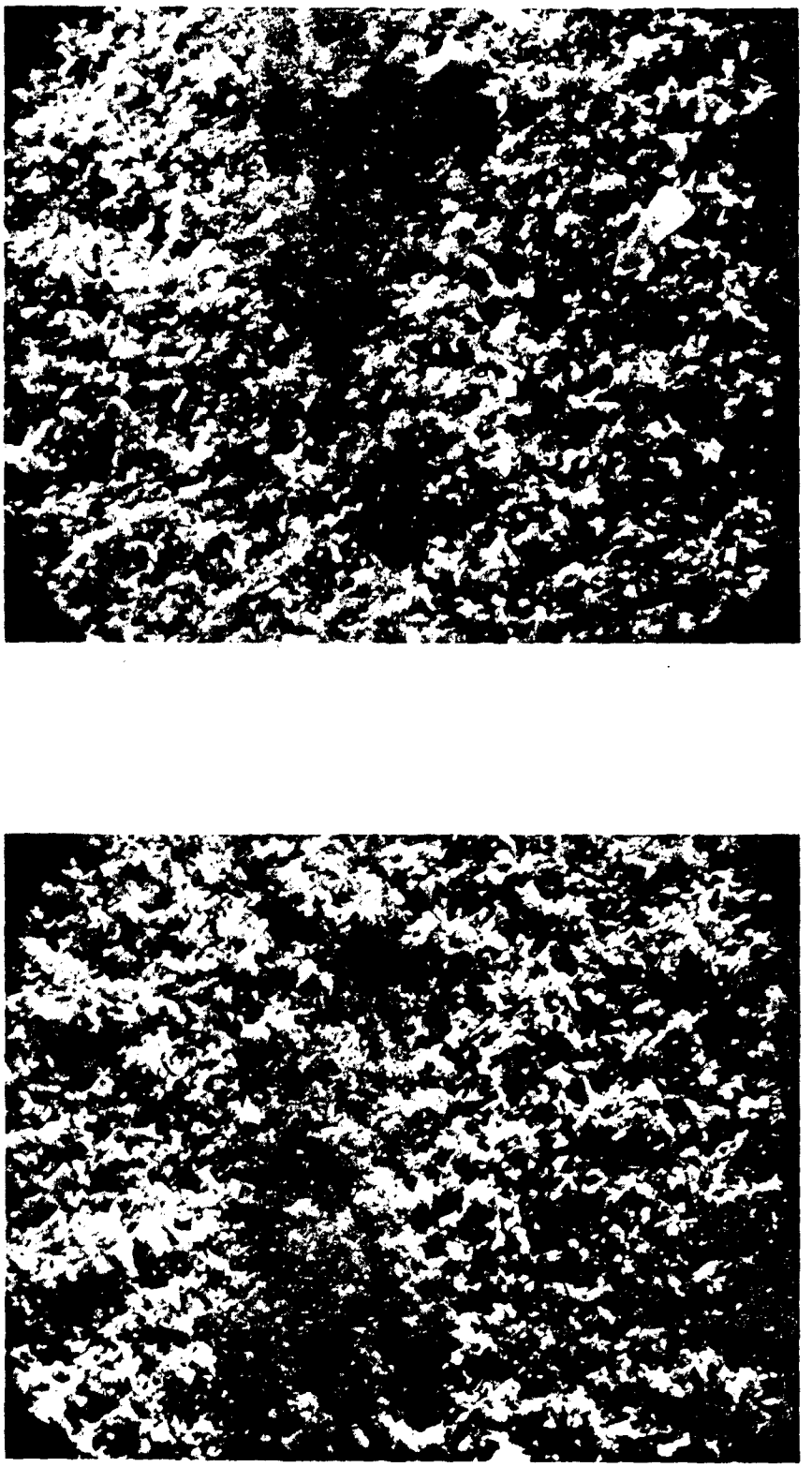

Figure 36. Fracture Initiation Site of Specimen X-4 at High Magnification.

1000X

Representative fracture surfaces in specimens with identified defects are shown in Figures 37-46. A well defined fracture mirror associated with a platelike or line defect is evident in Figures 37 and 38 (specimen 1-3). At high magnifications the defect appears as a crack with a sandwiched layer of flakelike material. This defect was almost perfectly aligned parallel to the tensile stress, during bend testing, and although failure obviously initiated at this location a fairly high fracture strength was observed. It is reasonable to assume that had the specimen been tested in the normal direction (bend axis rotated 90°), a very low strength value would have been obtained. A relatively high signal strength was noted for this defect and its estimated length (SEM) was about 875 μm.

Figure 39 shows fracture surfaces of specimen 1-4, the strongest specimen in this batch, with an apparent fracture initiation site close to the surface and about one-third of the width of the specimen from the right hand edge. There was a very small mirror portion with a small (~25 μm) void located at the center. For this specimen there appeared to be a good correlation between defect location and size, as determined from the ultrasonic signal, and from the SEM fractography. The seeded defect in specimen 3-3 was actually cut through so that it was exposed to the surface as shown in Figure 40. There was again a clearly defined mirror region identifying the fracture origin. The defect was clearly visible in the scanning electron microscope at 200X magnification on the ground surface, but was not visible optically. The difference in electron absorption indicated the presence of heavy elements and the defect was subsequently identified as WC. The image foreshortening effect is most evident from comparisons of Figures 40 and 41. In Figure 40 the angle between the beam and specimen ground surface was 90-23° or about 70°, and the tungsten carbide particle appears to have a circular section. In the lower photograph of Figure 41, the fracture surface was tilted about 50° from the beam so that the machined surface was now at about 40° to the beam and the defect looked elliptical (disc shaped in three dimensions). Bearing in mind that the pressing direction was horizontal with reference to Figure 40, this would be the anticipated shape of a spherical particle after deformation. From the SEM's, the estimated dimensions of this defect were that of an ellipsoid with major and minor axes of about 130 and 75 μm, respectively.

Fracture surfaces of another seeded specimen are shown in Figures 42 and 43. There was a problem of surface contamination with this specimen but since there was a very obvious cause of fracture in the form of a large inclusion, the residual contamination did not affect the evaluations. This specimen had a strength level of about 50% of the mean value. The fracture surface was very smooth and practically all mirror out to the compressive crack front. This defect was also machined through and had the apperance of a short rod-like inclusion of about 130 μm diameter.

The remaining specimen with a well defined fracture origin was 4-4 (Figure 44). This specimen broke off center near one of the loading pins, however, indicating that the ultrasonically identified defect was misplaced or lost during machining, or that the defect in the fracture surface was a more potent crack initiator. Because of the high signal strength (large defect), it is likely that the former was done. The fracture origin had some

16X

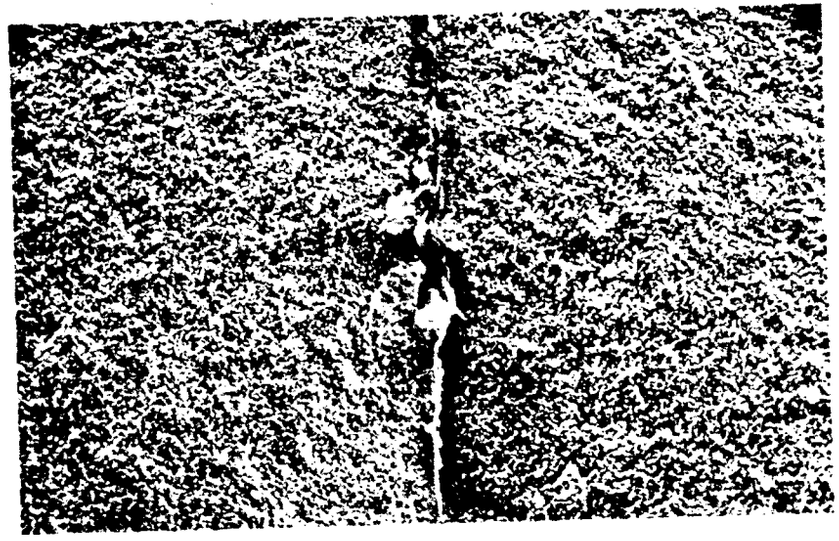

200X

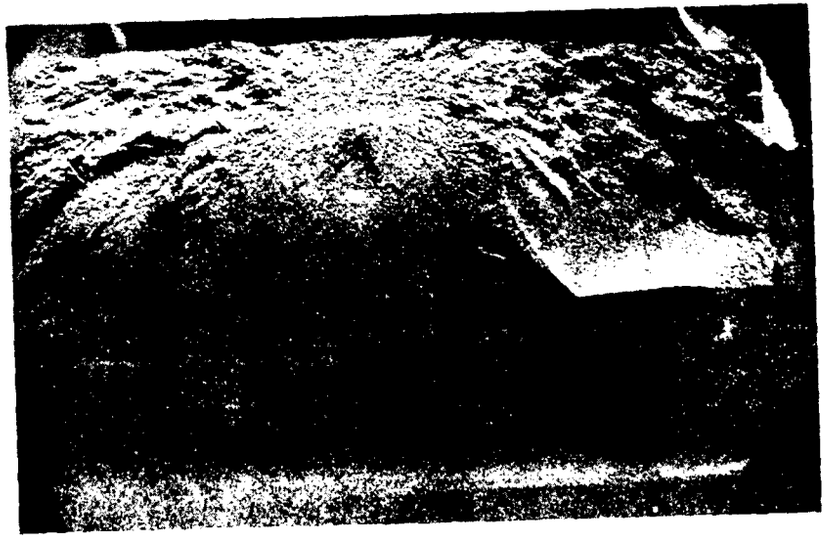

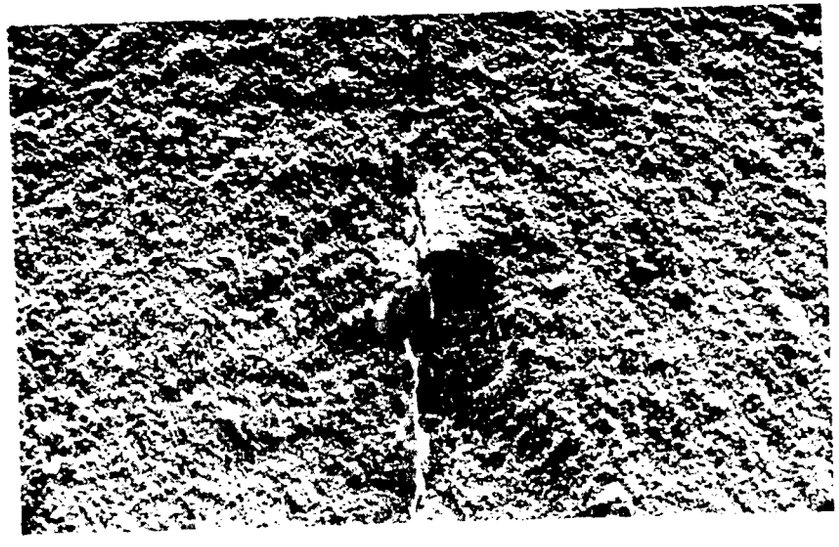

Figure 37. Fracture Surfaces of Hot Pressed Silicon Nitride Specimen 1-3, Showing Fracture Origin at Large Unidentified Linear Defect.

Figure 38. Fracture Initiation Site of Specimen 1-3 at High Magnification.

500X

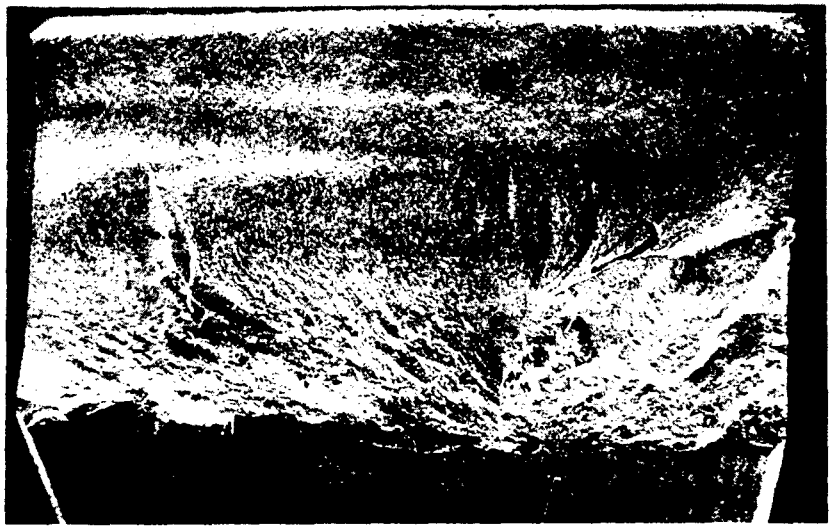

16X

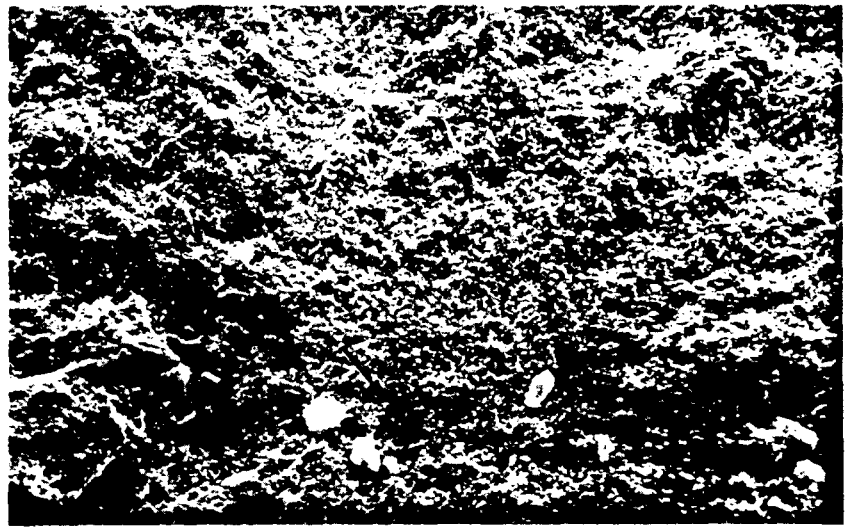

200X

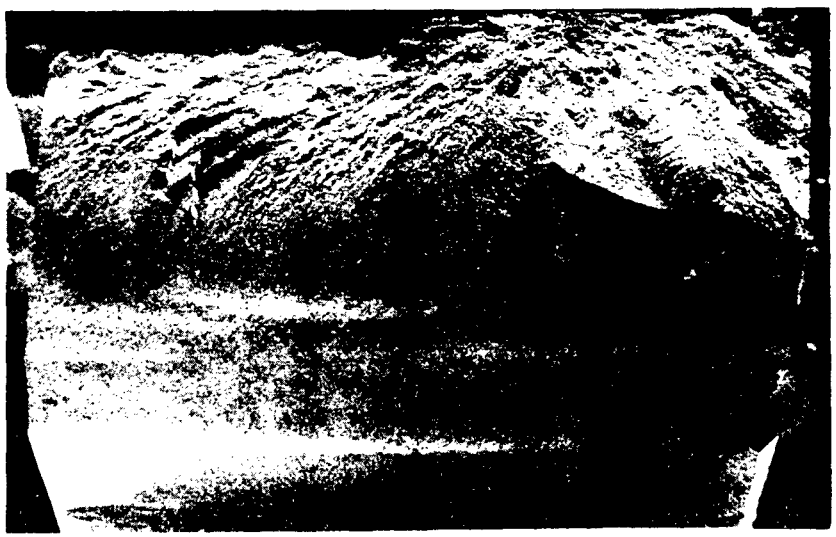

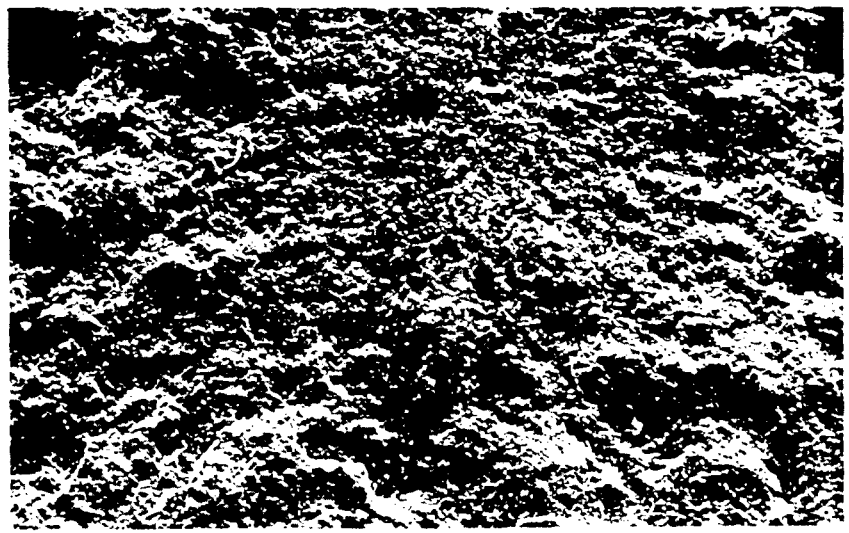

Figure 39. Fracture Surfaces of Hot Pressed Silicon Nitride Specimen 1-4, Showing Fracture Initiation Site at 25 μm Void.

16X

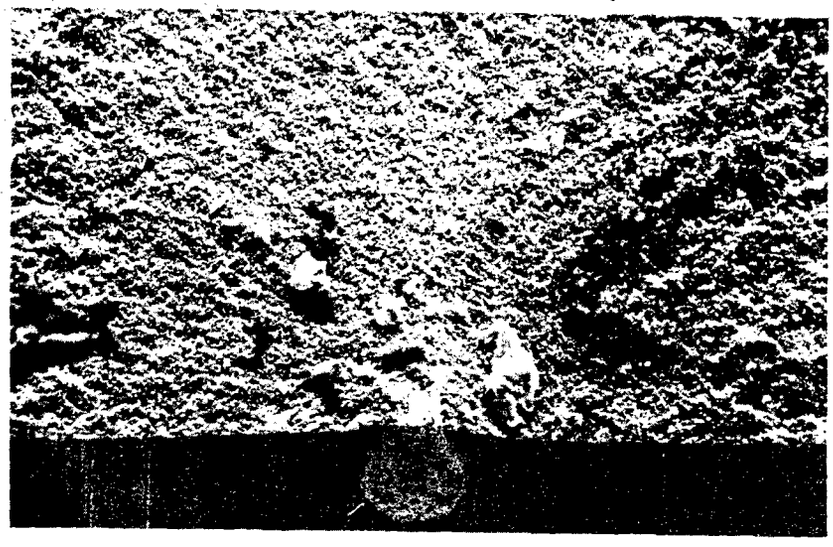

WC Seeded Defect 200X

Figure 40. Fracture Surfaces of Hot Pressed Silicon Nitride Specimen 3-3, Showing Fracture Initiation Site at Seeded High Density Inclusion.

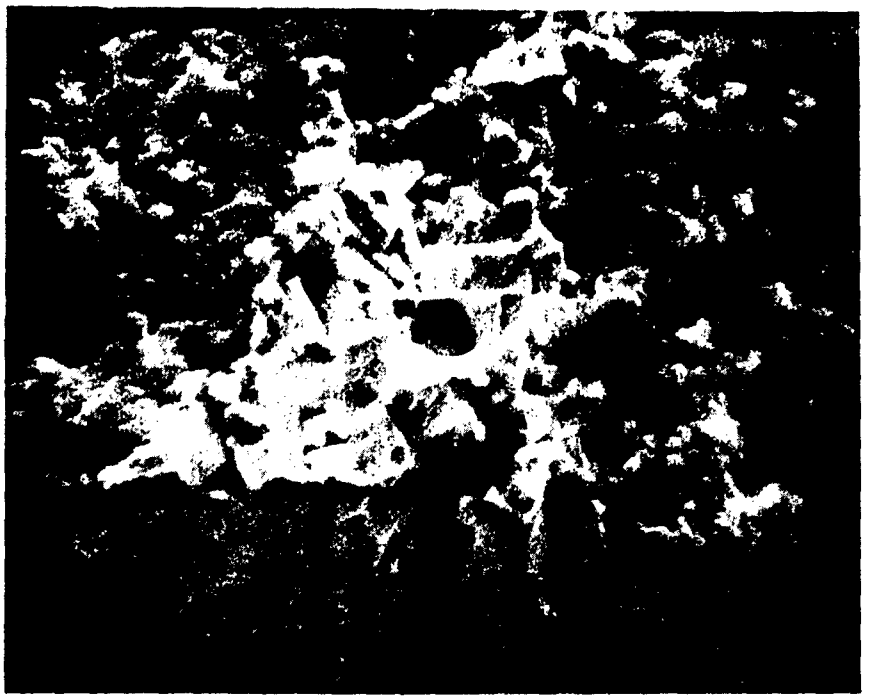

2000X

50° Tilt

1000X

Figure 41. Seeded Defect in Specimen 3-3 at High Magnifications.

16X

200X

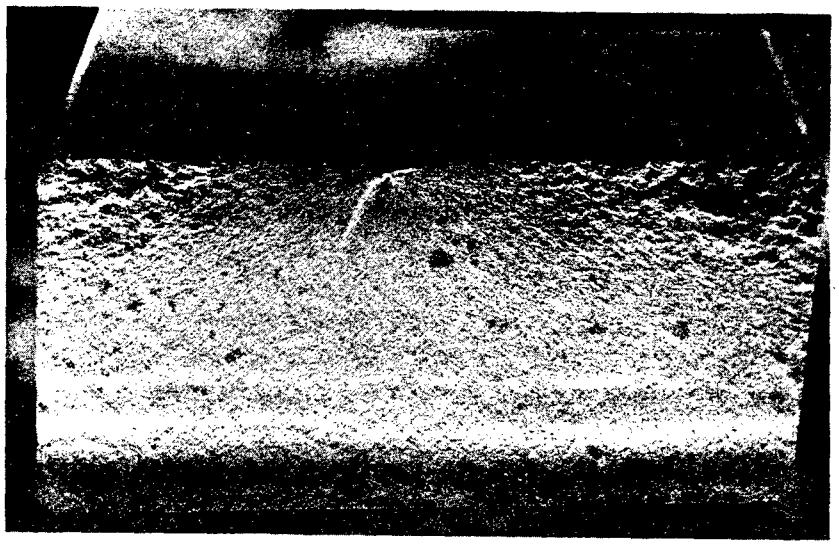

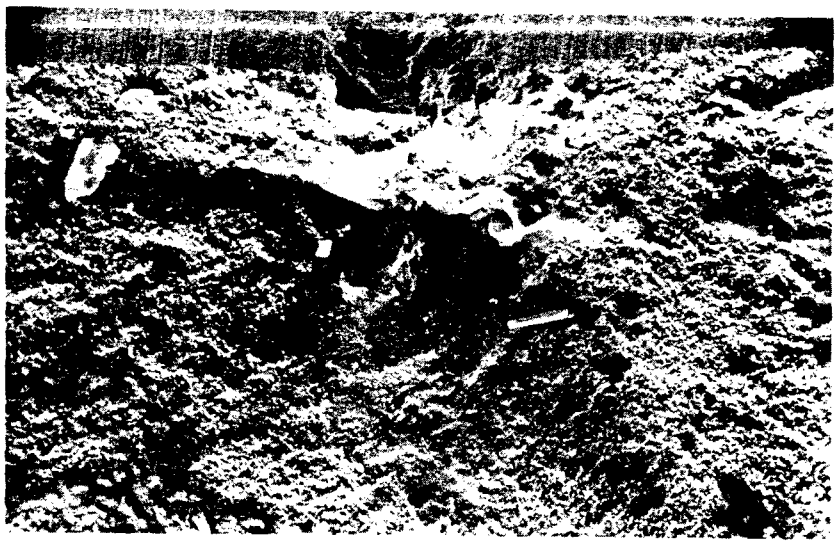

Figure 42. Fracture Surfaces of Hot Pressed Silicon Nitride Specimen 3-5, Showing Fracture Initiation Site at Seeded Low Density Inclusion.

Figure 43. Seeded Defect in Specimen 3-5 at High Magnification.

500X

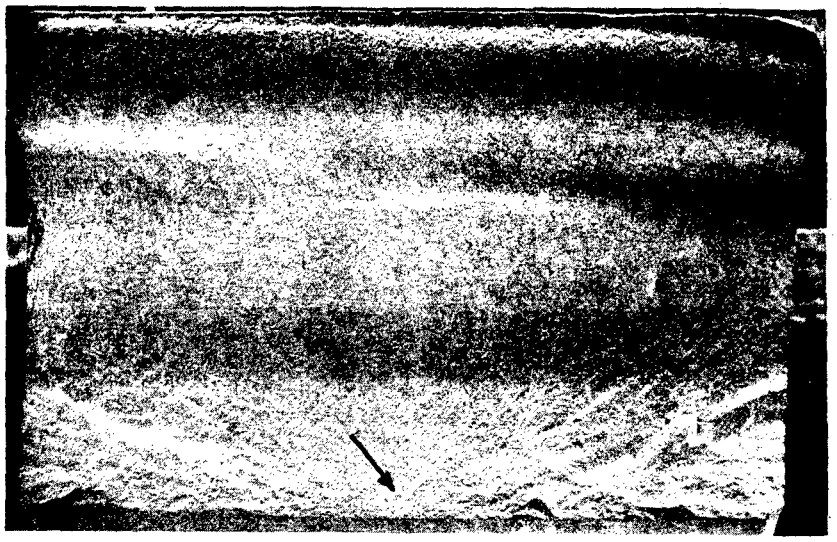

16X

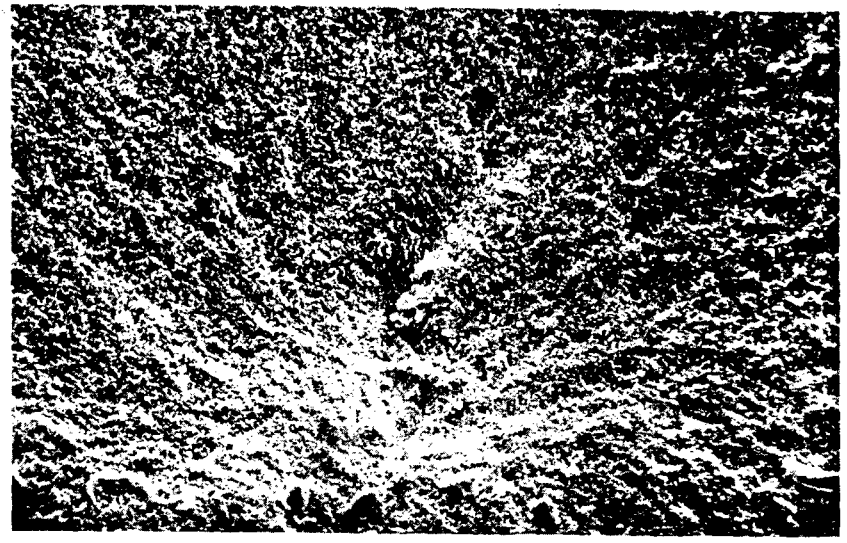

200X

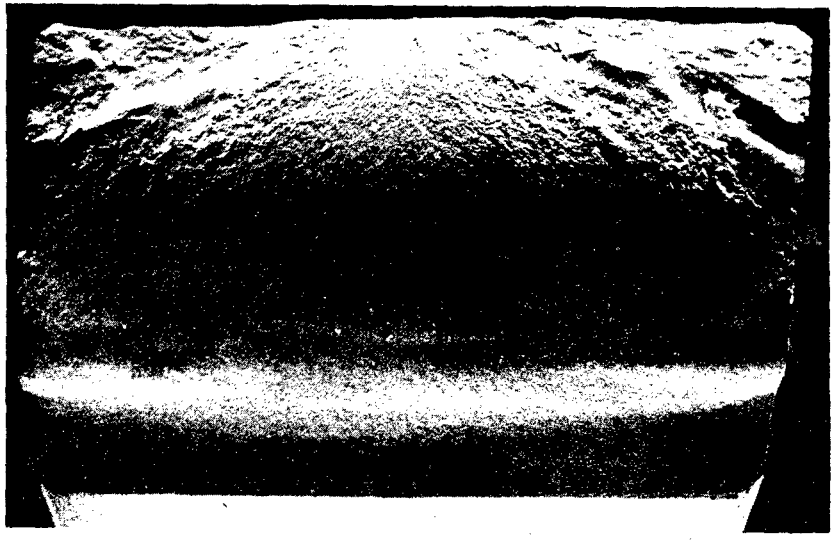

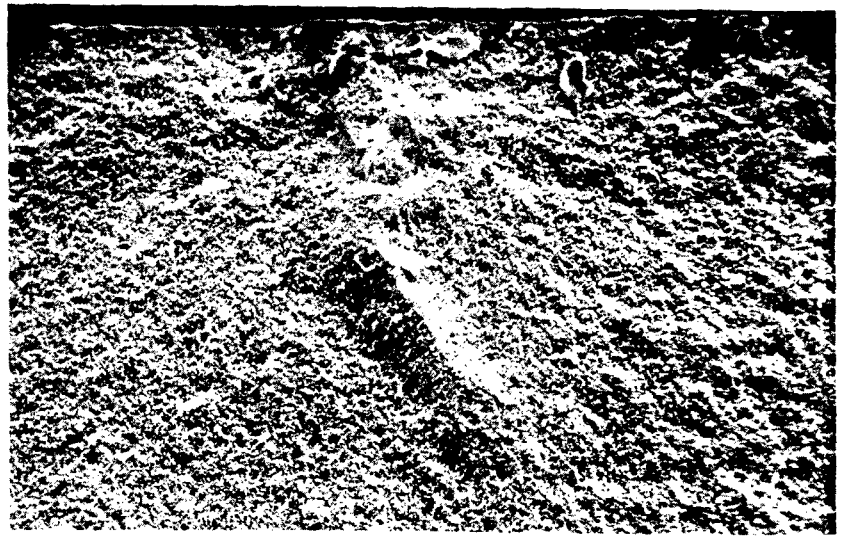

Figure 44. Fracture Surfaces of Hot Pressed Silicon Nitride Specimen 4-4, Showing Fracture Initiation Site at Unidentified Internal Flaw.

of the appearance of the smaller area in Figures 35 and 36 and, in fact, was also observed in other samples. In addition to the amorphous looking area, approximately 100 μm diameter, there was a groove with a crack at the base terminating in a "penetration flaw" referred to by Gruver et al (27). Figure 45 is included to show a frequently observed fracture behavior where initiation from one corner was evident. This type of failure would indicate the presence of surface damage from machining. In this case, however, closer examination (Figure 46) indicated the presence of a 10-20 μm diameter void close to the edge.

6.3.4 Microprobe Analyses

Quantitative electron beam microprobe analyses were performed on selected samples in an attempt to further characterize the defects. The actual fracture surfaces were examined and a multichannel analysis was first used to scan the total elemental spectrum at each defect. Slow scans were then performed for selected elements based on the indications of even trace amounts of these elements. Microprobe traces were obtained for the elements Si, N, C, S, O_2, Ca, B, Fe and W. Serious problems were encountered in interpreting the data due to the uneven topography, and only two specimens gave meaningful results. Microprobe traces for specimens 3-3 and 3-5 (see SEM's in Figures 40 and 42) are shown in Figures 47 and 48. The inclusion/defects in specimens 3-3 and 3-5 are clearly identified as WC and aluminum oxide (Al_2O_3). In the case of specimen 3-3, the scan was made on the ground surface.

It is likely that more meaningful data would have been obtained on specimen 1-3 if the specimen had been sectioned across the defect and polished. These additional evaluations were not possible within the program schedule, however. The results obtained on specimens X-4 and 4-4 indicate that refinements in the microprobe analysis technique will be required in order to obtain useful analytical data on the type of defect shown in Figures 35 and 44.

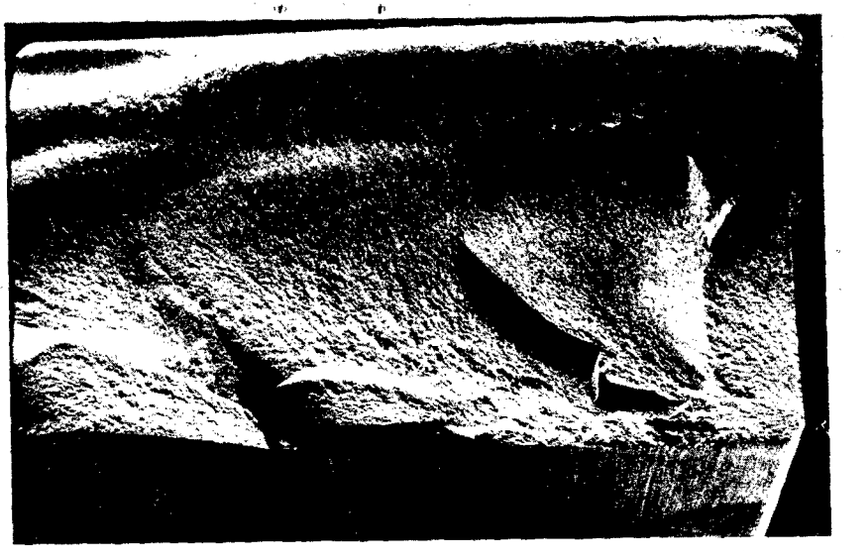

16X

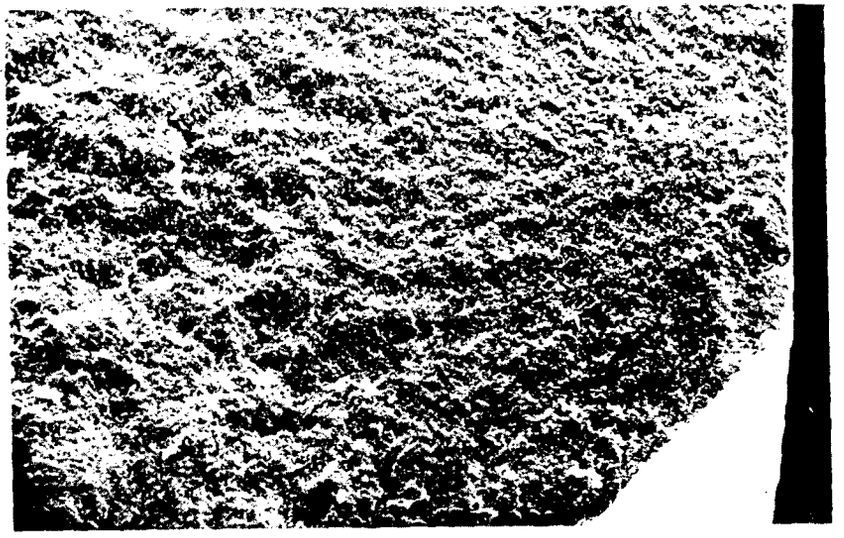

200X

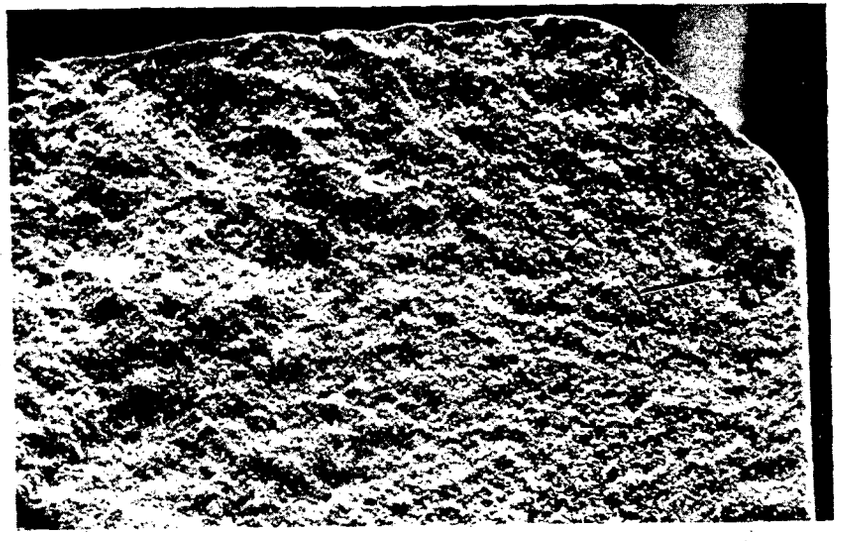

Figure 45. Fracture Surfaces of Hot Pressed Silicon Nitride Specimen 4-6, Showing Corner Fracture Initiation Site.

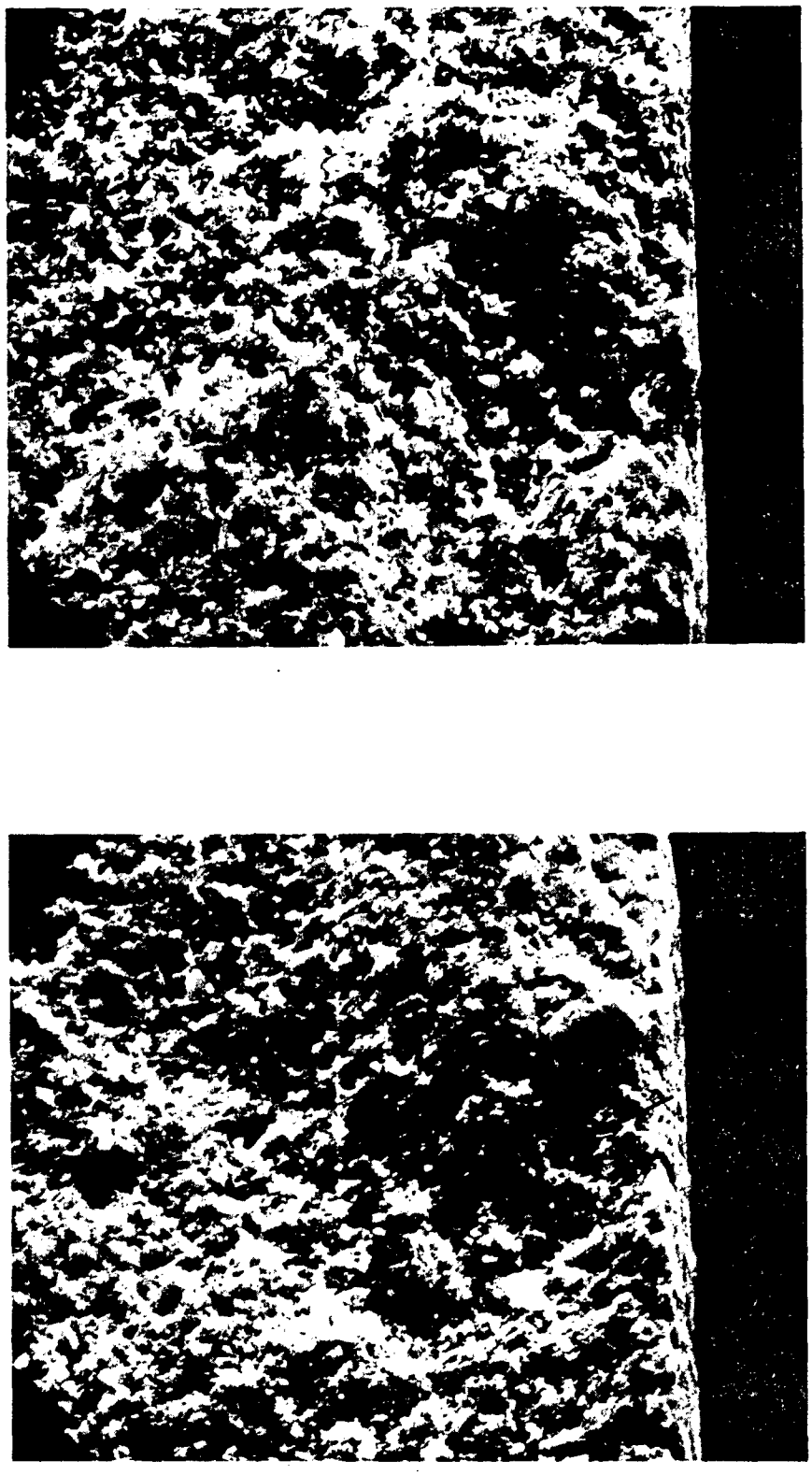

Figure 46. Fracture Initiation Site of Specimen 4-6 at High Magnification, Showing Large Void at Center of Fracture Mirror.

1000X

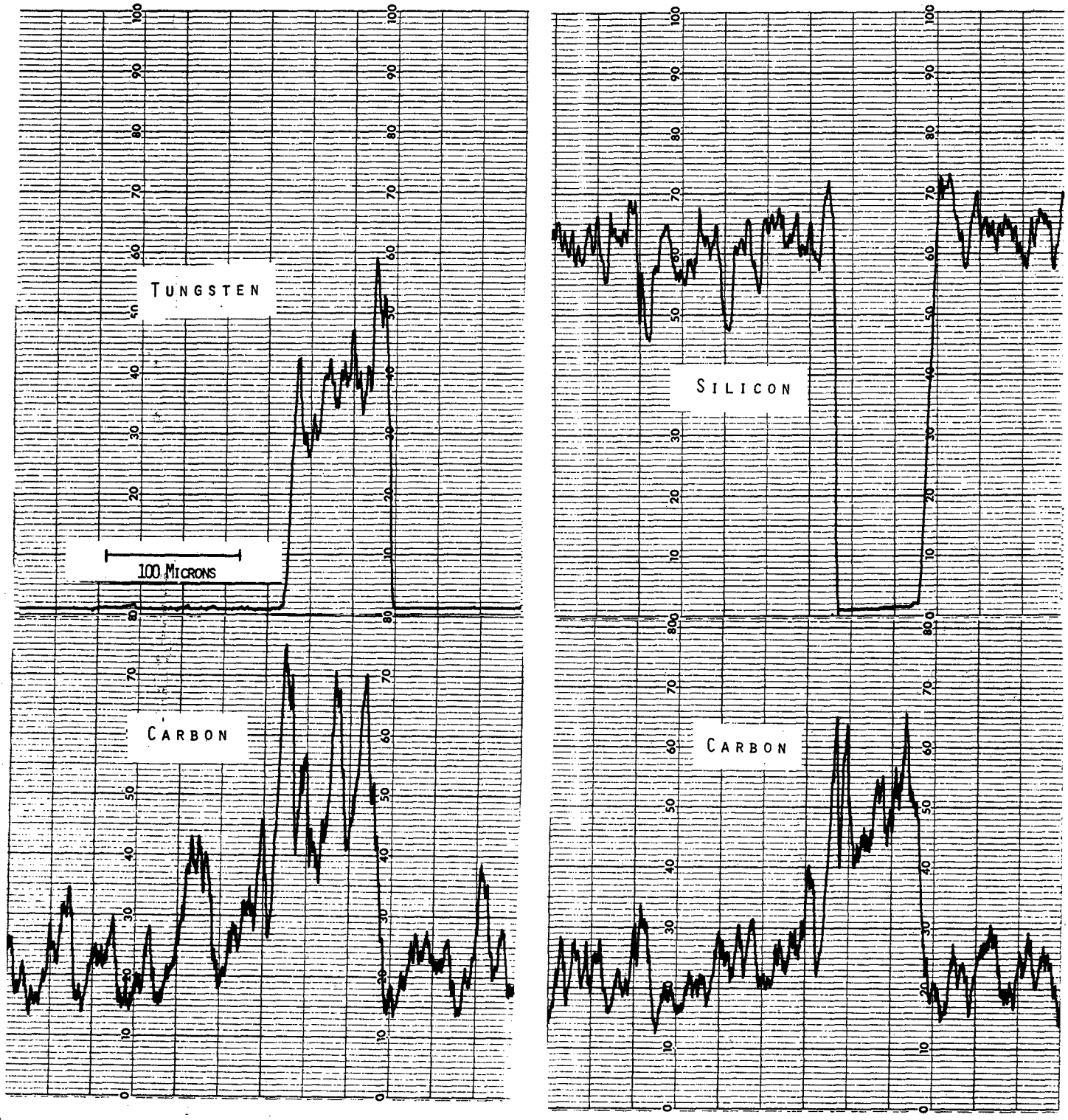

Figure 47. Electron Beam Microprobe Traces of the Seeded Defect in Specimen 3-3.

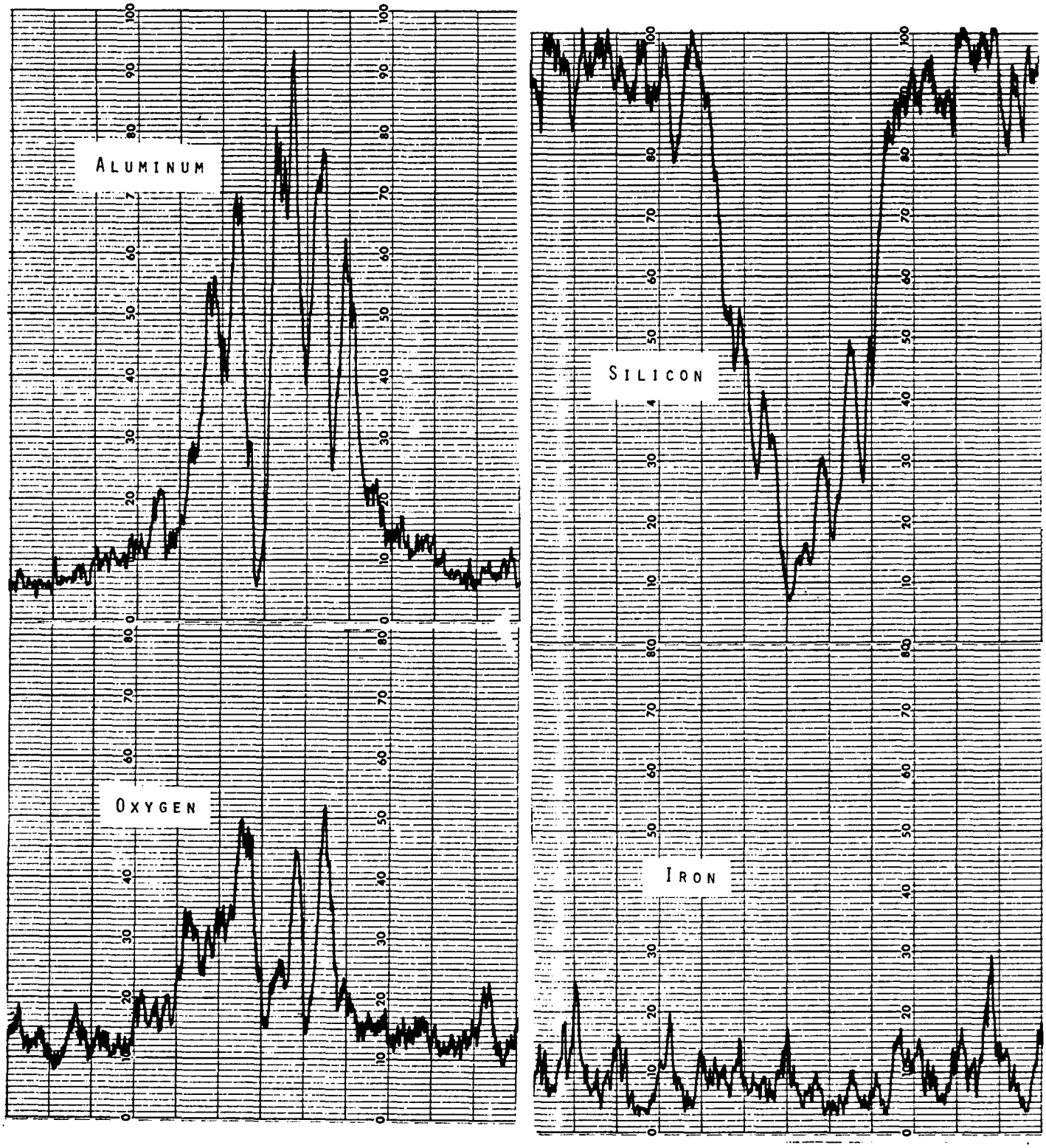

Figure 48. Electron Beam Microprobe Traces of the Seeded Defect in Specimen 3-5.

6.3.5 Correlation With Ultrasonic Results

Seven of the eight defect free control specimens tested broke without revealing any significant internal defects. One broke through a 60 μm defect which was not detected ultrasonically. Of the sixteen defect containing specimens, four (1-3, 1-4, 3-3, and 3-5) broke through defects that give every evidence of being the ultrasonically detected defects. Two other specimens gave uncertain results. Specimen 4-4 broke through a defect of about the right size (100 μm) and depth in the specimen, but located so far from the center that only a gross machining error could explain its location. Specimen 2-1 initiated fracture from a corner, but it broke through a 40 μm defect in the proper location to be the one detected ultrasonically. Furthermore, the ultrasonic signal strength correlates well with the defect size if the defect is WC. However, electron microprobe analysis failed to indicate the presence of WC at this location. Based on these results, it is difficult to draw any convincing conclusions about specimens 4-4 and 2-1.

In considering why the other specimens did not break through ultrasonically detected defects, two explanations can be supported by the existing evidence. The first is that the accuracy in locating the defects was not as good as expected and some of the defects were machined away. This explanation is supported by the fact that the two seeded defects broke the tensile surface of their specimens. The second explanation is that the specimens contained corner or surface flaws that caused the specimens to break at a lower strength than that associated with the defect. This explanation is supported by the fact that those that did break through ultrasonically detected defects showed higher strength than some of the specimens that broke from surface or corner flaws. Examination of the ultrasonically detected defects that were exposed by specimen fracture showed that the smallest defect that could be definitely identified as having been detected ultrasonically was the 25 μm void in specimen 1-4. Thus, the program goal of showing that high frequency ultrasonics is capable of detecting defects in the 10 to 100 μm size range was accomplished.

In Table IV, calculated defect sizes are shown, along with the values measured for defects examined by fractography. The calculated sizes are based on the theory that the ultrasonic signal amplitude is proportional to the cross-sectional area of the defect in the plane perpendicular to the ultrasonic beam. The values for low density inclusions were calculated based on the measured size of the seeded defect in specimen 3-5. The values for high density inclusions were calculated based on the measured size of the seeded defect in specimen 3-3. The 40 μm value calculated for specimen 1-4 indicates that a void is easier to detect than a low density inclusion. The values calculated for specimens 2-1 and 3-2 indicate that the defects, which could only be detected at 45 MHz, were in the 10 to 45 μm range, depending on their type.

No correlation was observed between the ultrasonic signal level and flexural strength. This is to be expected, of course, since most of the specimens did not initiate fracture at ultrasonically detected defects. However,

TABLE IV

RELATIONSHIP OF ULTRASONIC SIGNAL LEVEL AND DEFECT SIZE

Specimen (No.)	Signal Level[1] (mV)	Defect Size[2] (μm)		
		Calculated[3] for		Measured[4]
		Low Density Inclusions	High Density Inclusions	
1-3	5.4	150	-	25x850
3-4	5.2	145	-	-
4-4	5.7	155	-	100[5]
4-5	7.9	180	-	-
1-1	1.1	70	200	-
4-1	1.2	70	200	-
4-2	2.5	100	290	-
4-6	1.5	80	225	-
1-2	0.5	45	130	-
1-4	0.4	40	-	25
3-1	0.3	35	100	-
4-3	0.4	40	115	-
2-1	0.06	16	45	40[5]
3-2	0.04	13	35	-
3-3	0.5	-	-	130
3-5	4.1	-	-	130

NOTES:

(1) The "Signal Level" is the magnitude of the defect reflected acoustic signal, which was considered here in relation to the arbitrary reference magnitude obtained from Specimen No. 3-5. The signal level is expressed in the units in which the quantity itself is measured (mV).

(2) The "Defect Size" is expressed in the units in which the spherical shape defect itself is measured (diameter in μm).

(3) Defect sizes were calculated by using either specimen No. 3-5 (low density inclusion) or 3-3 (high density inclusion) as arbitrary reference points, and assuming that the signal level is proportional to the diameter squared of a circular cross-section reflector.

(4) Defect sizes were measured using SEM fractography.

(5) The correlation between the measured and the ultrasonically detected defect sizes is uncertain.

from the appearance of the defects that were exposed by fracture, it was concluded that no correlation should be expected for the experimental geometry employed. The defects observed were all compressed in the direction of hot pressing (the billet 1/4-inch (0.63 cm) thickness) so that their major axes were in the plane of the billet. Since the ultrasonic beam was parallel to the hot pressing direction, the defects were favorably oriented to produce the maximum ultrasonic defect signal. The specimens, however, were machined with their length in the plane of the billet, since the billet thickness was too small to allow specimens to be made parallel to the direction of hot pressing. Therefore, the defects were oriented in the specimens so as to have a minimum stress intensity factor with respect to the direction of testing. For the particular specimen geometry in question, ultrasonic shear wave inspection would be much more likely to show a correlation with flexural strength.

In the previous sections of this report the seeded defects are referred to as either voids or WC particles. The results of the fractography and microprobe analysis show that the seeded "void" is apparently aluminum oxide. This discrepency is a result of the fact that the billet manufacturer stated that he would insert a material in the billet that would be destroyed during billet fabrication in order to create a void. The material used was a piece of 125 μm diameter aluminum shot. Apparently, during processing it oxidized and remained intact as a low density inclusion. It is interesting to note that the low density and high density (WC) seeded inclusions were about the same size and were both open to the surface. But the specimen containing the low density inclusion was extremely weak, while the one containing the high density inclusion was only slightly below average in strength. In this case the relatively higher level of ultrasonic signal correlates with the weaker material.

In summary, although the data available from fractography is limited, a number of conclusions can be drawn from the experimental results.

1. High frequency ultrasonics is capable of detecting defects in the 10 to 100 μm range of interest in hot pressed silicon nitride. Detection of a 25 μm void at a frequency of 25 MHz has been verified.

2. The size defect that can be detected depends on the material of the defect (acoustic impedance mismatch). Voids are most easily detected. For smaller size inclusions, particularly high density ones, higher frequencies are needed.

3. Defects in pressed materials tend to be flattened in the plane perpendicular to the pressing direction (preferred orientation). In billets such as those used in this program, this causes the defects to be favorably oriented for detection using longitudinal waves, but unfavorably oriented to cause specimen failure in the directions that can be tested. For this reason shear wave inspection is more likely to provide a correlation with flexural strength.

6.4 Sintered Silicon Carbide Evaluations

The ultrasonic inspections of the billet of sintered silicon carbide showed areas of indications at 25 MHz similar to the lines found on a contour map (Figure 14). At 45 MHz these same patterns were superimposed on a general background of indications. Specimen areas were selected in this billet to provide a contrast between material exhibiting the pattern of defects and material containing only the general background indications.

6.4.1 Specimen Preparation

Eight specimens were cut out of corner #4 of the billet as shown in Figure 49, again with the billet thickness as the specimen width. Specimens 1-1 through 1-4 are in a relatively defect free area while specimens 2-1 through 2-4 intersect one of the major defect patterns. In order to maintain the two-to-one width-to-thickness ratio with this thin billet, the specimens were made 0.168 x 0.084 x 1.25inches (0.427 x 0.213 x 3.18 cm). As with the hot pressed silicon nitride, 0.002 inches (50 μm) was removed from the tensile surface by grinding along the length of the specimen and the corners were chamfered 0.005 inches (125 μm) at 45°.

6.4.2 Flexural Strength

The specimens were tested by the procedure described in Section 6.2. The four point-bend strength data are presented in Table V. The results did not indicate any strong correlation between strength and location within the panel, since there was considerable scatter within each group. The mean and standard deviation values for the total population, 249 and 78 MN/m^2 (36.2 and 11.3 ksi) were of the same order as determined separately for each group. These strengths appear to be low and with considerable variability, compared to published data on other sintered silicon carbide materials (Ref. 28). It should be observed however that during cutting with a diamond wheel there was more of a tendency for chipping with this material, and although the specimen corners were ground, residual machining damage may have been present.

6.4.3 SEM Fractography

The same procedures used to examine fracture surfaces in hot pressed silicon nitride were used with these specimens. In general, there was no obvious defect/fracture initiation correlation with the sintered silicon carbide specimens, in contrast to the data obtained on hot pressed silicon nitride. Several possible fracture initiation sites could be identified on each specimen.

Figure 50 is a series of SEM fractographs of Specimen 1-1 illustrating typical "flaws" found in most of these specimens. As before, the photographs are presented with the tensile surfaces, of the mating fracture surfaces, closest together. The markings visible on the compression surface in the low magnification photographs are due to residual wax pencil traces used to identify the desired load direction. In this specimen fracture appeared to

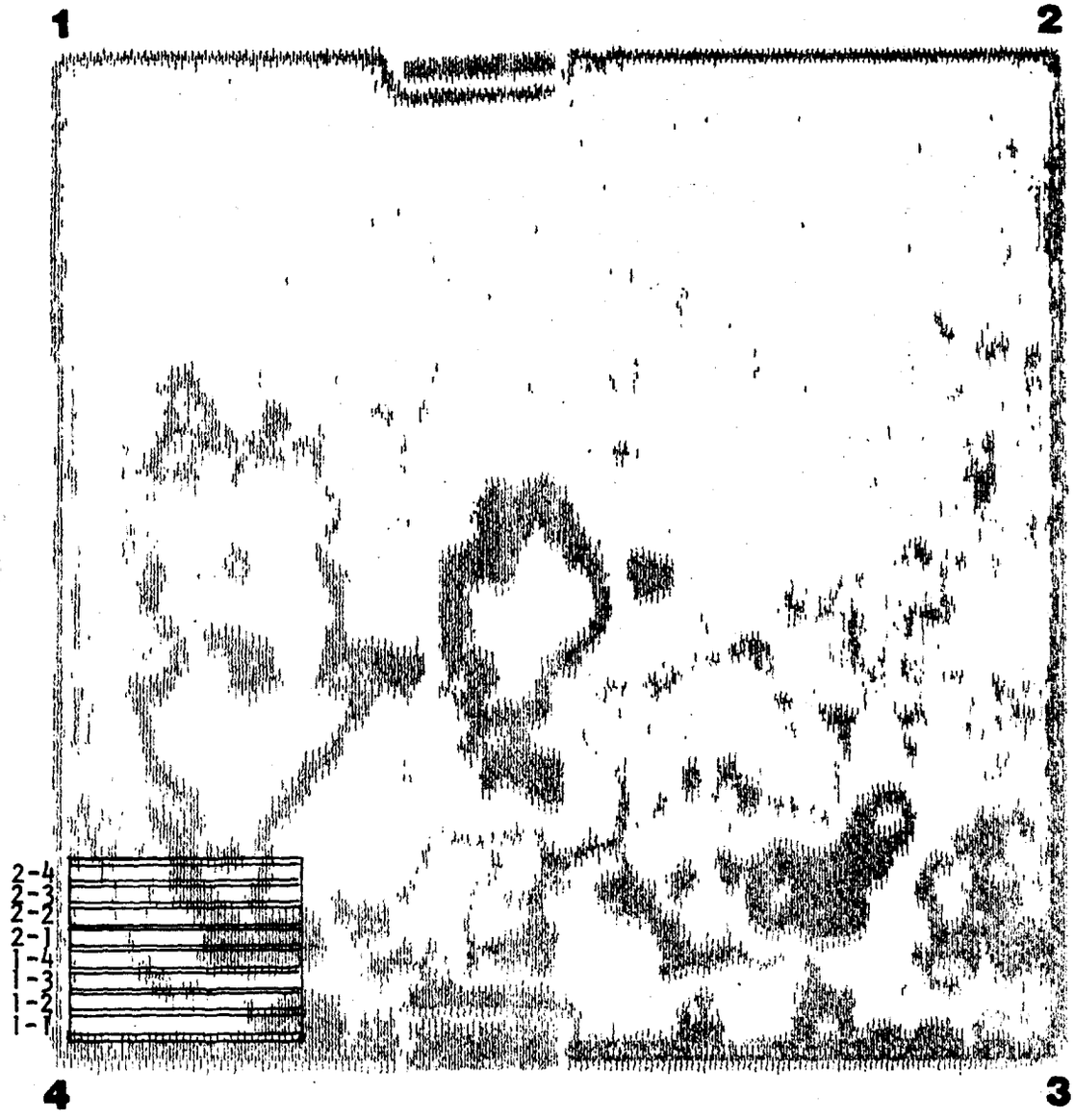

Figure 49. Location of Four Point-Bend Specimens With Respect to 25 MHz Inspection Results in Sintered Silicon Carbide.

TABLE V

FLEXURAL STRENGTH OF SINTERED SILICON CARBIDE SPECIMENS

Specimen (No.)	Flexural Strength MN/m2	ksi	Fracture Initiation Site/Flaw Type(1)
1-1	261	37.9	Corner Edge/A or C
1-2	346	50.2	Corner/E
1-3	163	23.6	Edge/E
1-4	314	45.5	Corner/E
2-1	185	26.9	Edge/E
2-2	172	24.9	Sub-Surface or Corner/A
2-3	207	30.0	Corner/E
2-4	347	50.4	Edge or Corner/E

NOTES:

(1) Flaw Types:
- A Large Void
- B Incluson
- C Line Defect
- E Unidentified

A. Corner and Edge Possible Initiation Sites Indicated.

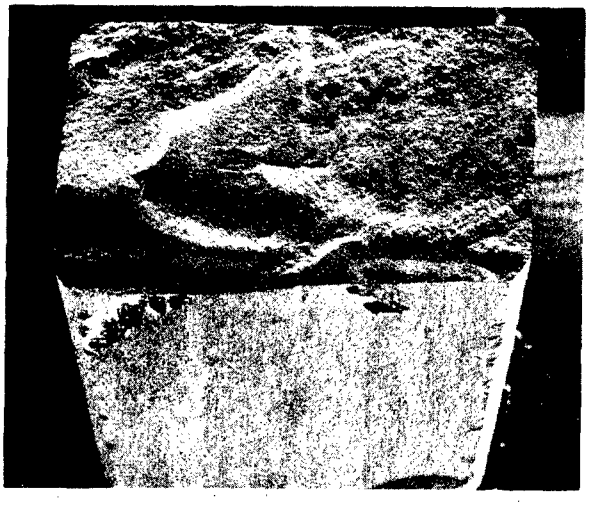

Figure 50. Fracture Surfaces of Sintered Silicon Carbide Specimen 1-1.

16X

B. Chipped Corner Indicated.

Large Void Indicated

Figure 50.
(cont.)

200X

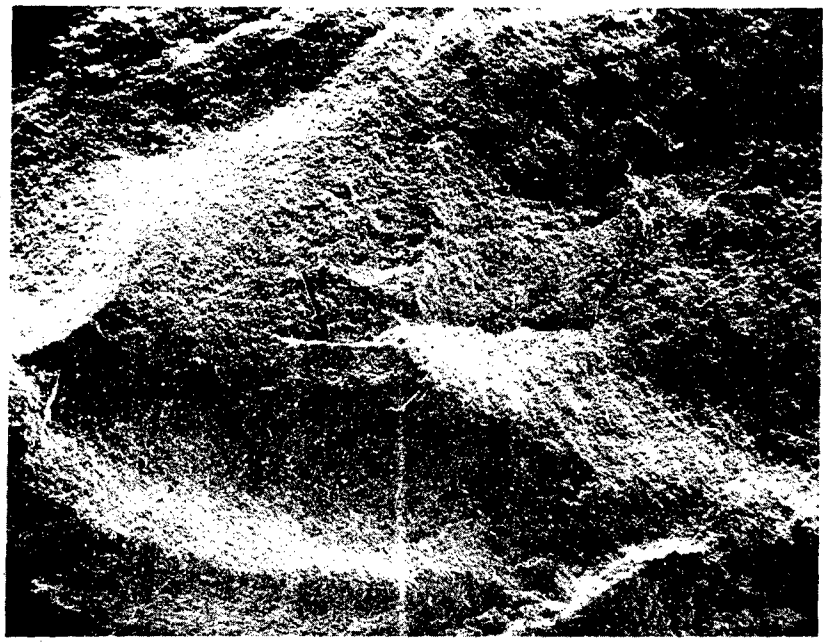

C. Internal Line Defect. 50X

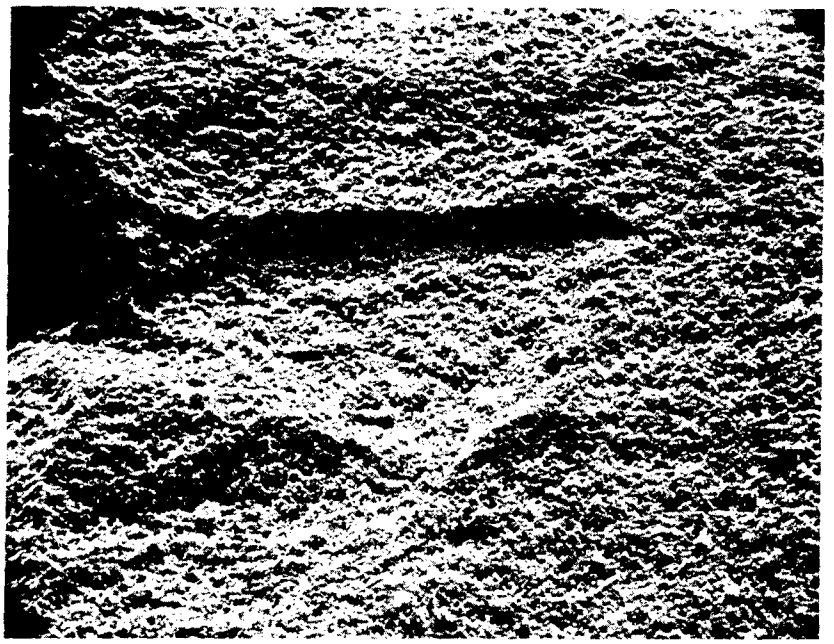

Same Area as Above Rotated 180° 200X

Figure 50.
(cont.)

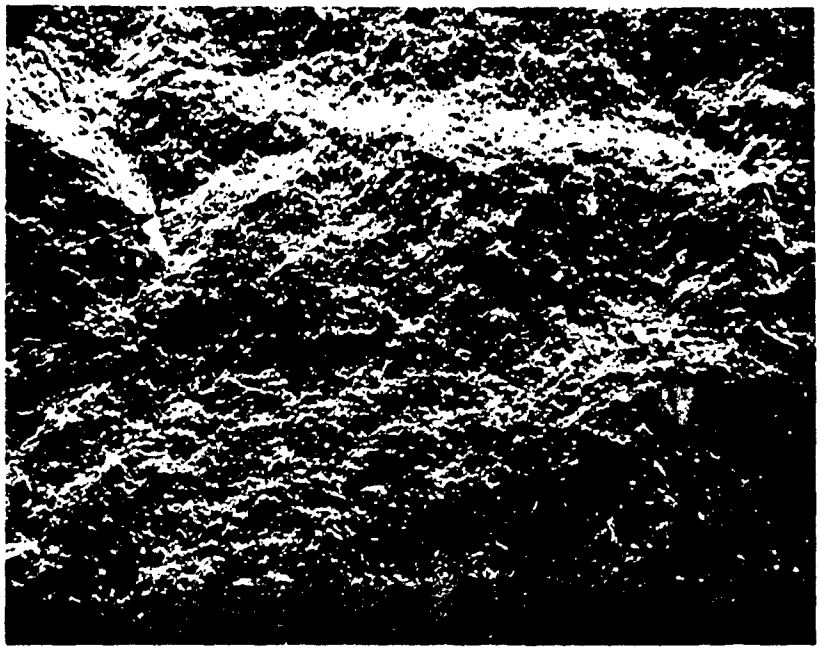

D. Line Defect and Void Indicated.

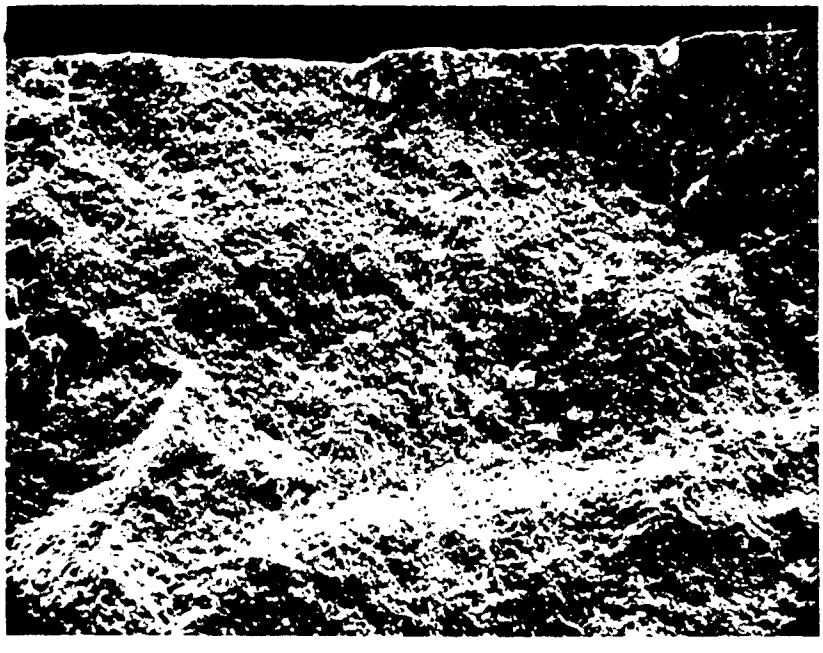

Figure 50.
(cont.)

200X

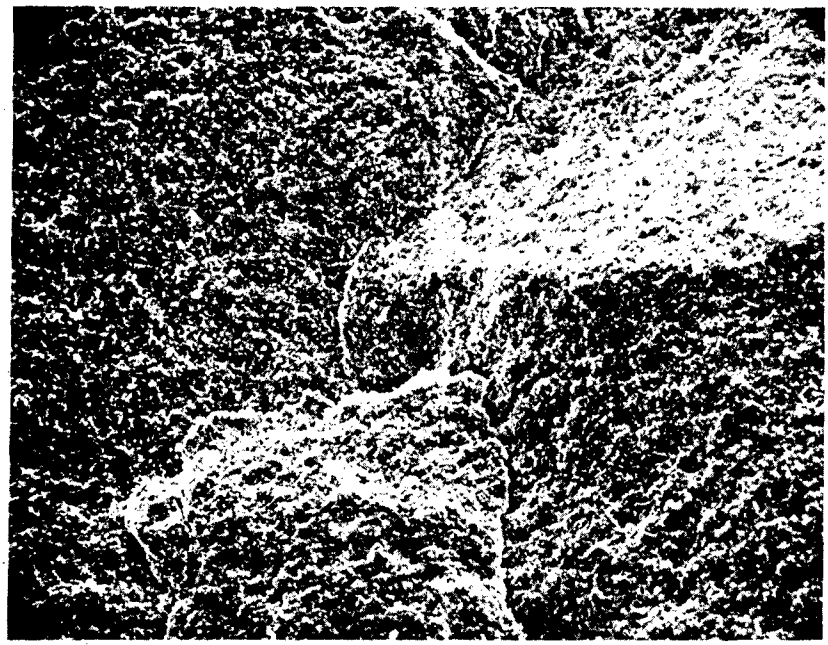

E. 200X

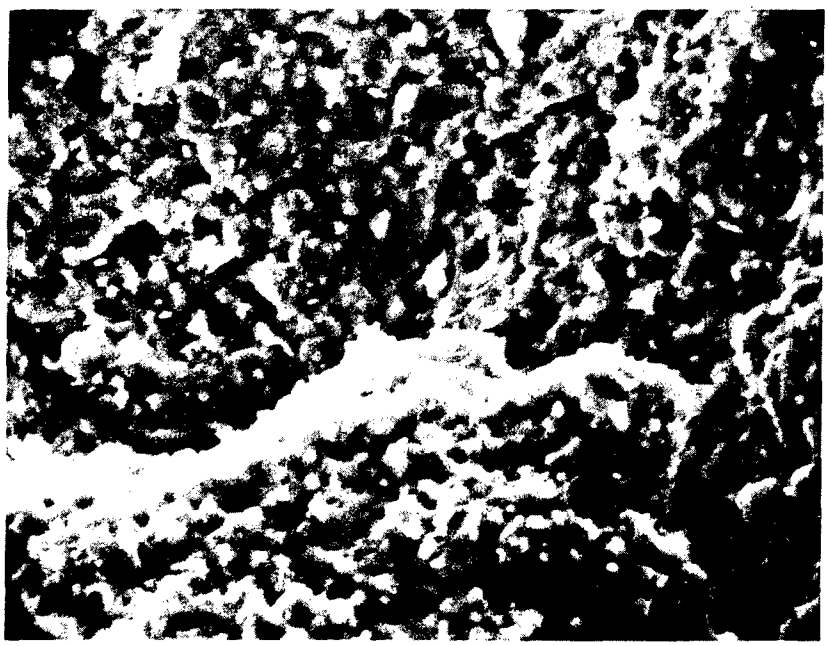

Secondary Cracks and Microporosity. 1000X

Figure 50.
(cont.)

have initiated at the right hand corner or edge (Figure 50-A), but there was not the well defined mirror area observed in many of the silicon nitride specimens. There was also a line defect visible running horizontally and close to the neutral stress axis. The micrographs in Figures 50-B to 50-E show representative "defects" which were typical of many of these specimens at higher magnifications. Figure 50-B shows the corner of Specimen 1-1 where fracture could have initiated. The apparent remains of a large chip is visible (top photograph) at the tensile surface which may have created sufficiently high stress concentrations to initial failure. The general area near the corner location however appeared to contain several larger-than-average pores of the order of 10 μ m diameter, and a large void (~40 μ m) is indicated in the lower photograph in a region roughly corresponding to the center of the mirror region. The horizontal line defect visible in the low magnification fractographs is shown in Figure 50-C. This has some of the appearance of the "stepped flaw" defect referred to by Gruver et al (Ref. 27) in hot pressed silicon nitride. A crack was visible at the end of this "defect" which may be just part of a multiple crack system in the fracture surface. Figure 50-D shows a region near the tensile surface and close to the center of the specimen which may have been a secondary fracture nucleation site. The only obvious structural details were the presence of a small trench with a crack running vertically (top picture) and a secondary crack system running parallel to the fracture surface. There is also a larger-than-average sized void indicated by the arrow, close to the specimen surface. Figure 50-E shows more secondary fragmentation regions and the high magnification photograph indicates an average pore size of about 1-1/2 μm.

Low magnification fractographs of Specimens 1-3 and 2-4, representing the lowest and highest strength materials from this series of specimens, are shown in Figures 51 and 52. The major difference in the appearance of the two fracture surfaces was that the weaker material had a much smoother or flatter topography and appeared to contain more of the 10-20 μ m size pores. There was also a stepped or faceted region at the right hand side of the weaker specimen and a small, but fairly well defined semi circular mirror region at one edge. It was difficult to assign an unambiguous fracture original site to either specimen.

More evaluations should be performed on this material, taking additional precautions to minimize surface damage during specimen machining.

6.4.4 Correlation With Ultrasonic Results

In examining the fracture surfaces of the sintered silicon carbide specimens, it is evident that the ultrasonic defect patterns are associated with the areas of secondary fragmentation, such as the one located about one-third of the specimen thickness from the left side in Figure 52. Areas of this type are typical of Specimens 2-1 through 2-4 and in each case the area is about one-third through the specimen and favorably located for ultrasonic detection. Areas of this type also show up in some of the specimens in the other group, such as Specimen 1-1 (Figure 50A). However, they tend to be oriented at a steep angle to the inspection direction which was unfavorable for defect detection. The nature of these flaws could not be determined by fractography. The only explanation observed for the general background of

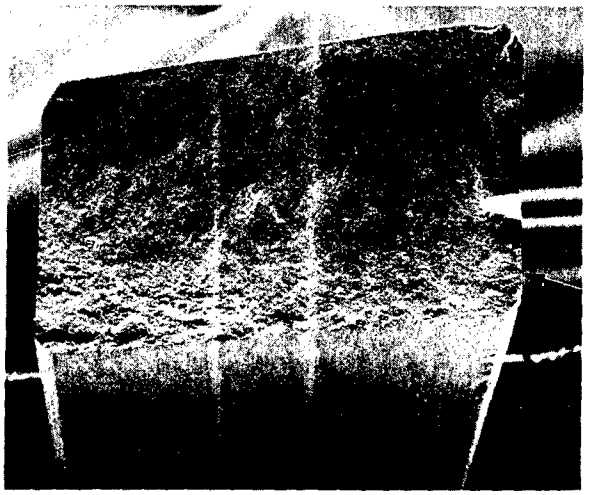

Possible Edge Initiation Site Indicated. 16X

Figure 51. Fracture Surfaces of Sintered Silicon Carbide Specimen 1-3.

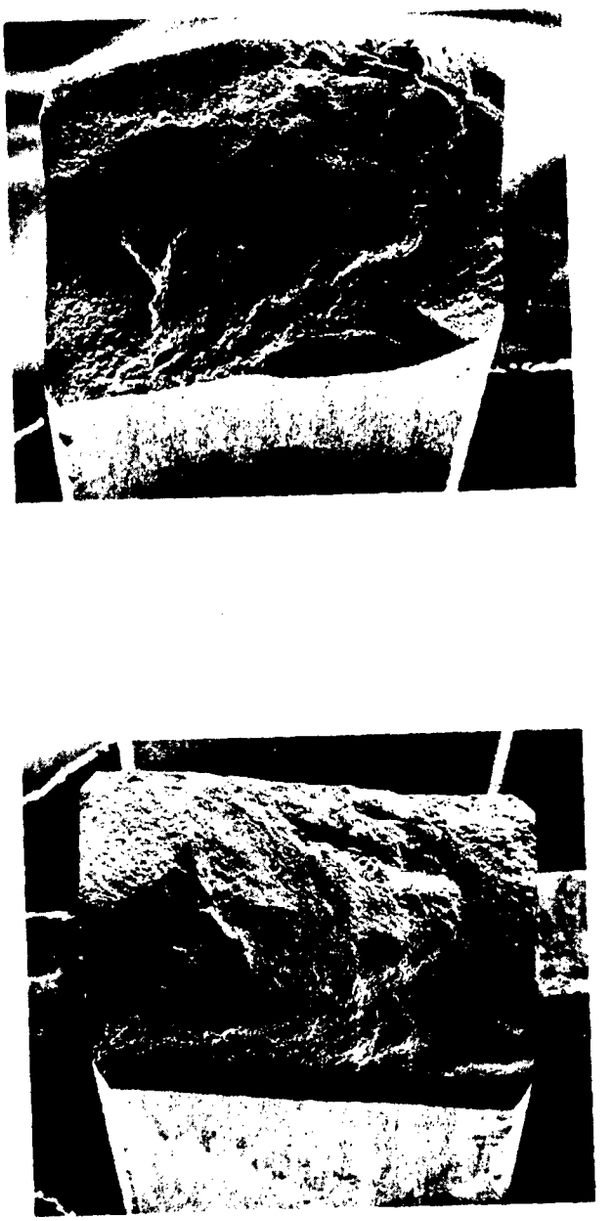

Figure 52. Fracture Surfaces of Sintered Silicon Carbide Specimen 2-4.

16X

indications seen at 45 MHz was the porosity of this material. These pores, however, were quite small, with the largest being in the 10 to 20 μm range. Since there is no significant difference between the flexural strengths of the two groups of specimens, no correlation could be shown between the material strength and the ultrasonic indications.

6.5 Reaction Bonded Silicon Nitride Evaluation

The ultrasonic inspections of the billet of reaction bonded silicon nitride revealed a general background of indications. Since the frequency of these indications was lower in areas of higher acoustic velocity (and, therefore, higher material density), it was assumed that these indications resulted from the pores in the material. Therefore, the specimens for flexural strength measurements were divided into two groups representing the extremes of indication frequency.

6.5.1 Specimen Preparation

Four specimens each were cut out of corners #1 and #4 of the billet as shown in Figure 53. Corner #1 was an area of low defect frequency and corner #4 was an area of high defect frequency. The specimens were made 1/8 x 1/4 x 1 1/4-inches (0.32 x 0.64 x 3.18 cm) using the billet thickness for the specimen width. The tensile surface was ground along the specimen length to remove 0.002 inches (50 μm) and the corners were chamfered 0.005 inches (127 μm) at 45°.

6.5.2 Flexural Strengths

The specimens were tested using the procedure described in Section 6.2. The four point-bend strength data from these tests are listed in Table VI. Although the number of tests were insufficient to obtain statistically meaningful strength distributions, there did appear to be a correlation with panel location, if specimen 1-4 was regarded as anomolous. The subsequent SEM fractography evaluations tended to confirm a correlation between acoustically indicated defect density, strength and observed defect density.

6.5.3 SEM Fractography

The same procedures as detailed before were used to examine all of the specimen fracture surfaces of reaction bonded silicon nitride. The large amount of porosity present in this material was evident even in the low magnification fractographs. The fracture surface of specimen 1-4, which had an anomalously low fracture strength, is shown in Figures 54 and 55. A large flaw (500 μm diameter) which appeared in the SEM as a bright powdery looking area was evident in the center of the specimen near the tensile surface. As can be seen in Figure 54, this flaw had a tail extending into the specimen giving a total length of about 1 mm. A similar but much smaller area was identified as the fracture origin in specimen 1-1. In other respects the fracture surfaces were very similar to those in the remainder of the specimens. Microprobe analyses to investigate the chemistry of this flaw have not so far been conducted. The average pore sizes in specimens 1-1 to 1-4 were of the order of 20 μm with a range of about 5 to 200 μm.

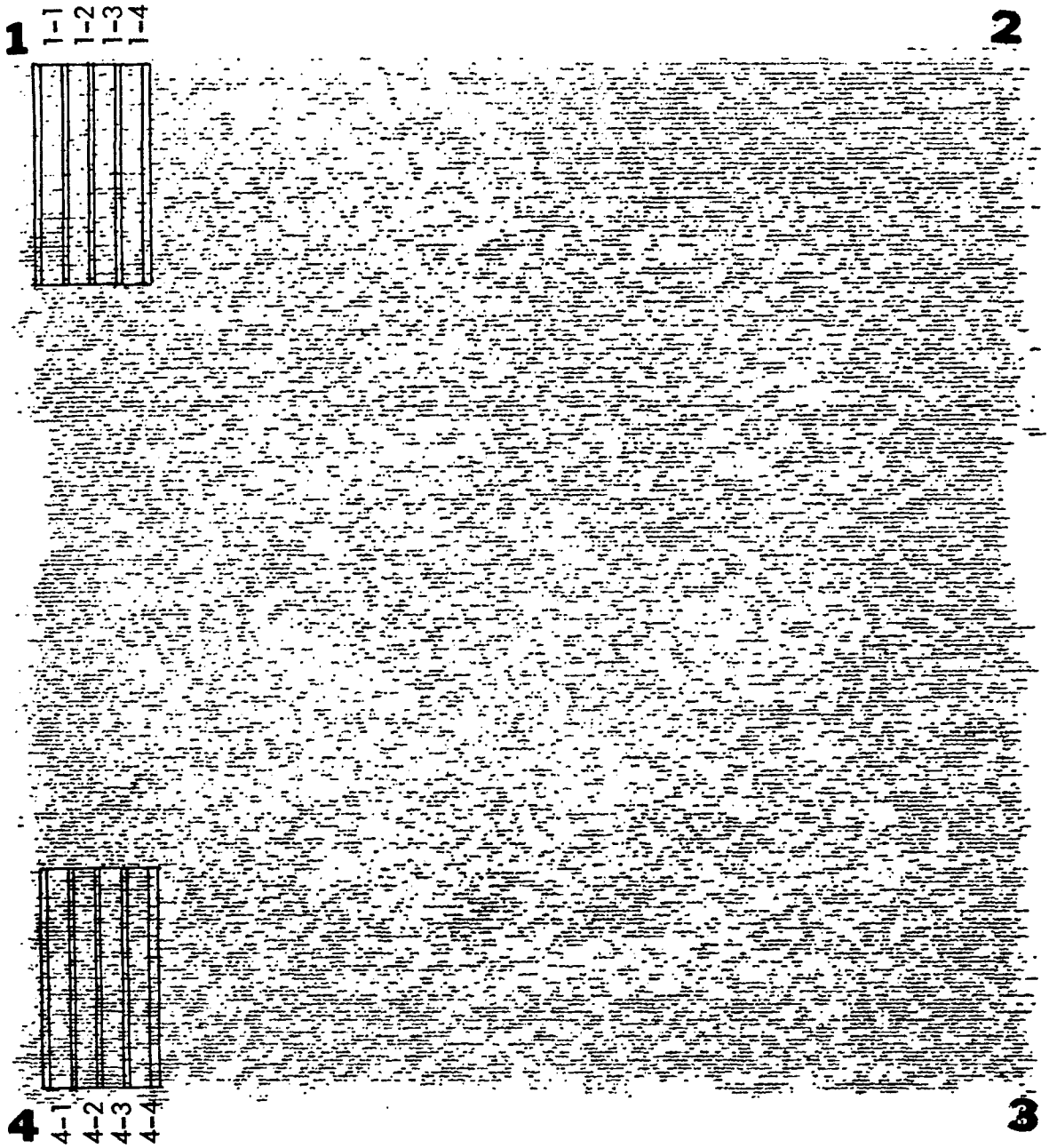

Figure 53. Location of Four Point-Bend Specimens With Respect to 25 MHz Inspection Results in Reaction Bonded Silicon Nitride.

TABLE VI

FLEXURAL STRENGTH OF REACTION BONDED SILICON NITRIDE SPECIMENS

Specimen (No.)	Flexural Strength MN/m^2	ksi	Fracture Initiation Site/Flaw Type(1)
1-1	130	18.9	Sub-Surface/B
1-2	139	20.2	Unidentified
1-3	152	22.1	Sub-Surface/A
1-4	103	14.9	Sub-Surface/B
4-1	87	12.6	Corner/D
4-2	128	18.6	No Obvious Initiation/C
4-3	122	17.7	" " " "
4-4	116	16.9	" " " "

NOTES:

(1) Flaw Types:
- A Large Void
- B Unidentified Inclusion
- C High Concentration of Voids
- D Surface Notch
- E Unidentified

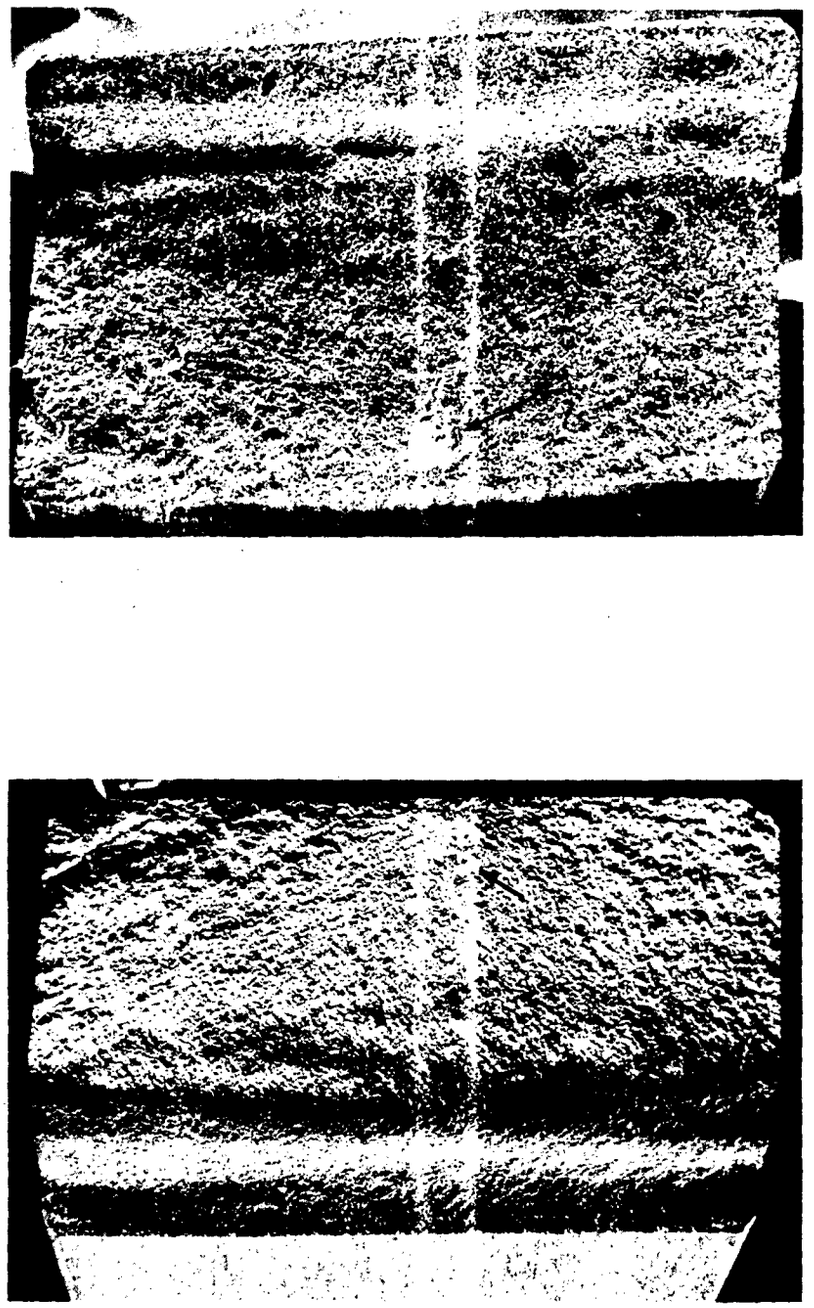

Figure 54. Fracture Surfaces of Reaction Bonded Silicon Nitride Specimen 1-4.

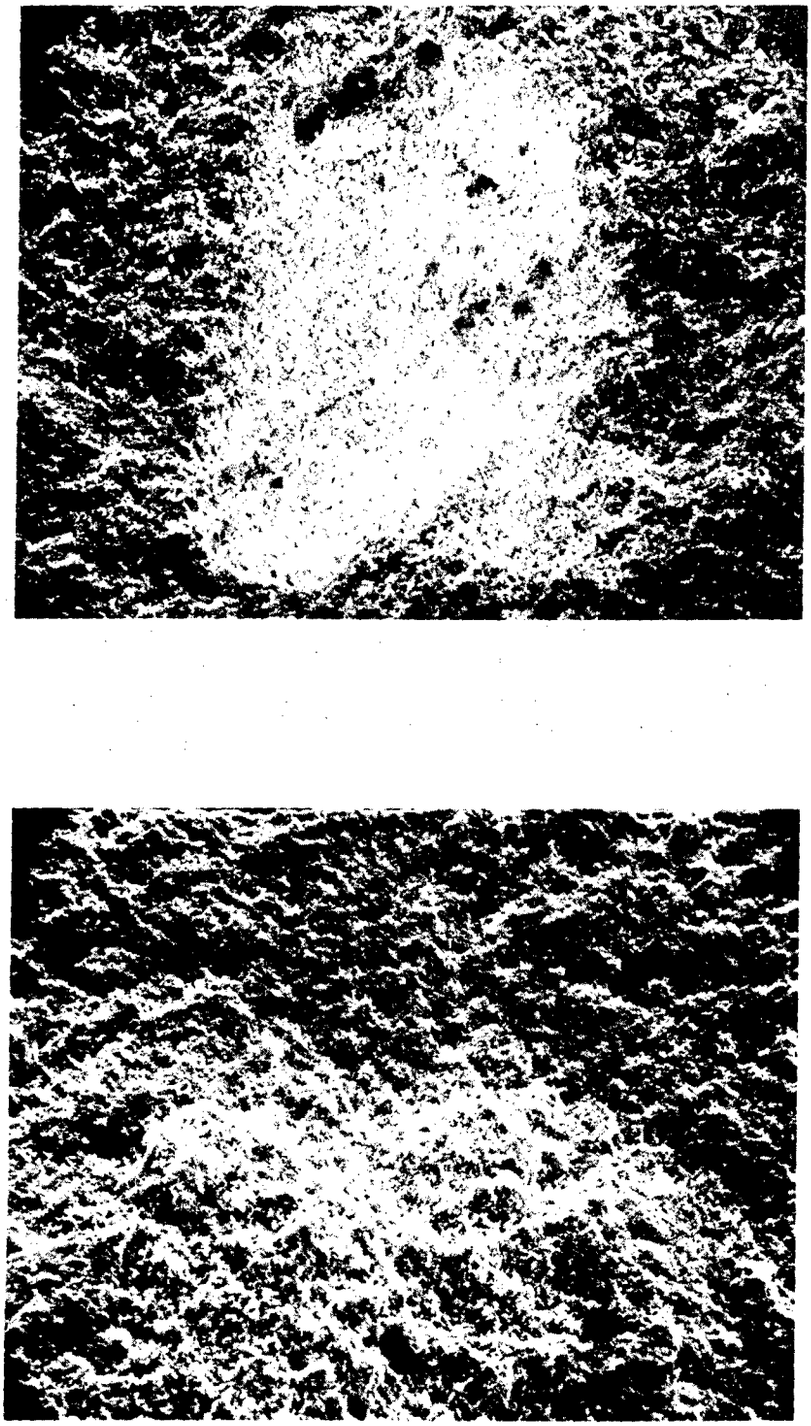

Figure 55. Unidentified Inclusion in Specimen 1-4. 200X

Figures 56 and 57 are SEM fractographs of specimen 4-2. A comparison of Figures 55 and 57 illustrates the differences in pore density between the two groups. The average pore size was not significantly different but as seen from Figure 57 there were many more of the 20 μm size, roughly spherical, voids present. In Figures 56 and 57 there are no obvious crack initiation sites visible.

6.5.4 Correlation With Ultrasonic Results

Examination of the fracture surfaces of the reaction bonded silicon nitride specimens verifies that the ultrasonic indications were primarily the result of pores. While some pores of about 200 μm were observed, the high density of ultrasonic indications can only be explained by assuming that pores on the order of 20 μm were detected.

The flexural strength data shows a correlation with the frequency of ultrasonic indications if the specimens that failed due to larger internal defects are ignored. On the other hand, the large defect in specimen 1-4 could not be distinguished from the general background of indications from the material pores. This suggests that this type of material should be inspected at a lower frequency and/or sensitivity in order to detect large defects without detecting pores. The results shown in Figure 16, for example, might be useful in identifying the larger defects in the material. Further work would be required to determine what size inclusion or other large defect could be detected at a sensitivity that would not show the general background of pores.

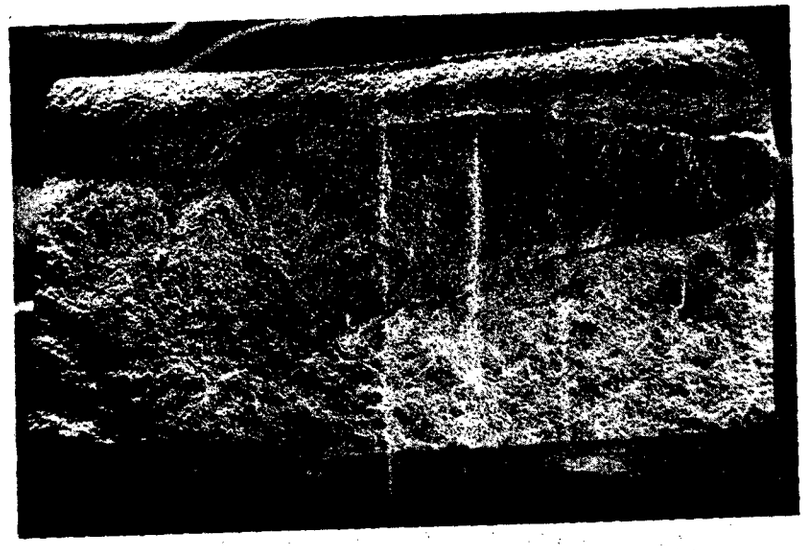

No Obvious Fracture Initiation Site. 16X

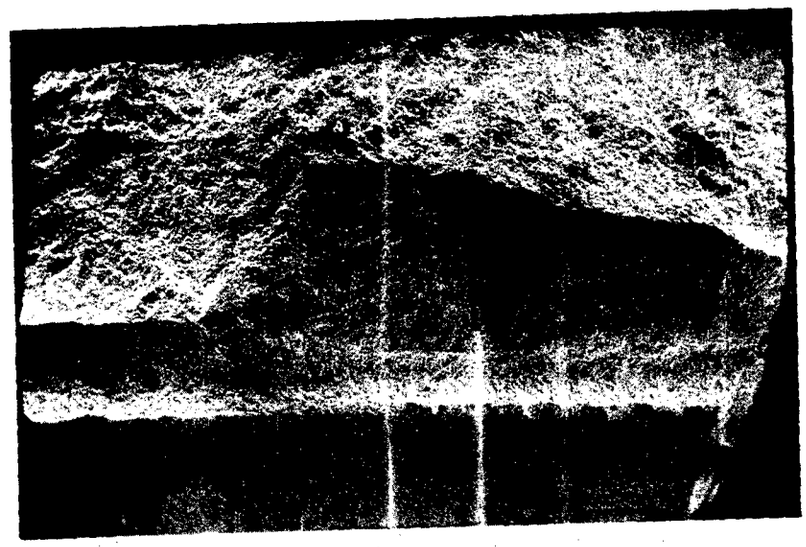

Figure 56. Fracture Surfaces of Reaction Bonded Silicon Nitride Specimen 4-2.

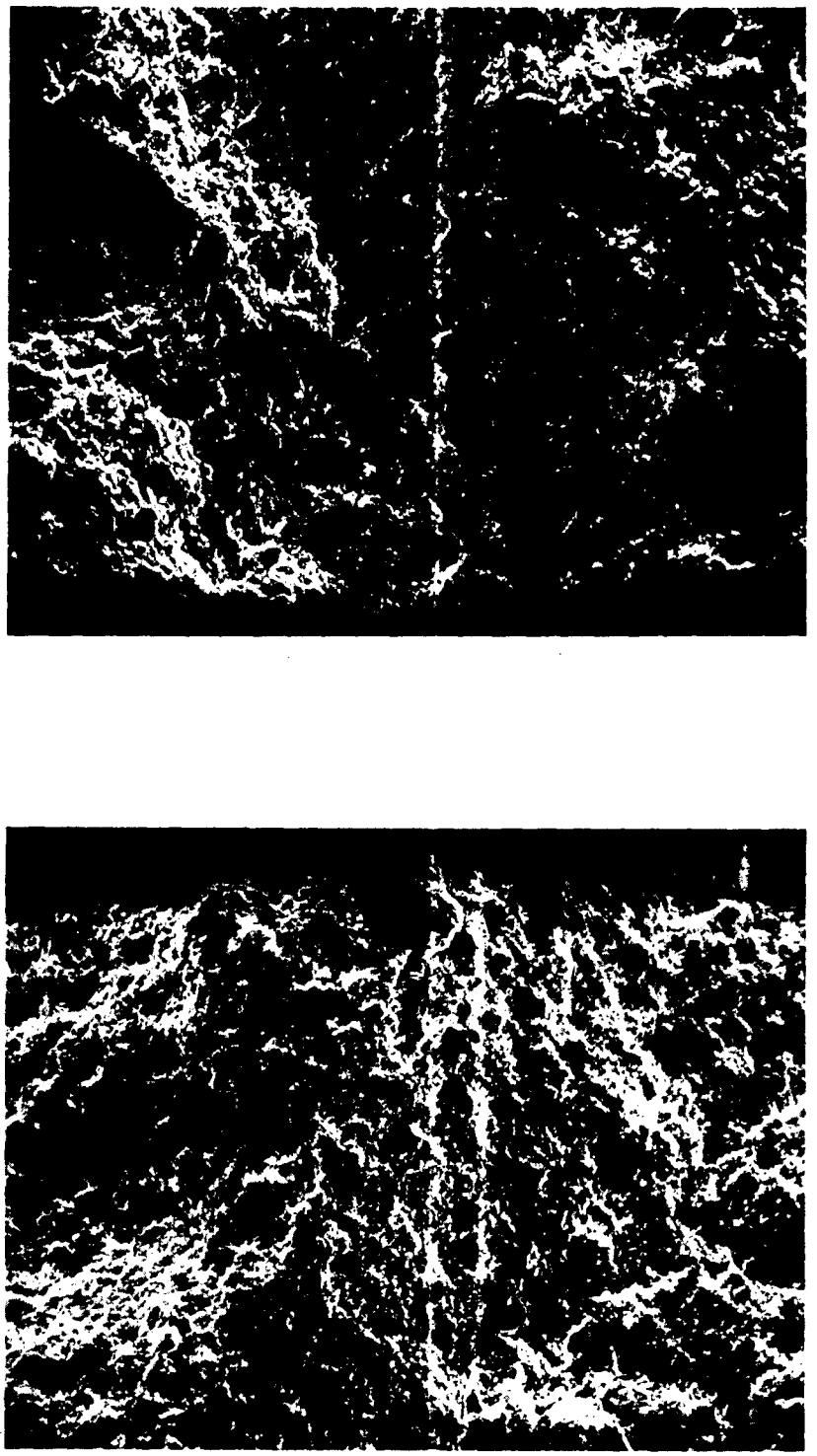

Figure 57. High Concentration of Voids in Specimen 4-2. 200X

7.0 CONCLUSIONS AND RECOMMENDATIONS

The program objective, demonstration of the capability of high frequency ultrasonics to detect defects in the 10 to 100 μm size range in gas turbine quality ceramics, has been accomplished. In addition, a number of conclusions have been drawn which indicate the direction that further investigation in this field should take. The four materials tested in this program all gave somewhat different results. Therefore, the specific conclusions and recommendations for each material are treated separately in the following sections.

7.1 Sintered Silicon Carbide

The general background of ultrasonic indications seen at 45 MHz seems to correlate with the pores in the material, the largest of which are in the 10 to 20 μm range. The contour patterns of ultrasonic indications correlate with areas of secondary fragmentation in the fracture surfaces. The nature of any defects associated with the secondary fragmentation, however, was not determined. The four point-bend specimens tested did not initiate fracture at the locations of ultrasonically detected defects and so no correlation could be established between the results of the ultrasonic longitudinal wave inspection and the material flexural strength.

It is recommended that further investigation of this material be carried out in order to establish the origin of the contour patterns of ultrasonic indications. It is further recommended that this material be inspected using ultrasonic shear waves in an effort to establish a correlation with flexural strength. In view of the general background of indications observed in the 45 MHz inspections, it is not recommended that higher frequencies be used unless a better quality material can be obtained.

7.2 Reaction Bonded Silicon Nitride

It was concluded that a correlation exists between the flexural strength of this material and the frequency of ultrasonic indications resulting from the general distribution of pores on the order of 20 μm in the material. However, the high density of ultrasonic indications from these small pores makes it difficult to identify indications from inclusions which were observed to have a significant effect on material strength.

There is some lower ultrasonic frequency which would allow the general background of pores to be ignored while detecting larger pores and inclusions. Further evaluations would have to be performed in order to determine what size defects could be detected under such circumstances and whether or not such a technique would be useful for quality control of this material. Such an investigation, however, was not considered within the scope of the present program.

7.3 Hot Pressed Silicon Carbide

This material was not submitted for mechanical testing because the ultrasonic inspections yielded so few defect indications that no significant results could be anticipated. It is recommended that this material be further evaluated at higher frequencies and using shear as well as longitudinal waves in an effort to identify enough defects to allow a statistically significant mechanical testing program to be conducted. It is further recommended that, since the seeded defects could not be detected in this material, a suitable reference standard be developed to allow an estimate to be made of the size defects that are detected in this material.

7.4 Hot Pressed Silicon Nitride

Three definite conclusions were drawn from examination of the defects that were exposed by specimen fracture:

1. The smallest defect that could be correlated with an ultrasonic signal was a 25 μm void (that was detected at an ultrasonic frequency of 25 MHz).

2. There is about a factor of ten difference in the signal level from a low and high density inclusion of about the same size, shape and depth in the material. Therefore, ultrasonic inspection possesses a preferred defect detection sensitivity for low density inclusions (high acoustic impedance mismatch).

3. The defects were deformed due to the process of hot pressing, making them favorably oriented for ultrasonic detection using longitudinal waves traveling in the billet thickness (hot pressing) direction, but not for affecting material strength in the direction tested. Defects favorably oriented to reduce material strength in the direction tested would be more easily detected by ultrasonic shear wave inspection.

In addition, several tentative conclusions are suggested by the data, but further investigation is required to prove or disprove them. For example, calculations based on the signal level for the seeded defects indicate that, at a frequency of 45 MHz, low density inclusions of about 13 μm and high density inclusions of about 35 μm should be detectable with the available instrument sensitivity. Furthermore, the relationship between the calculated and measured size of the 25 μm void suggests that voids are easier to detect than low density inclusions, so that a void less than 10 μm might be detectable at a frequency of 45 MHz. The small effect that such small defects would have on material strength makes it difficult to verify these calculations by initiating a specimen fracture at such a defect.

No definite conclusion could be drawn as to why more of the specimens did not break through ultrasonically detected defects. Evidence was found to support two conclusions, either or both of which could explain the results. One is that the asymmetry and orientation of the defects cause those defects that give strong ultrasonic signals to have little effect on material strength. The other is that due to larger than expected errors in defining the defect locations, many of the defects were machined away rather than being present in the specimens.

The results of the work done on hot pressed silicon nitride show that the goal of the program has been achieved. It has been shown that high frequency ultrasonics is capable of detecting defects well into the 10 to 100 μm range in fully dense material. In order to demonstrate that this is a useful tool for quality control of ceramic parts, further development is needed in two related areas. One is the establishment of a correlation between material strength and the various types of defects that can be detected ultrasonically. The other is the development of higher frequency techniques to allow detection of defects on the order of 10 μm for those types of defects for which a correlation can be established. Based on the results to date, it is recommended that ultrasonic shear wave inspection be explored, since it seems more likely than longitudinal wave inspection to correlate with flexural strength in the type of specimens that can be conveniently tested.

8.0 APPENDICES

8.1 Transducer Characterization

In selecting a focused transducer for ultrasonic inspection, one must consider that the ultrasonic beam is refracted by passing through the interface between two materials in the same way that light is refracted by a lens. In the case of a sonic beam, the index of refraction is determined by the ratio of the velocity of sound in the two materials. In the case of hot pressed silicon carbide, for example, the velocity of sound is about eight times the velocity of sound in water, so that a transducer with a focal length of two inches in water is required to focus the beam on the back surface of a one-quarter inch thick ceramic plate. After evaluation of several transducers, two transducers were purchased, one with a resonant frequency of 25 MHz and one with a resonant frequency of 45 MHz. Both transducers were Aerotech Laboratories' type alpha transducers with one-quarter inch elements and nominal focal lengths of two inches in water.

The transducers procured on the program were fully characterized by TRW in-house laboratory measurements. First the electrical impedance of each transducer was measured using a network analyzer consisting of a sweeping signal generator and phase/amplitude tracking detector with an impedance adaptor (Ref. 29). The transducers were then pulsed using a TRW Model 100 Ultrasonic Pulser/Receiver and the time domain response was analyzed to determine the resonant frequency of each transducer and the effect of water path on the frequency spectrum of the reflected signal.

Figure 58 shows the output of the pulser with no transducer. Figure 59 shows the same output with the 25 MHz transducer loading the pulser. The vertical scales of both figures are 50 V/cm and the horizontal scales are 10 ns/cm. The transducer pulse risetime (from 10% to 90% of pulse height) shown on Figure 59 is 0.8 cm or 8 ns. The risetime is 80% of a quarter wave or 20% of a full wave, so that the period of the pulse is 40 ns, corresponding to a transducer frequency of 25 MHz. Figure 60 shows the pulse reflected back to this transducer off the surface of a flat ceramic plate located at the focal point in water which was found to be 1.8 inches. Figure 61 shows the pulse from the same target at a water path of only 0.50 inches. The vertical scales are 0.05 V/cm and 0.01 V/cm, respectively. The horizontal scales are both 100 ns/cm. These photographs were taken to determine the extent of frequency degradation due to selective attenuation in the water. In both cases the frequency is degraded to about 12.5 MHz. However, the difference in water path makes no significant difference. Figure 62 shows the unloaded pulse reduced to 100 volts in order to avoid overloading the 45 MHz transducer. The vertical scale is 20 V/cm and the horizontal scale 10 ns/cm. Figure 63 shows the same output with the 45 MHz transducer loading the pulser. The scales are the same as for Figure 62. In this case the pulse risetime is 4.25 ns, which corresponds to a frequency of 47 MHz. Figures 64 and 65, respectively, show the reflected pulse off a ceramic plate at the focal point in water, which was determined to be 2.0 inches, and at a water path of 0.5 inches. In both figures the vertical scale is 0.005 V/cm and the

Figure 58. Unloaded Output of TRW Pulser.
50 V/cm vertical; 10 ns/cm horizontal.

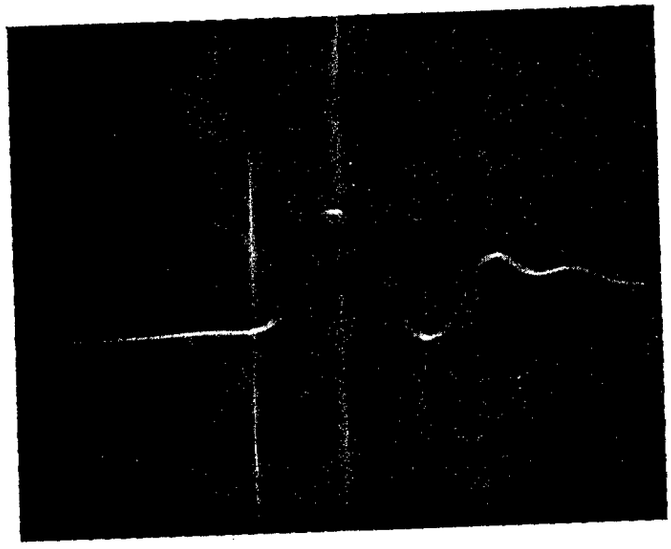

Figure 59. Output of TRW Pulser Loaded With 25 MHz Transducer.
50 V/cm vertical; 10 ns/cm horizontal.

Figure 60. 25 MHz Pulse Reflected From Ceramic Plate at Focal Point. .05 V/cm vertical; 100 ns/cm horizontal.

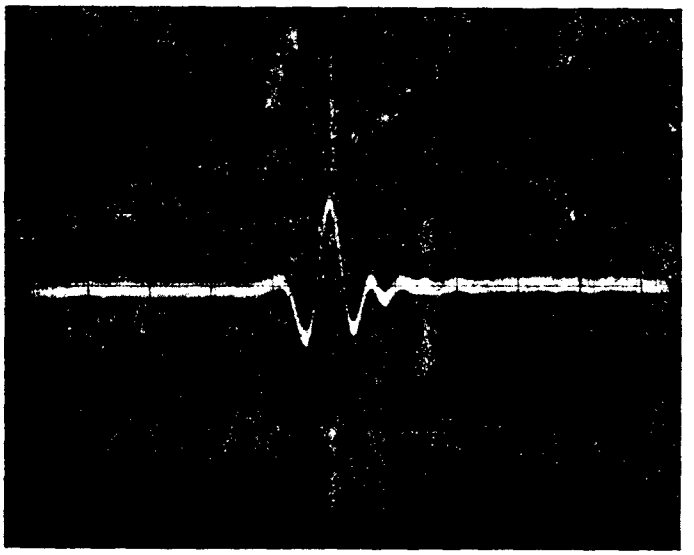

Figure 61. 25 MHz Pulse Reflected From Ceramic Plate at 0.5 Inch Water Path. .05 V/cm vertical; 100 ns/cm horizontal.

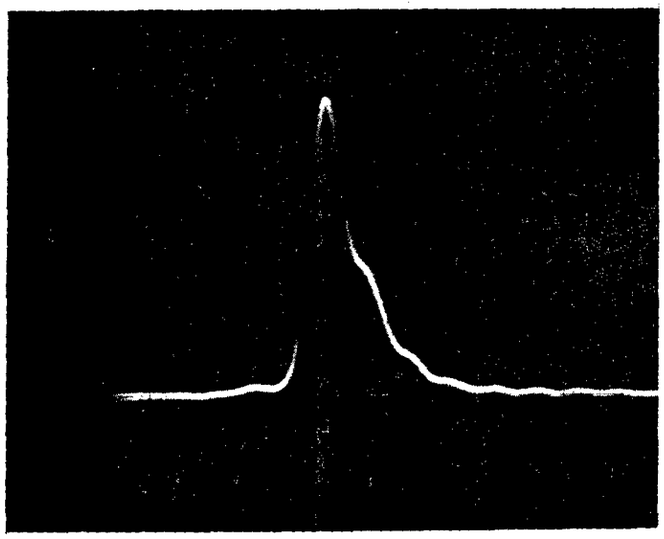

Figure 62. Unloaded Output of TRW Pulser Attenuated to 100 Volts. 20 V/cm vertical; 10 ns/cm horizontal.

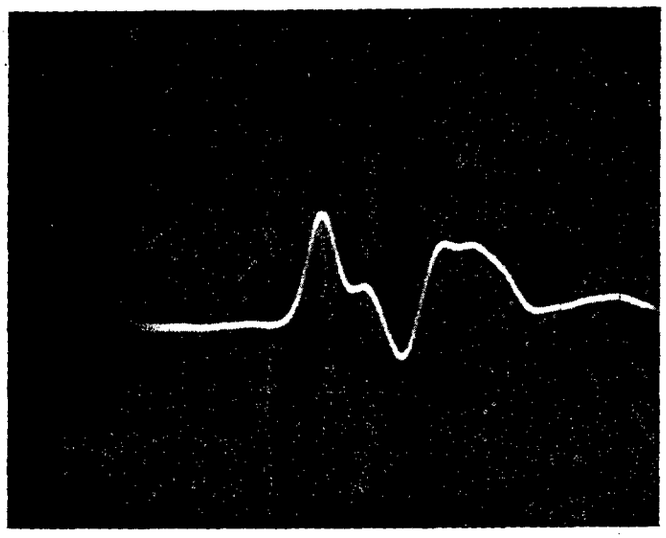

Figure 63. Output of TRW Pulser Loaded With 45 MHz Transducer. 20 V/cm vertical; 10 ns/cm horizontal.

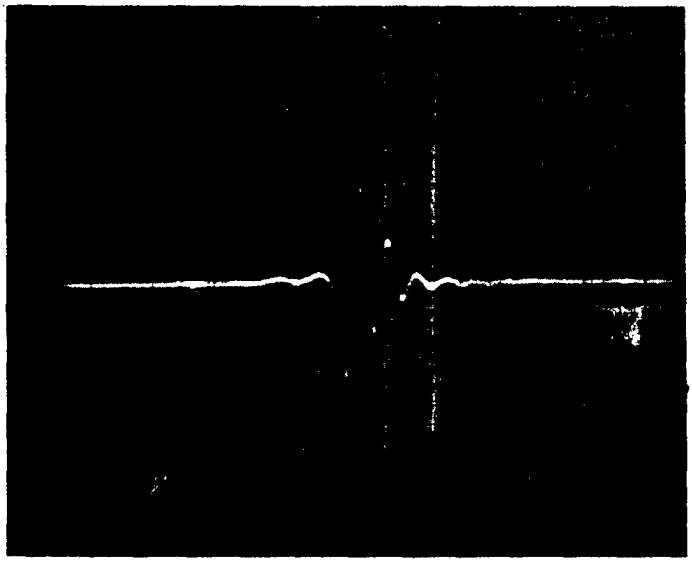

Figure 64. 45 MHz Pulse Relfected From Ceramic Plate at Focal Point. .005 V/cm vertical; 100 ns/cm horizontal.

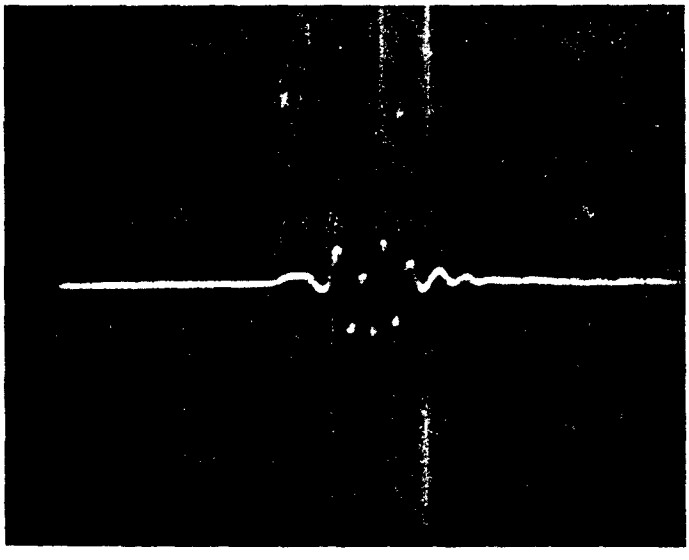

Figure 65. 45 MHz Pulse Reflected From Ceramic Plate at 0.5 Inch Water Path. .005 V/cm vertical; 100 ns/cm horizontal.

horizontal scale is 100 ns/cm. The pulse at 0.50 inches water path is 18 MHz while the pulse at 2.0 inches is 16 MHz, showing a slight frequency degradation due to the water path.

The low frequencies of the reflected pulses in these tests raised a question as to what frequency ultrasound is actually reaching the specimens. In questioning ultrasonic equipment manufacturers about this problem, two conflicting opinions were found. Instrument manufacturers expressed the belief that the lens used to focus the beam selectively attenuates the higher frequencies, causing the observed output to be predominantly lower than the transducer resonant frequency. The transducer manufacturer states that attenuation by the lens is small, and that the main problem is that even a high frequency pulser has a strong low frequency component which tends to dominate the transducer response.

Several experiments were run to obtain further data on this subject. First, a capacitive discharge pulser circuit was set up using a special fast turn-on time transistor. This circuit provided a critically dampened exponential time function pulse which was used to drive various ultrasonic transducers while varying the damping impedance to control the time function of the pulse to generate various pulse duration times to approximate the transducer frequencies. The ultrasonic beam was directed at a metal plate about one inch away, and the return signal was observed on a Tektronix 7844 high frequency oscilloscope. The results of this experiment are listed in Table VII. It was found that low frequency transducers, which usually have a very sharp resonance, respond at their resonant frequencies. High frequency transducers, however, respond at frequencies that depend on both the driving pulse rise time and duration. Even with a pulse rise time equivalent to 100 MHz and a duration equivalent to 45 MHz, the 45 MHz transducer only responded at 17 MHz. It is important to realize, however, that only the dominant frequency was measured in these experiments.

In order to determine the transducer response at specific frequencies, a sine wave generator with a range up to 65 MHz was used to drive each transducer. The 45 MHz transducer was used as a receiver when the 25 MHz transducer was driven. When the 45 MHz transducer was driven a thickness gaging transducer which is known to have a 45 MHz element was used as the receiver. Driving the 25 MHz transducer, signal output was detected up to 30 MHz. Driving the 45 MHz transducer, output was detected up to 50 MHz. In both cases the signal amplitude was stronger at frequencies below the resonant frequency and diminished gradually with frequency. This test indicates that high frequency ultrasound is reaching the specimen, but at a reduced amplitude which may be difficult to detect as a reflection from a defect.

8.2 Instrumentation Considerations

As a result of the initial inspections and the studies of transducer response as a function of driving pulse characteristics (see Appendix 8.1), it was evident that a modified pulser would provide improved defect detectability. The transducer frequency response depends on both the driving pulse rise time and pulse duration. While the pulser used in the preliminary inspection has a fairly good rise time (~10 ns), it has a long pulse duration and is badly loaded down by the low impedance of the high frequency transducers,

TABLE VII

TRANSDUCER FREQUENCY CHARACTERISTICS

Rise Time (1) (ns)	Duration Time (2) (ns)	Nominal Frequency (MHz)	Received Frequency (3) (MHz)
4	170	2.25	2
4	150	5	5
4	80	10	10
8	200	25	9
8	20	25	13
2	13	25	14
2	11	45	17

NOTES: (1) Pulse rise time is defined in accordance with IEEE recommended standards (E175/E203/42A65-9E4/19E4/31E3); namely, 10 and 90 percent of the peak pulse amplitude.

(2) Pulse duration time is defined as the time interval between the rise and fall of the pulse at which the instantaneous amplitude reaches a zero fraction of the peak pulse amplitude.

(3) In the case of the high frequency (25 and 45 MHz) transducers, a broad spectrum of received frequencies was present over a range of intensities, including frequencies at and above the transducers' resonant frequencies. The value listed in the table is the frequency of highest signal intensity.

resulting in a voltage on the transducer well below the maximum allowable. The TRW-100 pulser, which was used to measure transducer characteristics, provides a shorter rise time (equivalent to the resonant frequency of the transducer), a shorter pulse duration, and the capacity to provide the maximum allowable transducer voltage. In order to synchronize the TRW-100 pulser with the Erdman receiver and defect gate, the Erdman pulser was disabled and the trigger signal was used to trigger a signal generator which in turn could provide a strong enough trigger pulse for the TRW-100 pulser. This arrangement was used for all subsequent inspections. It provided superior defect detection capability, although the makeshift arrangement contributed significantly to noise problems which caused spurious indications on the C-scan recordings.

9.0 REFERENCES

1. "Silicon Carbide Parts Formed Easily Without High Pressures," Product Engineering, May, 1974, p. 31.

2. Lange, F.E., "Strong, High Temperature Ceramics," Technical Report Number 11, Contract N00014-68-C-0323, Office of Naval Research, (p. 5).

3. Parr, N.L. and May, E.R.W., Proc. Brit. Ceram. Soc., No. 7, 1967, (pp. 81-98).

4. Davidge, R.W., Gilling, D. and Wilyman, P.R., Special Ceramics V, ed. P. Popper, The British Ceramic Research Association, Stokes-on-Trent, England, 1972, (pp. 329-344).

5. Barnby, J.T., Special Ceramics V, ed. P. Popper, The British Ceramic Research Association, Stokes-on-Trent, England, 1972, (pp. 311-328).

6. Caws, R.B., Graham, R.P. and Stoddart, D.E., "Silicon Nitride Materials for Gas Turbine Components," ASME Pub. 73-GT-47, 1973. Presented at Gas Turbine Conf., Washington, D.C.

7. Jack, K.H., "The Production of High-Temperature, High-Strength Nitrogen Ceramics," Paper 111, 7, 1974.

8. Terwilliger, G.R. and Lange, F.F., "Task V, Pressureless Sintering of Si_3N_4," Final Report, Contract N00019-72-C-0278, Naval Air Systems Command.

9. Galasso, F. and Kuntz, V., J. Am. Ceram. Soc., No. 55.

10. Brennan, J.J., "Development of Fiber Reinforced Ceramic Matrix Composites," Third Quarterly Report on Contract N62269-74-C-0359, Naval Air Development Center.

11. Lange, F.F., Loc. Sit. (pp. 14-34).

12. Berry, J.P., Fracture Processes in Polymeric Solids, ed. B. Rosen, Wiley, New York, 1964, (pp. 157-194).

13. Lange, F.F., Loc. Sit. (pp. 7-8).

14. Lange, F.F., Loc. Sit. (p. 8).

15. Lange, F.F., Loc. Sit. (p. 9).

16. Charles, R.J., J. Appl. Phys., No. 29, 1958,(pp. 1657-62).

9.0 REFERENCES (Cont'd)

17. Lange, F.F., Loc. Sit. (p. 9).

18. Evans, A.G., J. Mater. Sci., No. 7, 1972 (pp. 1137-1146).

19. Charles, R.J., J. Appl. Phys., No. 29, 1958 (pp. 1657-62).

20. Lange, F.F., "High-Temperature Strength Behavior of Hot-Pressed Si_3N_4: Evidence for Subcritical Crack Growth," Amer. Cer. Soc. J., Vol. 57, No. 2, Feb. 1974 (pp. 84-87).

21. Terwilliger, G.R., "Properties of Sintered Si_3N_4," Amer. Cer. Soc. J. Vol. 57, No. 1, Jan. 1974 (pp. 48-49).

22. McLean, A.F., Fisher, E.A. and Bratton, R.J., "Brittle Materials Design, High Temperature Gas Turbine, Interim Report Number 6, January 1, 1974 to June 30, 1974," Contract Number DAAG46-71-C-0162, Advanced Research Projects Agency, April, 1974 (p. 157).

23. Torti, M.L., Alliegro, A., et al, "Silicon Nitride and Silicon Carbide for High Temperature Applications," British Ceramic Society Proceedings: 129-146 (1973).

24. Kossowsky, R., "Defect Detection in Hot Pressed Si_3N_4," Proceedings of the Second Army Materials Technology Conference, Nov. 1973 (pp. 685-684).

25. McLean, A.F., Fisher, E.A. and Bratton, R.J., Loc. Sit., (pp. 160-164).

26. McLean, A.F., Fisher, E.A., Bratton, R.J. and Miller, D.G., "Brittle Materials Design, High Temperature Gas Turbine, Interim Report Number 7, July 1, 1974 to December 31, 1974," AMMRC CTR 75-8, April, 1975, p. 97.

27. Gruver, R.M., Sotter, W.A., and Kirchner, H.P., "Fractography of Ceramics," Summary Report, Contract N00019-73-C-0356, Naval Air Systems Command, November 22, 1974.

28. Prochazka, S., Johnson, C.A. and Giddings, R.A., "Investigation of Ceramics for High Temperature Turbine Components," Final Report, Contract N6229-75-C-0122, Naval Air Systems Command.

29. Hurwitz, M.J., "Transducer for a High Resolution Ultrasonic Scanning System," Final Technical Report, Contract N00140-70-C-0065, Nov., 1970, pp. 6-11.

U.S. DEPARTMENT OF COMMERCE
National Technical Information Service
Springfield, Va. 22161

OFFICIAL BUSINESS

POSTAGE AND FEES PAID
U.S. DEPARTMENT OF COMMERCE
COM-211

U.S.MAIL

6322901 78 Z
NTIS CONTROL NUMBER

$ 4.90
VALUE OF SHIPMENT

22983 | 6C0165
DDC USER CODE | CONTRACT NO.

ORDER REF 085161
PURCHASE ORDER NO.

2436815
CARD SERIAL NO.

81091 1
DEPOSIT ACCT. NO.

NSCC/L 8767

PRINTED MATTER BOOKS

BATTELLE ADVANCED CONCEPTS LAB
ATTN
PO BOX 339 R F
WARREN MI 48090

NO. OF COPIES
PAPER COPY 001
MICRO FORM

ORDERED AS

AD A027357
FILED AS (DOCUMENT NO.)

THIS IS NOT A BILL. IT IS YOUR RECORD OF SHIPMENT. INVOICE WILL FOLLOW FOR SHIP AND BILL.
FOR ANY ADJUSTMENT ON THIS ORDER, PLEASE RETURN THIS CARD WITH YOUR CORRESPONDENCE.